0084019
Section 2 of 2

TABLE OF CONTENTS

B1.0 SUPPLEMENTAL RESISTIVITY RESULTS B-1
B1.1 HIGH-RESOLUTION RESISTIVITY LINES B-1
B1.1.1 High-Resolution Resistivity Line 0E B-1
B1.1.2 High-Resolution Resistivity Line 1E B-1
B1.1.3 High-Resolution Resistivity Line 2E B-4
B1.1.4 High-Resolution Resistivity Line 3E B-4
B1.1.5 High-Resolution Resistivity Line 4E B-5
B1.1.6 High-Resolution Resistivity Line 5E B-5
B1.1.7 High-Resolution Resistivity Line 6E B-6
B1.1.8 High-Resolution Resistivity Line 7E B-6
B1.1.9 High-Resolution Resistivity Line 8E B-7
B1.1.10 High-Resolution Resistivity Line 9E B-8
B1.1.11 High-Resolution Resistivity Line 10E B-8
B1.1.12 High-Resolution Resistivity Line 11E B-9
B1.1.13 High-Resolution Resistivity Line 12E B-9
B1.1.14 High-Resolution Resistivity Line 13E B-10
B1.1.15 High-Resolution Resistivity Line 14E B-10
B1.1.16 High-Resolution Resistivity Line 15E B-11
B1.1.17 High-Resolution Resistivity Line 16E B-11
B1.1.18 High-Resolution Resistivity Line 0N B-11
B1.1.19 High-Resolution Resistivity Line 1N B-12
B1.1.20 High-Resolution Resistivity Line 2N B-13
B1.1.21 High-Resolution Resistivity Line 3N B-13
B1.1.22 High-Resolution Resistivity Line 4N B-14
B1.1.23 High-Resolution Resistivity Line 5N B-14
B1.1.24 High-Resolution Resistivity Line 6N B-15
B1.1.25 High-Resolution Resistivity Line 7N B-15
B1.1.26 High-Resolution Resistivity Line 8N B-15
B1.1.27 High-Resolution Resistivity Line 9N B-16
B1.2 COMPILED HIGH-RESOLUTION RESISTIVITY CROSS SECTIONS B-16
B1.2.1 Horizontal Slice at 190 Meters B-17
B1.2.2 Horizontal Slice at 180 Meters B-18
B1.2.3 Horizontal Slice at 168.5 Meters B-19
B1.2.4 Horizontal Slice at 161 Meters B-20
B1.2.5 Horizontal Slice at 156 Meters B-20
B1.2.6 Horizontal Slice at 152 Meters B-21
B1.3 QUASI-THREE-DIMENSIONAL HIGH-RESOLUTION RESISTIVITY MODEL B-22
B1.4 TWO-DIMENSIONAL RESISTIVITY INVERSION OF HIGH-RESOLUTION RESISTIVITY DATA B-24

B2.0 SUPPLEMENTAL BACKGROUND SURVEY RESULTS B-28
B2.1 IN-FARM ELECTROMAGNETIC INDUCTION B-28
B2.2 IN FARM ELECTRICAL CONDUCTIVITY B-29
B2.2.1 Electrical Conductivity at 5 kilohertz B-30
B2.2.2 Electrical Conductivity at 7.5 kilohertz B-31
B2.2.3 Electrical Conductivity at 10 kilohertz B-32
B2.2.4 Electrical Conductivity at 15 kilohertz B-32
B2.2.5 Electrical Conductivity at 20 kilohertz B-33
B2.2.6 Total Electrical Conductivity B-33
B2.3 MAGNETOMETRY B-34
B2.3.1 In-Farm Magnetic Survey B-34
B2.3.2 Ex-Farm Magnetic Results B-35
B2.4 EX-FARM ELECTROMAGNETIC INDUCTION B-37
B2.4.1 In-Phase Electromagnetic Induction B-37
B2.4.2 In-Phase 5 kilohertz B-38
B2.4.3 In-Phase 7.5 kilohertz B-39
B2.4.4 In-Phase 10 kilohertz B-39
B2.4.5 In-Phase 15 kilohertz B-40
B2.4.6 In-Phase 20 kilohertz B-41
B2.4.7 Ex-Farm Electrical Conductivity B-41
B2.4.8 Electrical Conductivity at 5 kilohertz B-42
B2.4.9 Electrical Conductivity at 7.5 kilohertz B-43
B2.4.10 Electrical Conductivity at 10 kilohertz B-43
B2.4.11 Electrical Conductivity at 15 kilohertz B-44
B2.4.12 Electrical Conductivity at 20 kilohertz B-44
B2.4.13 Total Electrical Conductivity B-45
B2.5 IN-FARM GROUND-PENETRATING RADAR RESULTS B-45

B3.0 REFERENCES B-48

LIST OF FIGURES

Figure B-1. Variogram of Modeled and Experimental High-Resolution Resistivity Data for 190 Meters. B-17

Figure B-2. Variogram of Modeled and Experimental High-Resolution Resistivity Data at 180 Meters. B-18

Figure B-3. Variogram of Modeled and Experimental High-Resolution Resistivity Data at 168.5 Meters. B-19

Figure B-4. Variogram of Modeled and Experimental High-Resolution Resistivity Data at 161 Meters. B-20

Figure B-5. Variogram of Modeled and Experimental High-Resolution Resistivity Data at 156 Meters. B-21

Figure B-6. Variogram of Modeled and Experimental High-Resolution Resistivity Data at 152 Meters. B-22

Figure B-7. Cumulative Distribution Function for High-Resolution Resistivity at the T Tank Farm. B-23

Figure B-8. Sample Ground-Penetrating Radar Plot with Buried Pipelines. B-46

LIST OF TABLES

Table B-1. Summary of High-Resolution Resistivity Line Statistics. B-2

Table B-2. Summary of Two-Dimensional Inversion Model Parameters and Statistics. B-25

Table B-3. Summary Statistics for In-Phase Electromagnetic Induction Data. B-28

Table B-4. Summary Statistics for Electrical Conductivity Data. B-30

Table B-5. Summary Statistics for In-Farm Magnetic Data. B-34

Table B-6. Summary Statistics for Ex-Farm Magnetic Data. B-35

Table B-7. Summary Statistics for Ex-Farm, In-Phase Electromagnetic Induction Data. B-38

Table B-8. Summary Statistics for Ex-Farm, In-Phase Electromagnetic Induction Data. B-42

LIST OF TERMS

Abbreviations, Acronyms, and Initialisms

EM	electromagnetic induction
GPR	ground-penetrating radar
HRR	high-resolution resistivity
RMS	root mean square

B1.0 SUPPLEMENTAL RESISTIVITY RESULTS

B1.1 HIGH-RESOLUTION RESISTIVITY LINES

This section presents the results of the high-resolution resistivity (HRR) data collected on the 27 separate surface lines in the T tank farm. The HRR coverage area is shown in Figure A-46. The HRR data are shown in Appendix A, Figures A-27 through A-73. Table B-1 provides the summary statistics for each HRR line.

B1.1.1 High-Resolution Resistivity Line 0E

The results of HRR line 0E can be seen in Figure A-47.

The HRR line is the farthest west, adjacent to the T-7 tile field, and crosses lines 0N through line 6N. HRR line 0E shows distinctively resistive features within the body of the figure which begin at the surface stretching the length of the line from south to north to form two large formations. The resistive feature in the south extends beyond the limits of the survey, while the dominant feature extends beyond the limits of the survey to the north. Both features are delineated by the red/orange color representing apparent resistivity values from 320 to 450 ohm-meters. Within the main body of this resistive feature, apparent resistivity values go up to a high of 1,400 ohm-meters. At approximately 100 to 150 meters along the line, there is a moderate conductive feature coincident with the location of the T-7 tile field. This area is bound by the two large resistive areas on either side. The water table begins at approximately 136 meters above mean sea level and extends beyond the depth limits of the survey.

B1.1.2 High-Resolution Resistivity Line 1E

The results of HRR line 1E can be seen in Figure A-48. The location of the line with respect to the site boundaries can be seen in Figure A-46. This line was located 30 meters east of line 0E, placed in a north to south orientation, and adjacent to the T-36 crib and T-5 trench. Additionally, line 1E overlays the crib 216-T-7 tile field, and crosses lines 0N through 6N.

Table B-1. Summary of High-Resolution Resistivity Line Statistics. (2 Sheets)

Line #	Figure	Data Points (Total)	Apparent Resistivity (ohm-meter)			Std Dev	Nodes (Total)	Coordinates		Length (m)
			Min	Median	Max			Start	End	
0E	A-47	1,872	88	424	1,720	262	6,728	566640.3, 136542.2	566639.6, 136891.0	345
1E	A-48	1,251	72	370	1,091	183	5,292	566670.4, 136542.2	566669.1, 136890.3	321
2E	A-49	1,622	58	339	1,232	273	6,549	566700.6, 136542.2	566700.6, 136899.7	353
3E	A-50	4,546	33	253	1,186	250	7,181	566730.1, 136536.1	566729.4, 136882.3	334
4E	A-51	4,478	21	95	1,474	289	7,181	566760.9, 136536.8	566759.6, 136885.0	334
5E	A-52	4,105	10	80	856	180	7,224	566793.8, 136536.1	566792.4, 136881.6	335
6E	A-53	6,253	8	70	185	185	7,396	566824.6, 136535.5	566821.2, 136881.0	343
7E	A-54	6,206	11	83	686	147	7,396	566852.2, 136535.6	566853.7, 136880.3	343
8E	A-55	6,301	18	129	646	117	7,224	566887.7, 136535.1	566886.8, 136879.3	336
9E	A-56	5,580	6	134	496	134	7,568	566912.2, 136535.1	566913.7, 136882.2	343
10E	A-57	2,856	6	264	1712	264	8,621	566940.7, 136534.8	566940.1, 136999.4	466
11E	A-58	2,075	25	290	1,765	226	8,778	566958.3, 136532.3	566958.3, 137000.7	463
12E	A-59	1,934	25	297	1,188	200	8,816	566972.7, 136532.3	566972.7, 136999.4	463
13E	A-60	2,066	51	320	1,447	199	8,816	566972.7, 136532.9	566986.5, 136998.2	463
14E	A-61	2,220	21	327	1,273	195	8,816	566998.4, 136536.1	566998.4, 137000.7	463
15E	A-62	2,124	41	328	1,548	241	8,584	567014.7, 136532.3	567014.7, 136996.3	463
16E	A-63	2,037	36	349	1,620	268	8,584	567042.3, 136532.3	567042.9, 136996.9	462
0N	A-64	2,788	15	212	1,504	274	12,300	566535.7, 136617.9	567139.1, 136605.1	600
1N	A-65	7,222	18	213	1,303	247	14,812	566481.7, 136661.8	567132.4, 136655.0	642
2N	A-66	8,080	8	217	1,215	233	15,360	567042.3, 136532.3	567042.9, 136996.9	643
3N	A-67	8,080	8	217	1,215	233	15,360	566480.3, 136719.8	567127.7, 136715.8	643

Table B-1. Summary of High-Resolution Resistivity Line Statistics. (2 Sheets)

Line #	Figure	Data Points (Total)	Apparent Resistivity (ohm-meter)			Std Dev	Nodes (Total)	Coordinates		Length (m)
			Min	Median	Max			Start	End	
4N	A-68	6,529	8	225	1,079	211	15,456	566486.4, 136750.9	567125.6, 136746.2	643
5N	A-69	12,779	22	253	925	194	15,042	566489.1, 136781.3	567167.5, 136776.5	679
6N	A-70	1,700	43	327	872	148	5,488	566546.5, 136813.7	567131.0, 136802.9	686
7N	A-71	1,264	123	340	956	139	5,538	566844.5, 136833.2	567130.4, 136829.2	283
8N	A-72	1,272	158	345	1,074	148	5,396	566845.2, 136858.9	567130.4, 136854.9	283
9N	A-73	4,064	172	406	943	158	5,680	566844.5, 136882.5	567127.0, 136879.8	283

Notes:

m = meter.
max = maximum.
min = minimum.
std dev = standard deviation.

HRR line 1E shows distinctively resistive signatures within the body of the figure which begin at the surface stretching the length of the line to form three large formations. The resistive feature in the south extends beyond the limits of the survey while the central and northern most features are delineated by the red/orange color representing apparent resistivity values from 350 to 460 ohm-meters. Within the main body of this resistive feature, apparent resistivity values range up to a high of 1,400 ohm-meters. Line 1E extends along the western edge of the T-36 crib, through T-7 tile field, and along the western edge of T-5 trench. At approximately 180 to 200 meters along the line, there is a moderate conductive feature at the location of the T-5 trench at values in the range of 310 ohm-meters. This area is bound by large conductive areas on either side. A slightly conductive feature area also appears at the beginning of the line at approximately 60 meters and extends to 115 meters, which corresponds to the T-36 crib and the T-7 tile field. This area is also bound by large conductive areas. The water table begins at approximately 136 meters above mean sea level and extends beyond the depth limits of the survey.

B1.1.3 High-Resolution Resistivity Line 2E

The results of HRR line 2E can be seen in Figure A-49. The location of the line with respect to the site boundaries can be seen in Figure A-46. This line was located 30 meters east of line 1E, placed in a north-south orientation, and adjacent to the T-32 crib. Additionally, line 2E overlays crib T-36, the T-7 tile field, and crosses lines 0N through 6N.

HRR line 2E shows a large, distinctive break in the resistive signature observed in lines 0E and 1E. At approximately 80 to 180 meters along line 2E, there is a moderately conductive area corresponding to the T-7 tile field and the corner of crib T-32. While this area is only moderately conductive, it is bordered by two highly resistive regions. Additionally, the water table appears to rise with a convex swelling toward this area, with lower resistivities moving well beyond its average depth of 70 meters. The water table is highlighted by the light blue color representing apparent resistivity values of 160 ohm-meters. The bulk of water table signature shows values from 50 to 115 ohm-meters.

B1.1.4 High-Resolution Resistivity Line 3E

The results of HRR line 3E can be seen in Figure A-50. The location of the line with respect to the site boundaries can be seen in Figure A-46. Orientation for line 3E is directly north–south, located 30 meters east of line 2E, and crosses lines 0N through 6N, the T-36 crib, the T-7 tile fields, and the southeast corner of the T-32 crib. This line was placed parallel to lines 2E and 4E.

HRR line 3E shows a distinctively highly conductive plume signature extending the length of the line at varying depths and infiltrating the water table at 136 meters above mean sea level. At approximately 115 meters along line 3E, there is a peak rise in the plume which coincides with the T-7 tile field. The plume subsides at approximately 170 meters above mean sea level and then sharply rises to 180 meters above mean sea level at 160 meters along line 3E. At this intersection, line 3E crosses the corner of crib T-32, correlating with the plume convexity in this

area. Near both anomalies, the plume reaches within 20 meters of the ground surface. The plume recedes rapidly running north along line 3E. A thin light blue layer (160 ohm-meters) followed by a darker blue layer (106 ohm-meters) highlight the plume. Resistivity values ranging from 10 to 130 ohm-meters form the bulk of the plume and extend into the water table past the survey limits. Line 3E is bracketed by high resistivity areas in the range of 1,300+ ohm-meters at either end, and approximately 40 meters in length.

B1.1.5 High-Resolution Resistivity Line 4E

The results of HRR line 4E can be seen in Figure A-51. The location of the line with respect to the site boundaries can be seen in Figure A-46. Line 4E is oriented in a north-south direction, located 30 meters east of line 3E, and bounded by tanks T-204 through T-201 10 meters to the west, and tanks T-112, T-109, T-106, and T-103 5 meters to the east. Line 4E is adjacent to underground pipes and an underground electrical trench. Additionally, line 4E crosses east-west lines 0N through 6N, a large concrete pipe trench, and various stainless steel pipes.

To the east, line 4E shows a large continuous conductive anomaly beneath tanks T-112, T-109, T-106, and T-103. The anomaly reaches the surface to the south, and just below the ground surface to the north. This anomaly covers the bulk of the plot and is bound by highly resistive features on either side. The resistivity anomaly is likely related to the large network of pipes and electrical lines that make up the tank farm system. In the proximity of the tanks and infrastructure, there is high connectivity. The HRR results present a significant conductive anomaly forming a massive conductive signature in the bulk of the plot. This anomaly is likely noise, possible transmission problems, and potential short circuiting created by the linked tank farm infrastructure. It does not represent true conductive values. However, the conductive anomaly is bound by highly resistive features which are descriptive in the context.

B1.1.6 High-Resolution Resistivity Line 5E

The results of HRR line 5E can be seen in Figure A-52. The location of this line with respect to the site boundaries can be seen in Figure A-46. Line 5E is oriented in a north-south direction, located 30 meters east of line 4E, and bounded by tanks T-112, T-109, T-106, and T-103 approximately 5 meters to the west and tanks T-111, T-108, T-105, and T-102 approximately 2 meters to the east. Line 5E crosses east-west lines 0N through 6N as well as several pipelines.

HRR line 5E shows a large continuous conductive anomaly beneath tanks T-111, T-108, T-105, and T-102. To the south, the conductive anomaly stretches upward from approximately 37 meters to the edge of tank T-111 at approximately 123 meters. From tank T-102, the conductive anomaly stretches downward tapering off quickly to the north. This anomaly covers the bulk of the plot and is bound by highly resistive features to either side. The anomaly is likely related to the large network of pipes and electrical lines that make up the tank farm system. Steel pipes, electrical lines, and many other conductive materials can produce conductive shadows that radiate downward obscuring the true resistivity of the subsurface. In the proximity of the tanks and infrastructure, there is great connectivity among the associated pipes and

electrical lines. This anomaly is likely caused by noise, possible transmission problems, and potential short circuiting created by the interconnected tank farm infrastructure. It does not represent true conductive values. However, the conductive anomaly is bracketed by resistivity highs at either end in the range of 1,300+ ohm-meters, and approximately 60 meters in length to the south and 55 meters to the north.

B1.1.7 High-Resolution Resistivity Line 6E

The results of HRR line 6E can be seen in Figure A-53. The location of the line with respect to the site boundaries can be seen in Figure A-46. Line 6E is oriented in a north-south direction, located 30 meters east of line 5E, and bounded by tanks T-111, T-108, T-105, and T-102 approximately 3 meters to the west and tanks T-110, T-107, T-104, and T-101 approximately 5 meters to the east. Line 6E crosses east-west lines 0N through 6N. Line 6E parallels pipes and other infrastructure from approximately 160 meters to 260 meters.

HRR line 6E shows a large continuous conductive anomaly beneath tanks T-110, T-107, T-104, and T-101. From the south, the conductive anomaly stretches upward from approximately 38 meters reaching the surface at approximately 65 meters and then again at 85 meters, and finally to the middle of tank T-110 at approximately 137 meters along the line. From approximately 258 meters along line 6E stretching to the north, the conductive anomaly reaches downward tapering off quickly to 308 meters along the line. This anomaly covers the bulk of the plot and is bound by highly resistive features on either side. The anomaly is likely related to the large network of pipes and electrical lines that make up the tank farm system. Steel pipes, electrical lines, and many other conductive materials can produce conductive shadows that radiate downward obscuring the true resistivity of the subsurface. In the proximity of the tanks and infrastructure, there is great connectivity among the associated systems of pipes and electrical lines in the survey area. This anomaly is likely caused by noise, possible transmission problems, and potential short circuiting created by the interconnected tank farm infrastructure. It does not represent true conductive values. However, the conductive anomaly is bracketed by resistivity highs at either end in the range of 1,300+ ohm-meters and approximately 55 meters in length to the south and approximately 62 meters to the north.

B1.1.8 High-Resolution Resistivity Line 7E

The results of HRR line 7E are displayed in Figure A-54. The location of the line with respect to the site boundaries can be seen in Figure A-46. Line 7E is oriented in a north-south direction, located 30 meters east of line 6E, and flanked approximately 3 meters to the west by tanks T-110, T-107, T-104, and T-101. Line 7E crosses east-west lines 0N through 9N.

HRR line 7E shows a large continuous conductive anomaly beneath tanks T-110, T-107, T-104, and T-101. From the south, beyond the limits of the survey, the conductive anomaly begins at a depth of 178 meters above mean sea level and rises vertically to the surface reaching approximately 40 meters along the line. From this intersection, the anomaly stretches along the surface for approximately 109 meters and then dips down under tank T-110 and rises to

encompass tanks T-107, T-104, and T-101. At approximately 260 meters along the line, the anomaly tapers downward reaching the water table at 305 meters. This anomaly covers the bulk of the plot with highly conductive values in the range of 10 ohm-meters to 170 ohm-meters. To the north of the anomaly, there is a highly resistive feature beginning at the surface and reaching a depth of approximately 150 meters above mean sea level. Its length extends from 265 meters along the line to 343 meters north where the line ends. The resistive feature extends beyond the limits of the survey.

The highly conductive anomaly is likely related to the large network of pipes and electrical lines that make up the tank farm system. Steel pipes and electrical lines can produce conductive shadows that radiate downward obscuring the true values of the subsurface. In the proximity of the tanks and infrastructure, there is great connectivity among the associated systems of pipes and electrical lines in the survey area. This anomaly is likely caused by noise, possible transmission problems, and potential short circuiting created by the linked tank farm infrastructure. It does not represent true conductive values. However, the conductive anomaly is bracketed by resistivity highs at either end in the range of 1,300+ ohm-meters, and approximately 55 meters in length to the south and approximately 62 meters to the north.

B1.1.9 High-Resolution Resistivity Line 8E

The results of HRR line 8E can be seen in Figure A-55. The location of the lines with respect to the site boundaries can be seen in Figure A-46. Line 8E is oriented in a north-south direction, located 30 meters east of line 7E, and approximately 33 meters to the west of tanks T-110, T-107, T-104, and T-101. Line 8E crosses east-west lines 0N through 9N. Line 8E parallels electrical conduit, steam pipes, and a small pipe trench.

HRR line 8E shows a large conductive anomaly punctuated by an area of high resistivity. In the southern region, there is a moderately resistive area extending approximately 78 meters to the north along the line at 280 ohm-meters. In the north, there is a highly resistive area extending approximately 65 meters south along the line at 1,350 ohm-meters. Both theses features bracket the conductive anomaly at the center making up the bulk of the plot. The anomaly begins at a depth of 170 meters above mean sea level and 10 meters along line 8E. It then dips slightly before rising vertically to reach the surface at approximately 80 meters along the line. From this intersection, the anomaly stretches along the surface for approximately 190 meters and then drops down slightly under the conductive anomaly before reaching the water table at 300 meters along the line.

The conductive anomaly is likely related to the large network of pipes and electrical lines that make up the tank farm system. These areas produced conductive shadows and do not reflect the true resistivity of the subsurface. This anomaly is likely caused by noise, possible transmission problems, and potential short circuiting created by the interconnected tank farm infrastructure. It does not represent true conductive or resistive values. The punctuated resistive area located between 120 meters to 220 meters, and at an approximate depth of 145 meters above mean sea level, is likely noise.

B1.1.10 High-Resolution Resistivity Line 9E

The results of HRR line 9E can be seen in Figure A-56. The location of this line with respect to the site boundaries and the other 26 lines can be seen in Figure A-46. Line 9E is oriented in a north-south direction, located 30 meters east of line 8E, and flanked approximately 63 meters to the west by tanks T-110, T-107, T-104, and T-101. Line 9E crosses east-west lines 0N through 9N.

HRR line 9E shows a distinctive conductive signature across the bottom portion of line 9E. This feature begins at approximately 160 meters above mean sea level; it then rises toward the surface creating a convex lump reaching the surface at a value of 158 ohm-meters. The bulk of the conductive anomaly is at 10 ohm-meters. The conductive anomaly reaches the surface at approximately 80 meters along the line and then falls sharply at approximately 130 meters along line 9E. This 50-meter section of 9E is associated with a large cluster of pipes suggesting the effects of a conductive shadow, and does not reflect the true resistivity of the subsurface. Within the main body of this conductive anomaly, apparent resistivity values range from a low of 10 ohm-meters to a high of 130 ohm-meters. At 210 meters and 245 meters along line 9E, two additional distinctive pipe features appear. These have a traditional pant leg appearance, making their identification highly conclusive.

B1.1.11 High-Resolution Resistivity Line 10E

The results of HRR line 10E can be seen in Figure A-57. The location of this line with respect to the site boundaries and the other 26 lines can be seen in Figure A-46. Line 10E is oriented in a north-south direction, located 30 meters east of line 9E, and crosses east-west lines 0N through 9N. Additionally, line 10E runs to the west of and adjacent to the 207-T retention basin and crib T-14.

HRR line 10E shows a distinctive conductive anomaly at its beginning in the south while in the north, the signature graduates to become highly conductive. Beginning at approximately 10 meters along the line and at a depth of 170 meters above mean sea level, the conductive anomaly begins well above the water table, tapers upward reaching the surface at 25 meters, drops sharply to 165 meters above mean sea level, then rises sharply again reaching the surface at 70 meters along the line. From 70 meters to 115 meters along the line, the conductive anomaly stays at or just below the ground surface, tapers off reaching a depth of 155 meters above mean sea level, then rises again forming a moderate convex bulge stretching 100 meters before dipping into the water table. The anomaly is delineated by light blue at 160 ohm-meters followed by a deep blue color representing apparent resistivity values of 144 ohm-meters. The bulk of the anomaly is highlighted by light violet colors and has resistivity values in the range of 20 ohm-meters to 70 ohm-meters. The anomaly line has a similar appearance to that seen in line 9E, and likely represents pipes.

The highly conductive anomaly is likely related to the network of pipes and electrical lines composing the tank farm system. Underground infrastructure such as pipes and electrical lines can produce conductive shadows, and do not reflect the true resistivity of the subsurface.

Portions of this anomaly are likely caused by noise, possible transmission problems, and potential short circuiting created by the tank farm infrastructure.

B1.1.12 High-Resolution Resistivity Line 11E

The results of HRR line 11E can be seen in Figure A-58. The location of this line with respect to the site boundaries and the other 26 lines can be seen in Figure A-46. Line 11E is oriented in a north-south direction, located 18 meters east of line 10E, and crosses east-west lines 0N through 9N. Additionally, line 11E runs through the 207-T retention basin and to the east of crib T-14.

HRR line 11E shows distinctive conductive anomalies near the beginning of the line. The highly conductive anomaly is likely related to the network of pipes and electrical lines composing the tank farm system. Underground infrastructure such as pipes and electrical lines can produce conductive shadows and do not reflect the true resistivity of the subsurface. Portions of this anomaly are likely caused by noise, possible transmission problems, and potential short circuiting created by the tank farm infrastructure.

The end of line 11E shows a slight conductive anomaly deep within the vadose zone. The line runs adjacent to the trenches that received approximately 1 million gallons of liquid waste. This anomaly most probably represents changes in soil resistivity due to waste disposal efforts.

B1.1.13 High-Resolution Resistivity Line 12E

The results of HRR line 12E can be seen in Figure A-59. The location of this line with respect to the site boundaries and the other 26 lines can be seen in Figure A-46. Line 12E is oriented in a north-south direction, located 13 meters east of line 11E, and crosses east-west lines 0N through 9N. Additionally, line 12E runs through the 207-T retention basin and to the east of crib T-15.

HRR line 12E shows a conductive anomaly beginning in the south and extending midway through the figure. The northern half of the figure is highly conductive. Beginning at approximately 12 meters along the line and at a depth of roughly 167 meters above mean sea level, the conductive anomaly begins well above the water table. The anomaly extends sharply upward reaching the surface at 21 meters. The anomaly is likely related to the network of pipes and electrical lines composing the tank farm system. Underground infrastructure such as pipes and electrical lines can produce conductive shadows and do not reflect the true resistivity of the subsurface. Portions of this anomaly are likely caused by noise, possible transmission problems, and potential short circuiting created by the tank farm infrastructure.

The end of line 12E shows a slight conductive anomaly deep within the vadose zone. The line runs adjacent to the trenches that received approximately 1 million gallons of liquid waste. This anomaly most probably represents changes in soil resistivity due to waste disposal efforts.

B1.1.14 High-Resolution Resistivity Line 13E

The results of HRR line 13E can be seen in Figure A-60. The location of this line with respect to the site boundaries and the other 26 lines can be seen in Figure A-46. Line 13E is oriented in a north-south direction, located 14 meters east of line 12E, and crosses east-west lines 0N through 9N. Additionally, line 13E runs through the 207-T retention basin and to the east of crib T-15.

HRR line 13E shows a conductive anomaly beginning in the south that extends midway through the figure. The northern half of the figure is highly conductive. Beginning at approximately 3 meters along the line and at a depth of roughly 186 meters above mean sea level, the conductive anomaly begins well above the water table. The anomaly extends sharply upward reaching the surface at 9 meters. This anomaly is likely related to the network of pipes and electrical lines composing the tank farm system. Underground infrastructure such as pipes and electrical lines can produce conductive shadows and do not reflect the true ohm values of the subsurface. Portions of this anomaly are likely caused by noise, possible transmission problems, and potential short circuiting created by the tank farm infrastructure.

The end of line 12E shows a slight conductive anomaly deep within the vadose zone. The line runs adjacent to the trenches that received approximately 1 million gallons of liquid waste. This anomaly most probably represents changes in soil resistivity due to waste disposal efforts.

B1.1.15 High-Resolution Resistivity Line 14E

The results of HRR line 14E can be seen in Figure A-61. The location of this line with respect to the site boundaries and the other 26 lines can be seen in Figure A-46. Line 14E is oriented in a north-south direction, located 12 meters east of line 13E, and crosses east-west lines 0N through 9N. Additionally, line 14E runs through the western section of crib T-15.

HRR line 14E shows distinctively resistive signatures within the body of the figure which begin at the surface, stretch the length of the line from south to north, and form two large formations. The large resistive feature in the south is bound by a thin conductive anomaly extending beyond the limits of the survey southward in the range of 103 ohm-meters. The other dominant feature begins at approximately 318 meters and extends beyond the limits of the survey to the north. Both features are delineated by the red/orange color representing apparent resistivity values from 320 to 450 ohm-meters. Within the main body of this resistive feature, apparent resistivity values range to a high of 1,400 ohm-meters. At approximately 262 to 344 meters along the line, there is a moderate conductive feature coincident with the location of the T-16 crib. This area is bound by the two large resistive areas on either side. The water table is at 136 meters above mean sea level. There is no conductive signature visible for the water table, and therefore, it is likely lower than the limits of the survey.

Within line 14E, there is much less pipe infrastructure than in previous lines. However, portions of this anomaly may still relate to noise, possible transmission problems, and potential short circuiting caused by infrastructure.

B1.1.16 High-Resolution Resistivity Line 15E

The results of HRR line 15E can be seen in Figure A-62. The location of this line with respect to the site boundaries and the other 26 lines can be seen in Figure A-46. Line 15E is oriented in a north-south direction, located 16 meters east of line 14E, and crosses east-west lines 0N through 9N. Additionally, line 15E runs through the T-17 crib.

HRR line 15E has two main sections. The southern portion shows a response typical for infrastructure. At approximately 90 and 120 meters along the line, resistivity decreases and pant leg effects indicate the presence of pipes. These pant legs extend down to the water table, and obscure the resistivity of the soil.

The northern portion of the line, from about 220 to 340 meters along the line, shows a slight conductive region about 20 metes below ground surface. This conductive anomaly coincides with trenches that received approximately 1 million gallons of liquid waste. North of this anomaly, the soil returns to background condition resistivity (i.e., greater than 450 ohm-meters) suggesting the absence of waste plume contamination.

B1.1.17 High-Resolution Resistivity Line 16E

The results of HRR line 16E can be seen in Figure A-63. The location of this line with respect to the site boundaries and the other 26 lines can be seen in Figure A-46. Line 16E is oriented in a north-south direction, located 30 meters east of line 15E, and crosses east-west lines 0N through 9N. Additionally, line 16E runs approximately 20 meters to the east of crib T-17.

HRR line 16E has two main sections. The southern portion shows a response type for infrastructure. At approximately 90 and 120 meters along the line, resistivity decreases, and pant legs effects indicate pipes. These pant legs extend down to the water table, and obscure soil resistivity.

The northern portion of the line, from about 220 to 340 meters along the line, shows a slight conductive region at about 20 meters below ground surface. This conductive anomaly coincides with trenches that received approximately 1 million gallons of liquid waste. North of this anomaly, the soil conditions return to background resistivity (i.e., greater than 450 ohm-meters) suggesting the absence of a waste plume.

B1.1.18 High-Resolution Resistivity Line 0N

The results of HRR line 0N can be seen in Figure A-64. The location of this line with respect to the site boundaries and the other 26 lines can be seen in Figure A-46. Line 0N is oriented in a west-east direction, located 45 meters south of line 1N, and 10 meters south of 23rd Street. The line crosses north-south lines 0E through 16E. Additionally, line 0N runs parallel to the T-7 crib and tile field.

Line 0N has two sections. The first section to the west extends from the beginning of the line to about 280 meters. The second section starts at 280 meters to the eastern edge of the survey. Noise from infrastructure in the eastern section entirely obscures soil resistivity.

The western portion of line 0N shows responses typical for infrastructure near surface at approximately 140, 225, and 255 meters along the line. The first feature is caused by a well. The other two responses are likely caused by pipes. The removal of these features by filtering suggests the subsurface is more conductive at depth near the water table. A known inorganic plume exists in the saturated zone, with a high nitrate concentration, near this line. The HRR data likely reflect the presence of this plume. The plume probably originates in the western cribs, which received in excess of 30 million gallons of liquid waste discharges. However, the infrastructure makes it difficult to define the edges of the potential plume.

In addition to showing potential contamination, HRR line 0N shows areas in the west free from contamination. These areas are indicated by high resistivity values typical of clean or dry sand.

B1.1.19 High-Resolution Resistivity Line 1N

The results of HRR line 1N can be seen in Figure A-65. The location of this line with respect to the site boundaries and the other 26 lines can be seen in Figure A-46. Line 1N is oriented in a west-east direction, located 30 meters south of line 1N, 24 meters north of the T tank farm fence, and south of tanks T-110, T-111, and T-112. The line crosses north-south lines 0E through 16E. Additionally, line 1N runs through the middle of the T-7 tile field. Line 1N parallels a portion of the steel pipes from approximately 248 meters to approximately 366 meters.

To the north, HRR line 1N shows a single large conductive region encompassing the majority of the figure. The conductive anomaly is bracketed by two moderately sized resistive regions in the west and east, indicating a clean area in the vadose zone. The resistive feature in the west extends beyond the limits of the survey and stops at approximately 235 meters. The resistive feature in the east extends beyond the limits of the survey and abruptly begins at approximately 511 meters. Both features are delineated by the red/orange color representing apparent resistivity values from 320 to 450 ohm-meters. Within the body of the features, apparent resistivity values range to a high of 1,400 ohm-meters.

Several interesting features appear in line 1N. The tanks, which are plotted explicitly in the sections, do not create the same conductive signature as pipes. The three tanks do not appear grounded to the soil, and may actually have high resistivity. Pipes between and adjacent to tanks do show the typical pant leg feature. Two additional features, where of the line crosses lines 8E and 9E, also show a pant leg response. However, the pant leg has an atypical appearance. The effect may represent waste in the soil. However, the effects of the infrastructure preclude firm conclusions about the origin of the effect.

The western portion of the line, coincident with the T-7 tile field, shows a conductive anomaly most likely caused from liquid waste disposal. The end points of the tile field are located on the filtered section of line 1N. Directly below these boundaries, the resistivity decreases. From the

western edge of the tile field to the beginning of the line, the resistivity of the vadose zone returns to a background condition (i.e., free of waste).

B1.1.20 High-Resolution Resistivity Line 2N

The results of HRR line 2N can be seen in Figure A-66. The location of this line with respect to the site boundaries and the other 26 lines can be seen in Figure A-46. Line 2N is oriented in a west-east direction, located 30 meters north of line 1N, and 3 meters from tanks T-109, T-108, and T-107. The line crosses north-south lines 0E through 16E. Additionally, line 2N runs through the middle of the T-32 crib, the 207-T retention basin, and 2 meters south of tank T-202. Line 2N parallels a portion of the steel pipes and electrical conduit from approximately 300 meters to approximately 360 meters.

To the north, HRR line 2N shows a single large, central conductive region. The conductive anomaly is bracketed by two large resistive regions in the west and east. One resistive feature extends beyond the limits of the survey in the south and ceases at approximately 195 meters. The second resistive feature begins at approximately 511 meters and extends beyond the limits of the survey in the north. Both features are bordered by the red/orange color representing apparent resistivity values from 320 to 450 ohm-meters. Within the body of the resistive features, apparent resistivity values range to a high of 1,400 ohm-meters.

In many respects, line 2N has an appearance similar to 1N. The same resistive features at either end of the line are indicative of background. Moderately resistive areas are coincident with waste disposal regions. Very low resistivity areas caused by tank farm infrastructure preclude positive conclusions about the presence or absence of a waste plume.

B1.1.21 High-Resolution Resistivity Line 3N

The results of HRR line 3N can be seen in Figure A-67. The location of this line with respect to the site boundaries and the other 26 lines can be seen in Figure A-46. Line 3N is oriented in an east-west direction, located 30 meters north of line 2N, and 3 meters from tanks T-106, T-105, and T-104. The line crosses north-south lines 0E through 16E. Additionally, line 3N runs through the middle of the T-5 trench, the 207-T retention basin, and 4 meters north of tank T-201. Line 3N parallels a portion of the stainless steel pipes from approximately 270 meters to approximately 370 meters.

To the north, HRR line 3N shows a single large, central conductive region. The conductive anomaly is bracketed by two large resistive regions in the west and east. One resistive feature extends beyond the limits of the survey in the west and ceases at approximately 180 meters. The second large resistive feature begins at approximately 437 meters and extends beyond the limits of the survey in the east. Both features are bordered by the red/orange color representing apparent resistivity values from 320 to 450 ohm-meters. Within the body of the resistive features, apparent resistivity values range to a high of 1,400 ohm-meters. At 180 to 225 meters,

and 415 to 435 meters, two moderately resistive regions appear. These areas are coincident with the T-5 trench location and the tank farm fenceline, respectively.

Pipes, electrical lines, and wells located in the vicinity of line 3N may produce conductive or resistive shadows within the survey area. The data in these areas does not reflect the true resistivity of the subsurface. Portions of the conductive and resistive anomalies in line 3N may contain noise, possible transmission problems, and potential short circuiting created by the tank farm infrastructure.

B1.1.22 High-Resolution Resistivity Line 4N

The results of HRR line 4N can be seen in Figure A-68. The location of this line with respect to the site boundaries and the other 26 lines can be seen in Figure A-46. Line 4N is oriented in an east-west direction, located 30 meters north of line 3N, and 3 meters from tanks T-103, T-102, and T-101. The line crosses north-south lines 0E through 16E. Line 4N parallels the large pipe trench from 280 to 368 meters.

To the north, HRR line 4N shows a single large conductive region encompassing the center part of the figure. To the west, the conductive anomaly is flanked by a large continuous resistive region extending to 262 meters. To the east, the conductive anomaly is flanked by a resistive feature beginning at 443 meters and extending beyond the limits of the survey. Both features are delineated by the red/orange color representing apparent resistivity values from 308 to 450 ohm-meters. Within the body of the resistive features, apparent resistivity values range to a high of 1,400 ohm-meters.

Pipes, electrical lines, and wells located in the vicinity of line 4N may produce conductive or resistive shadows within the survey area. The data in these areas does not reflect the true resistivity of the subsurface. Portions of the conductive and resistive anomalies in line 2N may contain noise, possible transmission problems, and potential short circuiting created by the tank farm infrastructure.

B1.1.23 High-Resolution Resistivity Line 5N

The results of HRR line 5N can be seen in Figure A-69. The location of this line with respect to the site boundaries and the other 26 lines can be seen in Figure A-46. Line 5N is oriented in an east-west direction, located 30 meters north of line 4N, and 3 meters from tanks T-103, T-102, and T-101. The line crosses north-south lines 0E through 16E. Line 5N parallels many pipes from 272 to 396 meters.

The western portion of line 5N is generally resistive in the vadose zone and conductive in the saturated zone. The rail line, entry road, and tank farm fence stand out as conductive infrastructure. However, they do not appear as pipelines and do not have the same detrimental effects on data interpretation.

In the area between the fence and tank T-103, the vadose zone displays conductivity possibly indicative of inorganic waste.

The eastern portion of the line runs south of trenches T-14 through T-17. The resistivity decreases in this area indicating the southern boundary of the plume resulting from disposal activities in this area. The far eastern area shows the soil returning to a background condition.

B1.1.24 High-Resolution Resistivity Line 6N

The results of HRR line 6N can be seen in Figure A-70. The location of this line with respect to the site boundaries and the other 26 lines can be seen in Figure A-46. Line 6N is oriented in an east-west direction, located 30 meters north of line 5N, and 16 meters north of the T tank farm fenceline. The line crosses north-south lines 0E through 16E and cribs T-14, T-15, T-16, and T-17.

HRR line 6N shows a relatively resistive vadose zone and a conductive saturated zone. In the vadose zone, however, there is some character that may relate to increased moisture or inorganic salt content. In the center of the section, between 200 and 300 meters, the resistivity decreases. The values are similar to other waste disposal areas, such as the T-7 tile field. On the eastern end and directly over the waste trenches, the resistivity decreases substantially. Orthogonal and adjacent HRR lines show similar response for this area, which provides additional evidence for a vadose zone plume.

B1.1.25 High-Resolution Resistivity Line 7N

The results of HRR line 7N can be seen in Figure A-71. The location of this line with respect to the site boundaries and the other 26 lines can be seen in Figure A-46. Line 7N is oriented in an east-west direction, located 30 meters north of line 6N. The line crosses north-south lines 7E through 16E and cribs T-14, T-15, T-16, and T-17.

HRR line 7N shows a small conductive region at the bottom of the figure from 32 meters (150 meters above mean sea level) to 94 meters (136 meters above mean sea level). The area is highlighted by light blue and has resistivity values in the range of 150 to 170 ohm-meters. The bulk of the plot is resistive. Resistive features are delineated by the red/orange color representing apparent resistivity values from 310 to 450 ohm-meters. Highly resistive areas display apparent resistivity values from 500 ohm-meters to 1,400 ohm-meters.

B1.1.26 High-Resolution Resistivity Line 8N

The results of HRR line 8N can be seen in Figure A-72. The location of this line with respect to the site boundaries and the other 26 lines can be seen in Figure A-46. Line 8N is oriented in an

east-west direction, located 30 meters north of line 7N. The line crosses north-south lines 7E through 16E and cribs T-14, T-15, T-16, and T-17.

HRR line 8N shows an area with moderate resistivity at approximately 176 to 223 meters. It corresponds to the edge of crib T-17 and the railroad, and has values from 196 to 250 ohm-meters. While this area is only moderately conductive, it is bordered by two highly resistive regions. The regions extend from the west to 152 meters and from the east at 226 meters. Resistive features are delineated by the red/orange color representing apparent resistivity values from 310 to 450 ohm-meters. Highly resistive areas display apparent resistivity values from 500 to 1,400 ohm-meters.

B1.1.27 High-Resolution Resistivity Line 9N

The results of HRR line 9N can be seen in Figure A-73. The location of this line with respect to the site boundaries and the other 26 lines can be seen in Figure A-46. Line 9N is oriented in an east-west direction, located 30 meters north of line 8N.

HRR line 9N shows an area with moderate resistivity at approximately 175 to 223 meters corresponding to the railroad. It has values from 196 to 250 ohm-meters. While this area is only moderately conductive, it is bordered by two highly resistive regions. The regions extend from the west to 152 meters and from the east at 226 meters. Resistive features are delineated by the red/orange color representing apparent resistivity values from 310 to 450 ohm-meters. Highly resistive areas display apparent resistivity values from 500 to 1,400 ohm-meters.

Lines 8N and 9N mirror each other almost perfectly. Both lines contain a moderately resistive area at approximately 175 to 223 meters bound by two highly resistive areas. In contrast, the moderately resistive feature in line 8N is bound by crib T-17 and the railroad, whereas in line 9N, this feature is flanked to the east by the railroad. It is likely that the railroad is creating a conductive shadow within this section of the survey area.

B1.2 COMPILED HIGH-RESOLUTION RESISTIVITY CROSS SECTIONS

After processing each HRR line, the data were compiled into two-dimensional cross sections (horizontal slices) at coincident depths. A total of six cross sections were compiled, and their results are discussed below. Geostatistical analyses were employed to interpolate the missing resistivity data.

The same color scheme applied to the figures in Section B1.1 was applied to the cross sections: browns and reds represent high resistivity, and blues and purples represent low resistivities.

To create the contours of data, points were kriged over a grid of 3 by 3 meters. Before kriging, a variogram was created to show the statistical structure of the data, including the correlation length and variance. A variogram presents the variance of data pairs for each separation (lag).

Variogram analysis was conducted within Surfer8[1] that fit a variogram model heuristically to the experimental data set assuming no statistical anisotropy.

B1.2.1 Horizontal Slice at 190 Meters

Figure A-74 shows the results of all apparent resistivity data at a coincident elevation of 190 meters above mean sea level. Figure B-1 depicts the model and experimental variogram.

Figure B-1. Variogram of Modeled and Experimental High-Resolution Resistivity Data for 190 Meters.

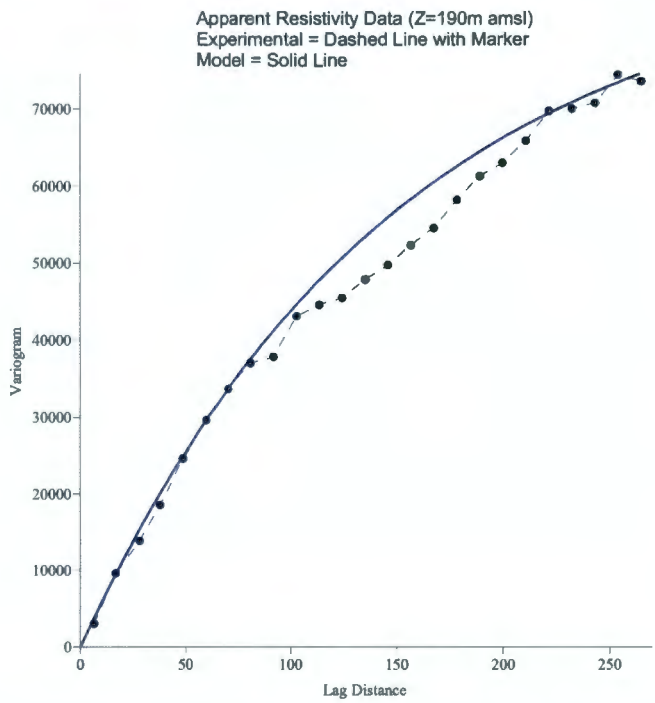

Figure A-74 shows the HRR data nearest the surface. It depicts a distribution of high resistivity values as orange to red colors on the outer edge of the site. The values in the central portion have lower resistivity and represent the background (i.e., 500 ohm-meters). The low resistivity values encompassed the area of the tank farm footprint shown in infrastructure maps. The low resistivity values may result from near surface inorganic waste or infrastructure related to the tank farm.

Several zones within the data show smaller than expected resistivity (indicated in colors other than brown). These include the areas over to the east and southeast, where no known disposal facility exists. Other anomalies, located to the west and northeast, coincide with known disposal facilities. A few of these low resistivity anomalies also appeared as anomalies in the electrical

[1] Surfer and Surfer8 are registered trademarks of Golden Software, Golden, Colorado.

conductivity plots from electromagnetic induction (EM) measurements in Figures A-21 through A-30.

B1.2.2 Horizontal Slice at 180 Meters

Figure A-75 shows the results of all apparent resistivity data at a coincident elevation of 180 meters above mean sea level. Figure B-2 shows the model and experimental variogram.

Figure B-2. Variogram of Modeled and Experimental High-Resolution Resistivity Data at 180 Meters.

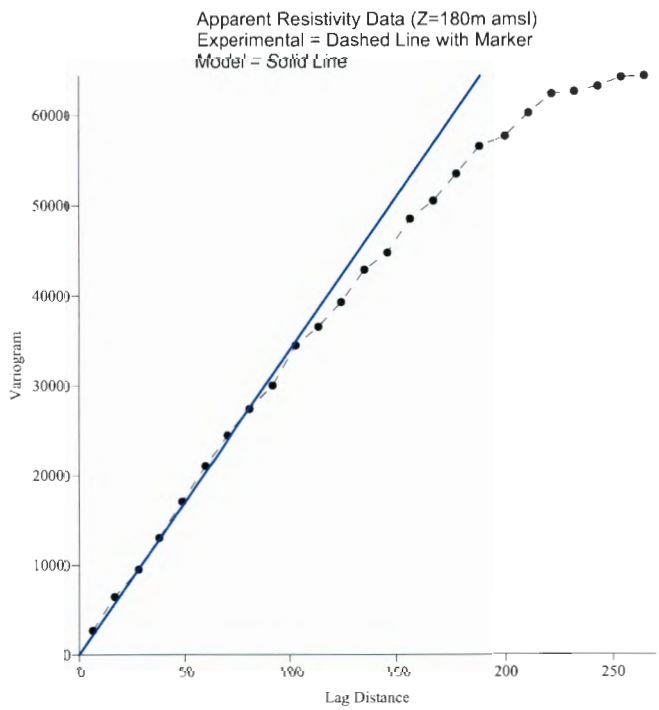

Figure A-75 shows high resistivity values as orange to red colors on the outer edge of the site. The values in the central portion have lower resistivity and represent the background (i.e., greater than 500 ohm-meters). The low resistivity values encompassed the area of the tank farm footprint shown in infrastructure maps. The low resistivity values may result from near surface inorganic waste or infrastructure related to the tank farm.

Several zones within the data show smaller than expected resistivity (indicated in colors other than brown). These include the areas over to the east and southeast, where no known disposal facility exists. Other anomalies, located to the west and northeast, coincide with known disposal facilities. A few of these low resistivity anomalies appeared also as anomalies on the electrical conductivity plots from EM measurements in Figures A-21 through A-30.

B1.2.3 Horizontal Slice at 168.5 Meters

Figure A-76 shows the results of all apparent resistivity data at a coincident elevation of 168.5 meters above mean sea level. Figure B-3 shows the model and experimental variogram.

Figure B-3. Variogram of Modeled and Experimental High-Resolution Resistivity Data at 168.5 Meters.

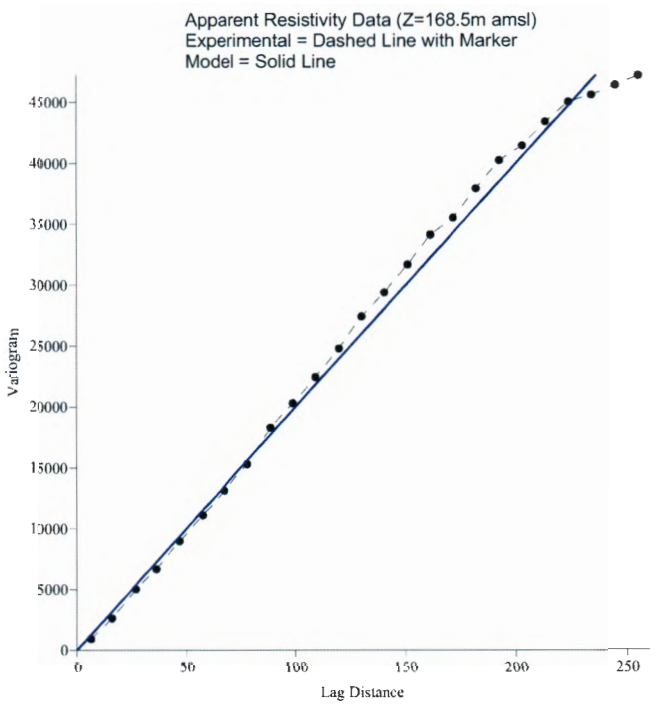

The HRR data of Figure A-76 shows that the apparent resistivity at 168.5 meters has become generally less resistive. The decrease in resistivity becomes most notably in the east and southeast portion of the survey site. Linear features extending from this region to outside the survey area would suggest the presence of pipelines. However, their large signature in the HRR data makes it impossible to determine if they have leaked. To address this limitation, the area was investigated using additional processing techniques, including three-dimensional surface resistivity inversion (Section 6.3.2) and well-to-well inversion (Section 6.3.3).

Other areas of interest in Figure A-76 include the waste disposal facilities outside the T tank farm fence. These include trenches T-14 through T-17 in the northeast and T-7, T-5, T-32, and T-36 to the west of the tank farm. These areas display characteristics consistent with possible waste migration beneath these facilities. The northeast trenches, for example, show T-16 and T-17 may have received more waste than T-14 and T-15. Additionally, areas around T-7 and T-32 show significant decreases in resistivity.

In addition to identifying areas possibly contaminated with waste, Figures A-74 through A-76 show areas free of waste. The absence of a plume appears as background apparent resistivity and is shown as a brown color. The data provide a high degree of confidence that these areas do not contain contamination in the upper vadose zone. Sampling could confirm the HRR results.

B1.2.4 Horizontal Slice at 161 Meters

Figure A-77 shows the results of all apparent resistivity data at a coincident elevation of 161 meters above mean sea level. Figure B-4 shows the model and experimental variogram.

Figure B-4. Variogram of Modeled and Experimental High-Resolution Resistivity Data at 161 Meters.

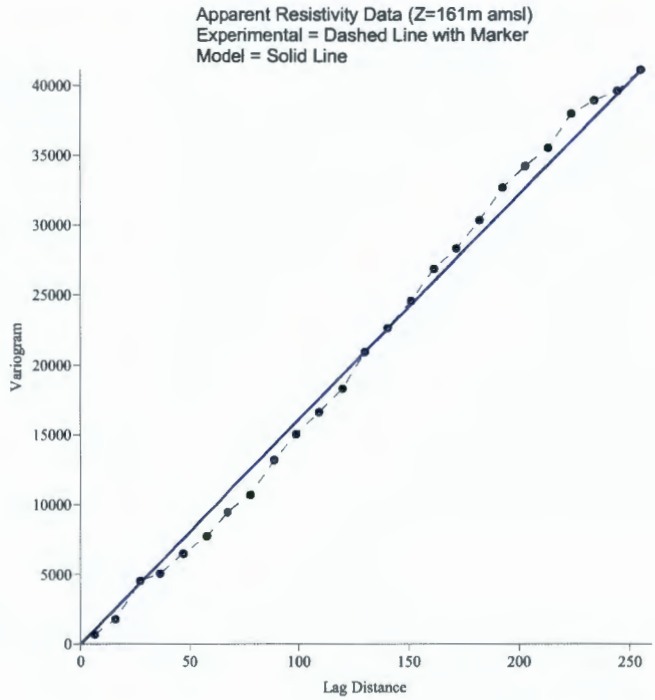

Figure A-77 shows many of the same features as Figure A-76. The central portion of the site, mainly within the T tank farm boundary and the southeastern portion, exhibits decreases in resistivity. Three possibilities could be causing this type of response in the HRR data. The first possibility is that the infrastructure including tanks, pipes, fences, wells, and other features could be saturating the signal by channeling the current. Current channeling causes short circuits making deep measurements appear more conductive than they actually are. The second possibility is that a large conductive plume, consisting of inorganic waste, has affected the resistivity of the soil causing the anomalous response. A plume this large does not fit the expected conceptual model based on previous leak/disposal events (RPP-23752, *Field Investigation Report for Waste Management Areas T and TX-TY*). The third possibility is a combination of the first two, causing the HRR data to be less resistive.

B1.2.5 Horizontal Slice at 156 Meters

Figure A-78 shows the results of all apparent resistivity data at a coincident elevation of 156 meters above mean sea level. Figure B-5 shows the model and experimental variogram.

Figure B-5. Variogram of Modeled and Experimental High-Resolution Resistivity Data at 156 Meters.

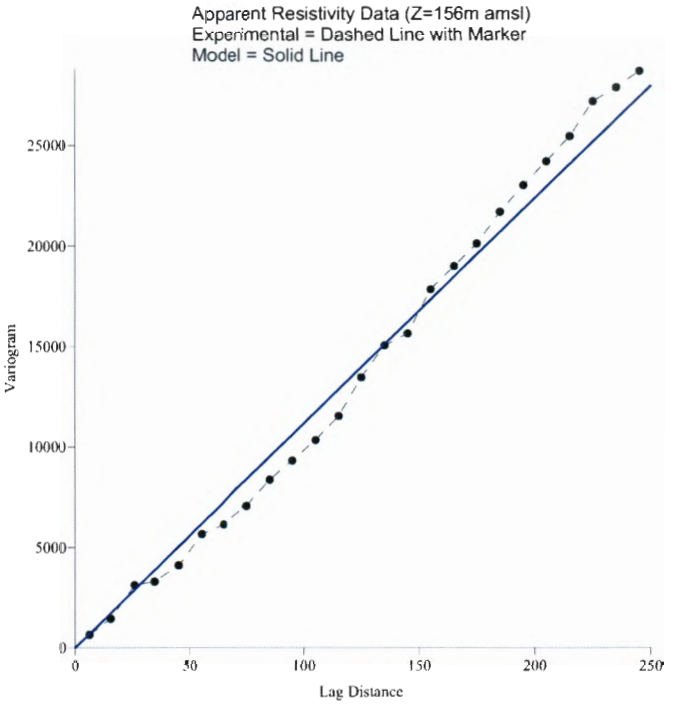

The conductive region identified in Figure A-77 appears to increase in size as the HRR data gets closer to the water table. The water table sits approximately 134 meters above mean sea level. From this point, HRR data cannot discriminate between infrastructure and plumes. Other processing methods presented in later sections of this report use inversion theory to calculate the distribution of electrical properties and provide additional visual clarity (Sections 6.3.2 and 6.3.3).

B1.2.6 Horizontal Slice at 152 Meters

Figure A-79 shows the results of all apparent resistivity data at a coincident elevation of 152 meters above mean sea level. Figure B-6 shows the model and experimental variogram.

Figure B-6. Variogram of Modeled and Experimental High-Resolution Resistivity Data at 152 Meters.

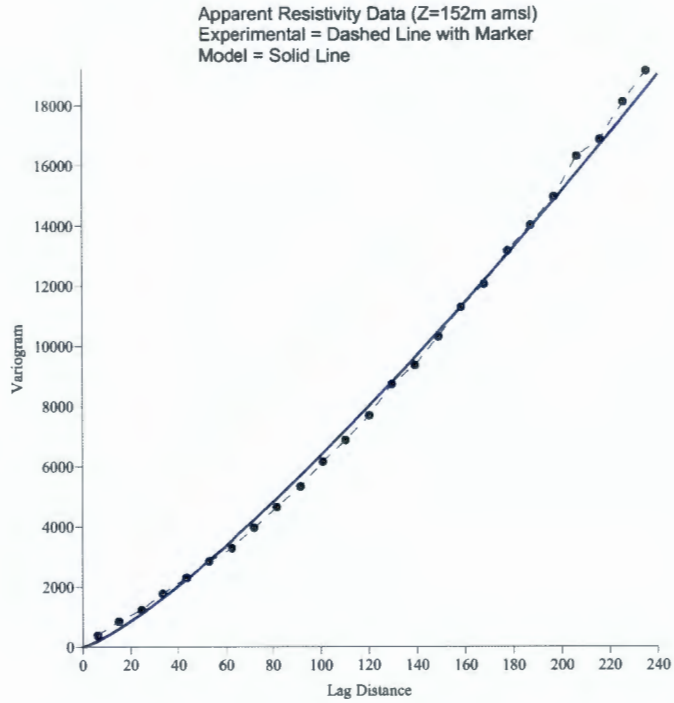

The HRR slice presented in Figure A-79 shows that the data are becoming less resistive. The maximum and median apparent resistivity for the 152 meter data set is much lower than the other slices. The decreased resistivity could be the result of water table influences. The apparent resistivity is affected by the water table at a much shallower depth than the actual location of the water table. This fact was explored in Appendix C, where the water table was modeled with HRR.

B1.3 QUASI-THREE-DIMENSIONAL HIGH-RESOLUTION RESISTIVITY MODEL

Figures A-80 and A-81 show three-dimensional rendering of the resistivity beneath the site. The modeled data appear as a solid mass with resistivity values less than 100 and 20 ohm-meters, respectively. The plot was interpolated in three dimensions using the compiled HRR data presented in Section B1.2. The RockWorks[2] program was used for interpolation. It employs an anisotropic inverse-distance weighting algorithm to interpolate the data.

The solid model renderings of HRR data in Figures A-80 and A-81 show a large conductive mass directly beneath the site. The 20 ohm-meters object in Figure A-81 shows that the conductive anomaly exists mostly around the tanks and to the southeast of the farm. The 100 ohm-meters object in Figure A-80 shows a much larger anomaly, which encompasses the waste trenches to the northeast and west of the T tank farm. It is difficult to separate a plume

[2] RockWorks is a registered trademark of RockWare, Inc., Golden, Colorado.

from infrastructure within these plots. However, HRR can define areas devoid of both infrastructure and plumes.

Volume estimates were produced for the conductive anomaly beneath the survey site. The volumes were computed by sorting the voxels (i.e., three-dimensional block representing an HRR data value) from the RockWorks interpolation file in ascending order and plotting against the total volume of voxels that represent that value or lower. Each voxel had a volume of 50 cubic meters. Figure B-7 shows the result of the volume plotting, which is similar to a cumulative distribution function. The bottom axis shows total voxel volume.

Figure B-7. Cumulative Distribution Function for High-Resolution Resistivity at the T Tank Farm.

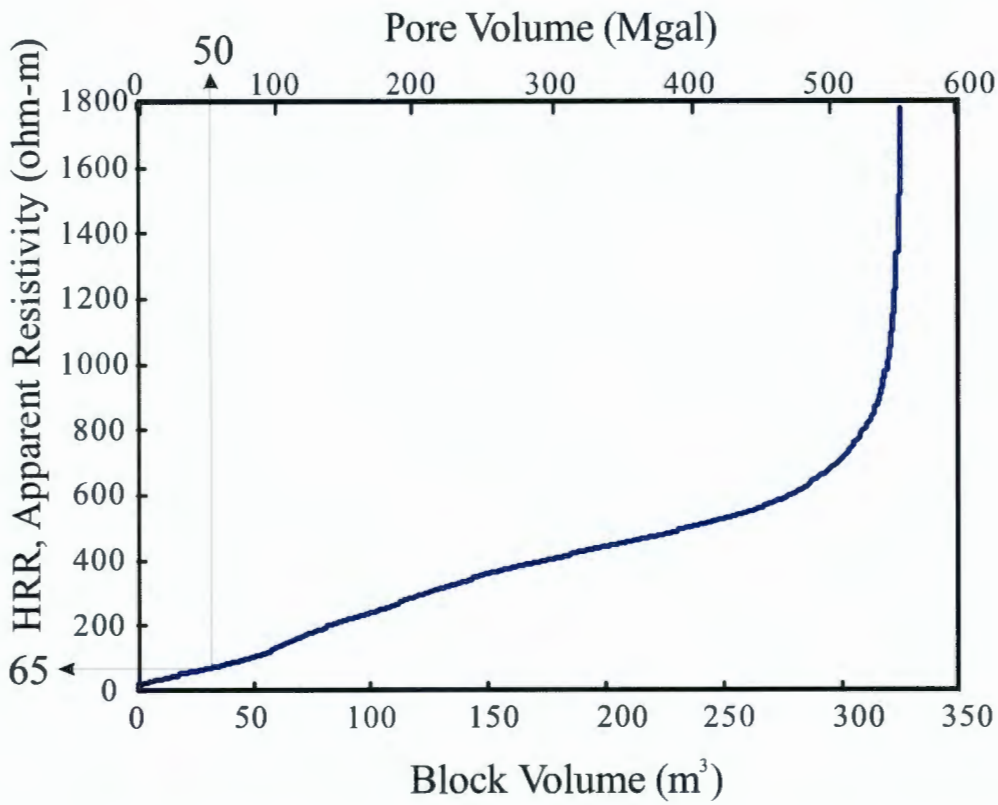

To read the plot, choose an HRR value, draw a line to the cumulative distribution function and down to the block volume axis. For example, the 100 ohm-meters HRR value presented in Figure A-80 has a volume of approximately 78 million cubic meters. The 20 ohm-meters value has a volume of 3.9 million cubic meters.

B1.4 TWO-DIMENSIONAL RESISTIVITY INVERSION OF HIGH-RESOLUTION RESISTIVITY DATA

Two-dimensional inversion of individual HRR data was accomplished with the software package EarthImager2D[3]. HRR data was imported into the program and inverted on a line-by-line basis. A total of 26 out of 27 lines of data were inverted. Line 8E was not inverted because of excessive noise in the data.

Inversion requires specification of a number of parameters. The code developers of EarthImager2D assisted with specification of these parameters. The modeling parameters for inversion include the starting model, the inversion scheme, *a priori* information, smoothing constraints, mesh refinement, and others. For the T tank farm resistivity data, parameters were tested for their ability to produce convergence and a hydrologically valid distribution.

Table B-2 lists the trials and models used in the inversion processes. Successful trials were those with the lowest root mean square (RMS) and L2 statistic. These statistics provided the basis for evaluating the performance of the model. For reference, the best RMS statistic has a value of less than three. Few trials produced an RMS statistic of less than three. Typically, each line typically required between 5 and 20 trials to identify the optimal parameters.

Appendix A, Figures A-82 through A-88, show the contoured results for each successful inversion. The same color file used for the HRR data was applied to the inversion results. Purples and blues represent low resistivity. Yellows and reds represent high resistivity.

Low resistivity can indicate a waste plume, infrastructure, or both. High resistivity indicates uncontaminated sand without infrastructure.

Figure A-82 shows lines 0E through 3E. Although the inverse models for these four lines converged to a low RMS and L2 statistic, the results do not appear to have hydrological validity. The area to the west of the tank farm has a moderate degree of infrastructure that includes several wells, pipes, fence, and roads. Although some of this information was incorporated into the inverse model, the results have an appearance unlike the expected subsurface conditions. Therefore, the two-dimensional inversion results for lines 0E through 3E do not provide a strong basis for making inferences about waste contaminant migration.

Figure A-83 shows the inversion results for lines 4E through 7E. These lines run north to south directly between tanks. The area has a dense network of pipes, tanks, and vaults that complicated the inversion process, and complicate the process of separating pipes and tanks from a plume or background sand. In general, all the lines show a very low resistive feature down to 100 meters below ground surface and beyond. The noise in the inversion results suggests the model does not display accurate subsurface features. The two-dimensional inversion results for lines 4E through 7E, therefore, do not provide a strong basis for making inferences about waste contaminant migration.

---

[3] EarthImager2D and EarthImager3D are trademarks of Advanced Geosciences, Inc., Austin, Texas.

Table B-2. Summary of Two-Dimensional Inversion Model Parameters and Statistics.

Line	File Name	Trial Number	Inversion Method	Starting Model	*A Priori* Information	Smoothing Level	Results L2	Results RMS
0E	0E-preproc-inv.stg	5	Smooth	Pseudosection	None	10	1.59	3.78
1E	1E-preproc-inv.stg	4	Smooth	Pseudosection	None	10	1.9	4.14
2E	2E-preproc-inv.stg	4	Smooth	Pseudosection	None	1	0.99	2.98
3E	3E-preproc-inv.stg	7	Smooth	Constant Value	Tanks	10	1.04	8.17
4E	4E-filt2-inv.stg	1	Smooth	Pseudosection	Pipes	10	15.98	12
5E	5E-filt2-inv.stg	1	Smooth	Pseudosection	Pipes	10	21.2	13.82
6E	6E-filt2-inv.stg	1	Smooth	Pseudosection	Pipes	10	70.47	25.21
7E	7E-filt2-inv.stg	1	Smooth	Pseudosection	Pipes	10	1.17	14.51
9E	9E-filt2-inv.stg	1	Smooth	Pseudosection	None	10	0.9	18.04
10E	10E-filt2-inv.stg	1	Smooth	Pseudosection	None	10	0.81	7.7
11E	11E-filt2-inv.stg	1	Smooth	Pseudosection	None	10	0.74	10.82
12E	12E-filt2-inv2.stg	4	Smooth	Pseudosection	none	1	0.7	13.5
13E	13E-filt2-inv.stg	1	Smooth	Pseudosection	None	10	0.87	10.84
14E	14E-preproc-inv.stg	1	Smooth	Pseudosection	None	10	0.83	8.04
15E	15E-filt-inv.stg	1	Smooth	Pseudosection	None	10	0.81	22.23
16E	16E-filt-inv.stg	1	Smooth	Pseudosection	None	10	0.76	13.86
0N	0N-preproc-inv.stg	1	Smooth	Pseudosection	none	10	0.94	12.42
1N	1N-preproc-inv.stg	5	Smooth	Pseudosection	none	1	3.2	12.96
2N	2N-preproc-inv.stg	1	Smooth	Pseudosection	Pipes	10	0.9	18.13
3N	3N-preproc-inv.stg	2	Smooth	Pseudosection	Pipes	10	0.8	15.96
4N	4N-preproc-inv.stg	3	Smooth	Constant Value	Tanks	1	3.71	15.42
5N	5n-preproc-inv2.stg	3	Smooth	Pseudosection	None	10	6.15	14.89
6N	6N-preproc-inv.stg	9	Robust	Constant Value	Tanks	10	0.81	5.41
7N	7N-filt-inv2.stg	1	Robust	Pseudosection	None	10	3.71	2.89
8N	8N-preproc-inv.stg	3	Smooth	Pseudosection	None	10	0.85	2.68
9N	9N-preproc-inv.stg	4	Smooth	Pseudosection	Water table	10	0.75	3.11

Note:
RMS = root mean square.

Figure A-84 shows the two-dimensional inversion results for lines 9E through 12E. These lines are located to the east of the tank farm. A dense network of pipes, tanks, and vaults complicated the inversion process. Line 9E suffers from many of the same limitations as Figure A-83 for lines 4E through 7E. The high RMS statistic confirms a poor fit between the model and the measured data.

Lines 10E through 12E appear more receptive to inversion. In general, these lines show a coherent degree of resistivity that is smooth in the central-north portion of the line (north = larger distance values along the line). This area is known for liquid waste disposal totaling approximately 1 million gallons. The southern portion of the line, however, shows complications in the resistivity inversion. This is likely caused by the density of pipes that carried fluids (e.g., tank waste, water, steam, sewer) to and from the T tank farm. The low resistivity values, that would otherwise indicate a plume, are likely noise from the inversion process. The two-dimensional inversion results for lines 9E through 12E, therefore, do not provide a strong basis for making inferences about waste contaminant migration.

Figure A-85 shows the two-dimensional inversion results for lines 13E through 16E. These lines run in the north-south direction and are located on the eastern boundary of the survey area. The inversion statistics, RMS and L2, show that the model has a poor fit to the data. The densely packed pipe network in the southeastern portion of the site likely accounts for the limitations of this model. However, similar to lines 10E through 12E in Figure A-84, the results to the north have more value than results for the south. The northern portions show a more cohesive resistivity distribution that may indicate a waste plume. In all, the two-dimensional inversion results for lines 13E through 16E do not provide a strong basis for making inferences about waste contaminant migration.

Figure A-86 shows the two-dimensional inversion results for lines 0N through 1N. These lines run in the west to east direction at the southern boundary of the site. The inversion statistics, RMS and L2, show that the inversion model does not have a good fit with the data. The densely packed pipe network in the southern and southeastern portion of the site has a deleterious effect on the model. The two-dimensional inversion results for lines 0N through 1N, therefore, do not provide a strong basis for making inferences about waste contaminant migration.

Figure A-87 shows the two-dimensional inversion results for lines 2N through 3N. These lines run in the west to east direction towards the southern boundary of the site. The inversion statistics, RMS and L2, show that the inversion model does not have a good fit with the data. The densely packed pipe network in the southern and southeastern portion of the site has a negative effect on the model results. The two-dimensional inversion results for lines 2N through 3N, therefore, do not provide a strong basis for making inferences about waste contaminant migration.

Figure A-88 shows the two-dimensional inversion results for lines 4N through 5N. These lines run in the west to east direction in the middle of the site. The inversion statistics, RMS and L2, show that the inversion model does not have a good fit with the data. The densely packed pipe network in the southern and southeastern portion of the site has a negative effect on the model results. The two-dimensional inversion results for lines 4N through 5N, therefore, do not provide a strong basis for making inferences about waste contaminant migration.

The inversion results from the last set of lines, 6N through 9N, appear in Figure A-89. The results from these lines are the best of any group presented thus far. Both inversion statistics, the RMS and L2, are quite low. The excellent convergence statistics are noticeable in the actual results. Line 6N, the first line north of the fence and a line completely free of infrastructure, shows two coherent low resistivity features. The first feature appears in the center of the plot and extends down to groundwater. The feature is quite large and its exact source is unknown. The second feature is to the east on the right hand side of the plot. This feature is much smaller and is well contained within the vadose zone. This region is coincident with the southern boundary of trenches T-14 through T-17, which received a combined total of 1 million gallons of discharge waste.

Lines 7N though 9N show results from directly over the trenches. Line 9N is immediately north of the trench boundary. A conductive feature between about 10 and 45 meters below ground surface is likely the result of a plume from historical disposal activities. The plume has a coherent shape and meets expectations for a hydrologically significant feature. Additionally, this feature appears in the north-south lines of 10E through 15E, confirming its existence and size. Of all the two-dimensional inversion results, lines 6N through 9N provide the strongest basis for inferring the presence and migration of a contaminant plume.

B2.0 SUPPLEMENTAL BACKGROUND SURVEY RESULTS

B2.1 IN-FARM ELECTROMAGNETIC INDUCTION

Appendix A presents 11 graphical depictions of the EM data. Both in-phase data and quadrature data were collected. Typically, in-phase data show magnetic susceptibility. Quadrature data show electrical conductivity. Both data types vary as a function of signal frequency, the vertical distance from the coils to the ground, coil orientation (horizontal or vertical), and coil separation. Figures A-10 through A-14 show the contours of the in-phase data for the frequencies of 5, 7.5, 10, 15, and 20 kilohertz, respectively.

The in-farm, in-phase EM data in Figures A-10 through A-14 graphically depict results after processing and reduction as described in Appendix C. The data were kriged on a 2-meter square grid. The kriging semi-variogram was linear. Arithmetic averaging was used for multiple data points within the interpolated grid. Table B-3 provides the summary statistics for each frequency (i.e., minimum, maximum, median, and standard deviation) for Figures A-1 through A-5.

Table B-3. Summary Statistics for In-Phase Electromagnetic Induction Data.

Figure	A-10	A-11	A-12	A-13	A-14
Frequency	5 kHz	7.5 kHz	10 kHz	15 kHz	20 kHz
Data count	34,882	34,882	34,882	34,882	34,882
Minimum (ppm)	-8,406	-8,456	-7,449	-6,668	-6,195
Median (ppm)	1,560	1,716	1,823	1,979	2,192
Maximum (ppm)	38,453	38,408	35,853	35,649	36,132
Standard deviation (ppm)	5,252	5,459	5,454	5,354	5,426

Notes:
kHz = kilohertz.
ppm = parts per million.

Data for all frequencies exhibit the same characteristics. The color ranges in Figures A-10 through A-14 depict changes in the data values. White areas show areas with no data coverage. The saturated brown color shows areas with high magnetic susceptibility and value ranges from 9,600 to 14,720 parts per million. Red, orange, and yellow hues show areas of moderate magnetic susceptibility and value ranges from 1,900 to 8,960 parts per million. Blues and violets show data from 0 to 1,920 parts per million, represent the statistical median, form the bulk of the background data, and show slight capacity for magnetic susceptibility. The pronounced contrast between characteristics demonstrates that localized features are anthropogenic and do not represent large-scale geologic phenomena.

Plans of T tank farm show many subsurface structures. Steel drains, sewer lines, stainless steel pipes, wells, concrete platforms, and the tanks show up as in-phase responsive, localized features. In-phase data show the 12 large tanks in the T tank farm as circular saturated dark brown color (i.e., 10,240 to 14,720 parts per million). In addition, the data show a large pipe trench running through the northeastern portions of the tank farm between tanks T-101 and T-104, and tanks T-102 and T-105. The pipe trench produces the same response as the tanks. This brown response indicates reinforced concrete containing steel rebar and steel pipes.

Many of the linear structures on existing maps and in the EM figures run congruently, in close proximity, or overlap creating a large bulk response. Infrastructure such as electrical conduit and steel pipe create a saturated yellow appearance (i.e., 1,920 to 2,560 parts per million) that encircles each tank and forms linear features that extend to other structures associated with the tanks. The data show an anomaly in the southeastern corner of T tank farm. A cluster of pipes in this area creates a large localized magnetic response that accounts for the anomaly. Three linear structures project outward from the pipe cluster/anomaly. Their linear arrangement matches the steel pipes found on existing infrastructure maps. The faint north to south linear anomaly that bisects the far eastern portion of the tank farm is consistent with the location of the 4-inch service waterline.

The data show little response for the monitoring wells because the sensor was not sited directly over the location of the wells. Lastly, the chain link fence around the site likely accounts for the visible edge effects, rather than buried features.

B2.2 IN-FARM ELECTRICAL CONDUCTIVITY

Figures A-15 through A-19 in Appendix A show the contours of frequency-dependent electrical conductivity data at 5, 7.5, 10, 15, and 20 kilohertz, respectively. Figure A-20 shows the total electrical conductivity plot. The data were obtained through inversion using quadrature data (Huang and Won 2000, "Conductivity and Susceptibility Mapping Using Broadband Electromagnetic Sensors"). The quadrature data are the real component of the complex quantity that relates the secondary magnetic field normalized to the primary field. Unlike magnetic and electromagnetic in-phase data, changes in soil moisture, salt deposits, and additions of ferrous and non-ferrous metals can produce anomalous responses in electrical conductivity.

The data were kriged on a 2-meter square grid. The kriging semi-variogram was linear. Arithmetic averaging was used for multiple data points within the interpolated grid. Table B-4 provides the summary statistics for each frequency (i.e., minimum, maximum, median, and standard deviation) associated with Figures A-15 through A-20.

Table B-4. Summary Statistics for Electrical Conductivity Data.

Figure	A-15	A-16	A-17	A-18	A-19	A-20
Frequency	5 kHz	7.5 kHz	10 kHz	15 kHz	20 kHz	Total
Violet bracket (min to max)	0 to 24	0 to24	0 to 37	0 to 37	0 to 25	0 to 25
Data count	34,833	34,833	34,833	34,833	34,833	34,833
Minimum (mS/m)	0	0	0	0	0	0
Median (mS/m)	32.7	20.4	16.5	15.1	13.9	19.6
Maximum (mS/m)	2,668.5	2,008.9	1,373.7	842.9	572.1	1068.8
Standard deviation (mS/m)	301	218	154	97	69	136

Notes:
kHz = kilohertz.
min = minimum.
max = maximum.
mS/m = millisiemens per meter.

The figures show color changes corresponding to changes in electrical conductivity. The saturated brown to red color indicates high electrical conductivity and prominent features. Orange and yellow hues are nearly absent from the figures. The median violet colors form the background. The lower values may represent the true background electrical conductivity of the existing soil. White areas show areas with no data coverage. The contrast demonstrates that color variations relate to anthropogenic structures and do not represent large-scale geologic phenomena.

The data show little response for the monitoring wells because the sensor was not sited directly over the well locations. Lastly, the chain link fence around the perimeter of the site likely accounts for the visible edge effect, rather than buried features.

B2.2.1 Electrical Conductivity at 5 kilohertz

Figure A-15 shows electrical conductivity data at 5 kilohertz after processing and reduction as described in Appendix C.

Figure A-15 depicts the pronounced features of the tanks in T tank farm and the associated infrastructure at 5 kilohertz. These areas show a wide range of electrical conductivity response due to variability in the feature and their depth. Plans of T tank farm show a wide variety of subsurface structures. Steel drains, sewer lines, stainless steel pipes, wells, concrete platforms, and the tanks all produce an electrical conductivity response. However, similar features may not produce the same response. For example, tanks T-101 through T-105 have a similar medium brown hue near the center of each tank. Tanks T-106 through T-112 do not appear as conductive. Electromagnetic coupling influenced by the geometric relationship between the transmitter loop, the receiver loop, and the earth and other objects may account for the differences. Depending on the geometric relationship, the same target may produce a strong or

weak response. Other features appear linear and are likely buried networks of pipelines and electrical lines.

In addition to the tanks, a large pipe trench runs through the northeastern portions of the tank farm between tanks T-101 through T-104, and tanks T-102 through T-105. The pipeline has a similar response to the tanks, suggesting both structures are constructed from similar materials.

Many of the linear structures on existing drawings, and in the electrical conductivity figures, run congruently, in close proximity, or overlap creating a bulk response. Infrastructure such as electrical conduit, steel pipe, and an electrical trench create a dark violet appearance in the range of 20 to 50 millisiemens per meter. This infrastructure forms linear features leading to the tanks. An anomaly within the southeastern corner of T tank farm indicates the presence of a cluster of pipes showing a large, localized, electrically conductive response.

B2.2.2 Electrical Conductivity at 7.5 kilohertz

Figure A-16 shows electrical conductivity data at 7.5 kilohertz after processing and reduction as described in Appendix C.

Figures A-15 and A-16 have similar color, contrast, and detail. The features in Figure A-16 depict the T tank farm tanks and associated infrastructure, as well as steel drains, sewer lines, stainless steel pipes, wells, and concrete platforms. Historical plans of T tank farm show a variety of subsurface structures (both linear and nonlinear). Many of the subsurface structures display a definite electrical conductive response. However, similar features may not produce the same response. For example, tanks T-101 through T-105 have a similar medium brown hue near the center of each tank. Tanks T-106 through T-112 do not appear as conductive.
The orientation of the GEM-2[4] in relation to the tank surface structures likely accounts for the difference. Other features appear linear and are likely buried networks of pipelines and electrical lines.

In addition to the tanks, a large pipe trench runs through the northeastern portions of the tank farm between tanks T-101 through T-104, and tanks T-102 through T-105. The pipeline has a similar response to the tanks, suggesting both structures are constructed from similar materials.

Many of the linear structures on existing drawings, and in the electrical conductivity figures, run congruently, in close proximity, or overlap creating a bulk response. Infrastructure such as electrical conduit, steel pipe, and an electrical trench create a dark violet appearance in the range of 20 to 50 millisiemens per meter. This infrastructure forms linear features leading to the tanks. An anomaly within the southeastern corner of T tank farm indicates the presence of a cluster of pipes showing a large, localized, electrically conductive response.

---

[4] GEM and GEM-2 are registered trademarks of Geophex, Ltd., Raleigh, North Carolina.

B2.2.3 Electrical Conductivity at 10 kilohertz

Figure A-17 shows electrical conductivity data at 10 kilohertz after processing and reduction as described in Appendix C.

Figure A-17 shows more contract than Figures A-15 and A-16. Figure A-15 depicts the pronounced features of the tanks in T tank farm and the associated infrastructure. Steel drains, sewer lines, stainless steel pipes, wells, concrete platforms, and the tanks all produce an electrical conductivity response. At 10 kilohertz, the tanks show approximately the same response. For example, all tanks have a medium brown hue near the center in the range of 200 to 900 millisiemens per meter. A high gradient marks the transition from the tanks to background over a short distance.

In addition to the tanks, a large pipe trench runs through the northeastern portions of the tank farm between tanks T-101 through T-104, and tanks T-102 through T-105. The pipeline has a similar response to the tanks, suggesting both structures are constructed from similar materials.

Many of the linear structures on existing drawings, and in the electrical conductivity figures, run congruently, in close proximity, or overlap creating a bulk response. Infrastructure such as electrical conduit, steel pipe, and an electrical trench create a dark violet appearance in the range of 20 to 50 millisiemens per meter. This infrastructure forms linear features leading to the tanks. An anomaly within the southeastern corner of T tank farm indicates the presence of a cluster of pipes showing a large, localized, electrically conductive response.

B2.2.4 Electrical Conductivity at 15 kilohertz

Figure A-18 shows electrical conductivity data at 15 kilohertz after processing and reduction as described in Appendix C.

At 15 kilohertz, Figure A-18 shows more punctuated gradients than at lower frequencies, and a stronger response to subsurface structures. The T tank farm tanks, steel drains, sewer lines, stainless steel pipes, wells, and concrete platforms all show a color shift toward dark blue at 36 millisiemens per meter. At 15 kilohertz, the tanks show variable characteristics. For example, the center of each tank ranges from 180 to 832 millisiemens per meter.

In addition to the tanks, a large pipe trench runs through the northeastern portions of the tank farm between tanks T-101 through T-104, and tanks T-102 through T-105. The pipeline has a similar response to the tanks, suggesting both structures are constructed from similar materials.

Many of the linear structures on existing drawings, and in the electrical conductivity figures, run congruently, in close proximity, or overlap creating a bulk response. Infrastructure such as electrical conduit, steel pipe, and an electrical trench create a dark violet appearance in the range of 20 to 50 millisiemens per meter. This infrastructure forms linear features leading to the tanks. An anomaly within the southeastern corner of T tank farm indicates the presence of a cluster of pipes showing a large, localized, electrically conductive response.

B2.2.5 Electrical Conductivity at 20 kilohertz

Figure A-19 shows electrical conductivity data at 20 kilohertz after processing and reduction as described in Appendix C.

A large pipe trench runs through the northeastern portions of the tank farm between tanks T-101 through T-104, and tanks T-102 through T-105. The pipeline has a similar response to the tanks, suggesting both structures are constructed from similar materials.

Many of the linear structures on existing drawings, and in the electrical conductivity figures, run congruently, in close proximity, or overlap creating a bulk response. Infrastructure such as electrical conduit, steel pipe, and an electrical trench create a dark violet appearance in the range of 10 to 25 millisiemens per meter. This infrastructure forms linear features leading to the tanks. An anomaly within the southeastern corner of T tank farm indicates the presence of a cluster of pipes showing a large, localized, electrically conductive response.

B2.2.6 Total Electrical Conductivity

Figure A-20 depicts a total electrical conductivity contour plot for all of the electrical conductivity data. Total electrical conductivity is calculated by arithmetically averaging the data for each frequency.

Figure A-20 shows several pronounced features that contrast with the median electrical conductivity value (light purple). The median violet color brackets the values from 0 to 8 millisiemens per meter, and a solid line contour is located at 0 millisiemens per meter. The lower values, represented by the color violet (0 to 4 millisiemens per meter), may represent the true background electrical conductivity of the existing soil.

The tanks, buried pipe, and other structures in the T tank farm likely account for many of the pronounced features. The areas immediately in the vicinity of the tanks show a range of conductivity from 80 millisiemens per meter (purple) to approximately 1,800 millisiemens per meter (medium brown). These areas show a wide range of electrical conductivity response due to variability in the feature and their depth. Plans of T tank farm show a wide variety of subsurface structures. Steel drains, sewer lines, stainless steel pipes, wells, concrete platforms, and the tanks all produce an electrical conductivity response. Linear features likely represent a buried network of pipelines. Figure A-20 explicitly outlines pipes inferred in Figures A-15 through A-20.

B2.3 MAGNETOMETRY

B2.3.1 In-Farm Magnetic Survey

Appendix A contains four figures (Figures A-1 through A-4) that visually depict the results of in-farm magnetic surveys after data processing and reduction as described in Appendix C. The figures show coverage maps and color contour maps of the residual total magnetic field recorded by the top sensor at 2 meters above ground.

Figure A-1 shows in-farm coverage as blue dots. The dots correspond to GPS locations recorded during the surveys. Because magnetic data was recorded more frequently than GPS coordinates, the position of the magnetic data points was inferred using linear interpolation.

Table B-5 summarizes the statistics for the in-farm magnetic data. The data were kriged on a 2-meter square grid with a total of 76,472 grid nodes. The semi-variogram used for the kriging algorithm was linear. Arithmetic averaging was used for multiple data points within the interpolated grids.

Table B-5. Summary Statistics for In-Farm Magnetic Data.

Statistic	Total Field Magnetics	Magnetic Gradient
Data count	65,535	65,535
Minimum value (nT or nT/m)	-26,573	-9,132
Median value (nT or nT/m)	-848	187
Maximum value (nT or nT/m)	29,664	12,225
Standard deviation (nT or nT/m)	3,825	1,114

Notes:
nT = nanotesla.
nT/m = nanotesla per meter.

Often, the total magnetic field masks separate magnetic features as pipes, tanks, or other near surface infrastructure. The wells, which are closer to the surface or rise above the ground, generally have the largest response. The tanks have the next highest response, and appear as large structures. Pipes in the vicinity of the wells do not appear in the data. The dipolar nature of the magnetic data, typical of the declination of the Earth's magnetic field, has lower values to the northeast of each tank and higher to the southwest.

The vertical magnetic gradient in Figure A-3 shows the difference between the magnetic field of the bottom sensor and the top sensor, divided by the separation distance of 1 meter. This calculation provides a tool for mapping pipe locations. Features closer to the surface (e.g., pipes) stand out prominently compared to deep objects (e.g., tanks). Figure A-4 shows an interpretation map of pipeline locations using the gradient map. This data is used to constrain the HRR and resistivity inversion data discussed in Sections 6.2 and 6.3.

B2.3.2 Ex-Farm Magnetic Results

Appendix A contains five figures (Figures A-5 through A-9) that visually depict ex-farm magnetic survey results. Table B-6 summarizes the statistics for the ex-farm magnetic data.

Table B-6. Summary Statistics for Ex-Farm Magnetic Data.

Statistic	Total Field Magnetics	Magnetic Gradient
Data count	65,535	65,535
Minimum value (nT or nT/m)	-9,793	-6773
Median value (nT or nT/m)	-139	71
Maximum value (nT or nT/m)	18,323	8,292
Standard deviation (nT or nT/m)	571	272

Notes:
nT = nanotesla.
nT/m = nanotesla per meter.

Figure A-5 shows ex-farm coverage as blue dots in roughly parallel survey lines. Blank areas indicate no coverage due to railways, structures, cordoned off areas, or heavily traveled roadways.

Figure A-6 shows single sensor, contoured total magnetic field data with the diurnal corrections and processing as described in Appendix C. This plot shows several pronounced monopolar and dipolar magnetic anomalies that stand out against the yellow background. The yellow hues show areas relatively clear of ferrous objects. The yellow background color brackets the values from -507 to -130 nanoteslas. Localized features, not regional geologic features or conditions, account for noticeable anomalies.

Localized monopolar features appear as an extreme positive response in the total magnetic field. Ferrous metallic objects that extend deep into the subsurface account for these responses. These responses usually correlate to the plotted drywell casings. For example, several drywells appear in the southwestern portion of the figure within the T-7 tile field area.

A chain link fence causes a low magnetic response in the T tank farm western, eastern, and northern perimeter. Lateral lows that progress outwards from the northern fence may be caused by nearby vehicles and associated site staging equipment.

Within the 207-T retention basin, located in the east central portion of the plot, rectangular dipolar magnetic signatures exist. These responses probably represent reinforced concrete and an associated piping network on top of, and leading away from, the basin.

Near, and surrounding the T-14 to T-17 cribs, a few localized magnetic anomalies exist. These are caused by small ferrous debris or possible basalt boulders, or simply noise in the data. No major magnetic responses are indicated within this crib area indicating the absence of metallic debris. The area west of the access road and east of the T-36 trench is filled with

magnetic anomalies that mask over one another. This may be caused by infrastructure density, ferrous scrap, or basalt boulders.

Figure A-6 shows several distinct linear anomalous features that indicate ferrous metallic pipelines. These linear features have various orientations.

The contoured vertical gradient magnetic data (top sensor response subtracted from the bottom sensor response) are presented as Figure A-8. As with the total field data, the vertical gradient data indicate several pronounced monopolar and dipolar magnetic gradient anomalies that stand out against the background (yellow). The yellow background color brackets values from -104 nanoteslas per meter to 121 nanoteslas per meter. The anomalies represent localized features and not large-scale geologic phenomena.

The well casings cause localized dipolar or monopolar responses. The response depends on sensor to well casing geometry and proximity. The gradient responses associated with the 207-T retention basin are more localized and rectangular in appearance, suggesting that the basin has some type of reinforcement. The area west of the access road and east of the T-36 trench is saturated by gradient responses. This may be caused by infrastructure density, ferrous scrap, or basalt boulders.

As with the total field results, the vertical gradient magnetic results in Figure A-8 show several distinct linear responses that indicate ferrous metallic pipelines. These linear features have different orientations.

Many of the linear ferrous responses in Figures A-7 and A-9 are likely buried steel pipelines. The vertical gradient and total field magnetic results were used in order to interpret buried pipelines. To better visually reference pipelines with report text, the interpreted utilities are labeled numerically. Overall, 10 steel pipelines are interpreted to exist outside of the main T tank farm installation.

The railroad spur in Figures A-7 and A-9 appears as a north-south oriented response along the western edge of the surveyed area. This response is caused by a sand covered railroad spur that comes into the T tank farm area from the north. Sporadic lengths of the railroad spur are exposed at surface.

A linear magnetic response oriented north-south in the northeastern portion of the plot, appears to emanate from the northwest-southeast oriented railroad line and continues past the northern mapped boundary. This response is interpreted as a large diameter pipeline and is labeled as "1" on the figures.

Two ferrous pipelines emanate from the eastern side of the 207-T retention basin. These are oriented northeast-southwest for most of their route. One of these pipelines (labeled as "2" on the figures) appears to cross underneath 23rd Street and continue past the surveyed area. The other, labeled as "3," appears to terminate at the northern edge of the asphalt. This pipeline response is identified as "4" on the plots.

Two east-west oriented pipelines are south of 23rd Street. One is located immediately south of the road and is referenced on the figures as "5." The other is located approximately 20 meters

south of the roadway, and is labeled as "6." Both pipelines appear to continue past the north-south oriented access road. Pipeline 5 appears to turn north at approximately 566770E. Pipeline 6 intercepts the T-36 trench, terminating at approximately 566740E. A possible pipeline emanates from the western edge of the T-36 trench (labeled as "7"). It has a north-south orientation at 566660E. A nearby response associated with a drywell at the northwest corner of the T-36 trench partially masks the linear response, making interpretation of this pipeline suspect.

Two steel pipelines come into the southwestern survey area at approximately 566980E and 136550N, and continue northwest towards 23rd Street. These pipeline responses are collectively labeled as "8" on the figures.

Identified as "9" on the figures, the longest and one of the most discernible buried pipeline anomalies begins at the southwestern survey area (566580E, 136575N), crosses 23rd Street, and continues northwards the western T tank farm fence. At the northwestern fence corner, the pipeline bears eastwards. It intercepts the mobile field office, continues in a northeastern orientation past the T-4-1/T-4-2 ditch, turns south at approximately 56880E, and terminates at a fenced off area located at the northeastern fence corner.

B2.4 EX-FARM ELECTROMAGNETIC INDUCTION

B2.4.1 In-Phase Electromagnetic Induction

Appendix A contains 11 figures (Figures A-21 through A-31) representing the EM measurements taken outside the T tank farm fence. Both in-phase and quadrature data were collected.

Figures A-21 through A-25 show the contours of the in-phase data for the frequencies of 5, 7.5, 10, 15, and 20 kilohertz, respectively. Table B-7 provides the summary statistics for the 5 kilohertz data.

Table B-7. Summary Statistics for Ex-Farm, In-Phase Electromagnetic Induction Data.

Statistic	5 kilohertz	7.5 kilohertz	10 kilohertz	15 kilohertz	20 kilohertz
Figure	**A-21**	**A-22**	**A-23**	**A-24**	**A-25**
Data count	43,033	43,033	43,033	43,033	43,033
Minimum (ppm)	-2,804	-2,795	-2,882	-2,970	-2,912
Median (ppm)	1,347	1,419	1,473	1,559	1,713
Maximum (ppm)	16,931	16,897	16,885	16,866	16,845
Standard deviation (ppm)	1,666	1,690	1,700	1,706	1,710

Notes:
ppm = parts per million.

The data were contoured to show the spatial representation of relevant subsurface features. The data were kriged on a 2-meter square grid. The kriging semi-variogram was linear. Arithmetic averaging was used for multiple data points within the interpolated grid.

Colors in the figure represent changes in the data values. Midrange hues diverge toward contrasting colors to indicate high and low data extremes. White areas represent areas of no data coverage. The saturated brown color indicates high magnetic susceptibility. The orange and yellow colors represent moderate magnetic susceptibility. The saturated green hue represents the background. Blues and violets represent the slightest magnetic susceptibility. The pronounced contrast and morphology between distinctive characteristics demonstrate that localized features are tank farm infrastructure related and do not represent any large-scale geologic phenomena.

The figures show sporadic in-phase responses over the entirety of the site. These responses are likely noise due to subtle differences within the soil, and the limitations of the survey instrument. Additionally, the monitoring wells produce little response because the sensor was not placed directly over top of their locations.

B2.4.2 In-Phase 5 kilohertz

The in-phase, ex-farm data at 5 kilohertz were processed and reduced according to the description in Appendix C.

Several key features are identified from the in-phase magnetic data shown in Figure A-21. A faint blue anomaly, at approximately 1,200 parts per million, appears in and between cribs 216-T-14 and 216-T-15. The 207-T retention basin appears as an obvious dark brown rectangular object located south of cribs 216-T-15 and 216-T-14, and east of the T tank farm fence. The 207-T retention basin was concrete lined and constructed from reinforced concrete. It has a high response of 3,000 parts per million and 7,000 parts per million. Anomalies located between the T tank farm fence and the 207-T retention basin, and north of T tank farm, all show the same dark brown color and response (i.e., 3,000 parts per million to 7,000 parts per million).

It is likely that these objects are constructed using the same materials, concrete reinforced with steel rebar. Linear features delineated by yellow highlights in the southeast corner of the figure show an in-phase response between 1,550 parts per million and 1,420 parts per million. This response likely corresponds to sewer lines and pipelines going to and from the 207-T retention basin and T tank farm.

A linear anomaly appears to follow Camden Road north, turn west along 23rd Street, then turn north into T tank farm. This linear arrangement coincides with an electrical trench detailed in historical site documents.

B2.4.3 In-Phase 7.5 kilohertz

The data in Figure A-22 were processed and reduced according to the description in Appendix C.

Figure A-22 shows several key features. A saturated light blue anomaly, at approximately 1,300 parts per million, appears within and between cribs 216-T-14 and 216-T-15. The 207-T retention basin appears as an obvious dark brown rectangular object located south of cribs 216-T-15 and 216-T-14, and east of the T tank farm fence. The 207-T retention basin is concrete lined and constructed out of reinforced concrete. It has a high response of 2,600 parts per million to 5,000 parts per million. Anomalies located between the T tank farm fence and the 207-T retention basin, and north of T tank farm, all appear as the same dark brown color (i.e., 2,600 parts per million to 5,000 parts per million). It is likely that these objects are constructed using the same material; concrete reinforced with steel rebar. Figure A-22 shows a larger response than Figure A-21 (i.e., 5 kilohertz).

Linear features with yellow highlights appear in the southeast corner of Figure A-22. These features display an in-phase response between 1,600 parts per million and 1,800 parts per million. This response likely corresponds to sewer lines and pipelines going to and from 207-T retention basin and T tank farm. Another linear anomaly appears to follow Camden Road north, turn west along 23rd Street, then turn north into T tank farm. This linear arrangement coincides with an electrical trench detailed in historical site documents. Three anomalies appear in the west portion of the figure. Two of the anomalies run diagonally in the top northwest corner, and one runs along the far west side oriented north-south. They have responses of 1,180 to 2,200 parts per million, and may represent subsurface electrical lines.

B2.4.4 In-Phase 10 kilohertz

The data in Figure A-23 were processed and reduced according to the description in Appendix C.

Key features in Figure A-23 include a pronounced light blue anomaly at approximately 1,300 parts per million within and between cribs 216-T-14 and 216-T-15. The 207-T retention basin appears as the obvious dark brown rectangular object located south of cribs 216-T-15 and 216-T-14, and east of the T tank farm fence. The 207-T retention basin is concrete lined and constructed out of reinforced concrete. It has a high response of 2,600 parts per million to

5,000 parts per million. Anomalies located between the T tank farm fence and the 207-T retention basin and north of T tank farm all show the same dark brown color and responses between 2,600 parts per million to 5,000 parts per million. It is likely that these objects are constructed using the same material, concrete reinforced with steel rebar. Compared to the 5 and 7.5 kilohertz in-phase data, Figure A-23 shows the anomalies more clearly because it mutes background noise.

Linear features, bracketed by yellow and highlighted by orange, in the southeast corner of Figure A-23 have responses between 1,550 parts per million and 1,800 parts per million. This response likely corresponds to sewer lines and pipelines going to and from 207-T retention basin and T tank farm. Another linear anomaly follow Camden Road north, turns west along 23rd Street, then turns north into T tank farm. This arrangement coincides with an electrical trench detailed in historical site documents. There are three violet features in the western portion of the figure. Two run diagonally in the top northwest corner, and one linear response runs along the far west side oriented north-south. They have responses of 800 to 1,400 parts per million and may represent subsurface electrical lines.

B2.4.5 In-Phase 15 kilohertz

The data in Figure A-24 were processed and reduced according to the description in Appendix C.

Figure A-24 shows a dramatic shift in background color and response. The background color shifts from predominately yellow at 1,500 parts per million to predominately light blue at 1,600 parts per million. This effect creates high contrast between the background and features. Within and between cribs 216-T-14 and 216-T-15 a dark blue feature appears at approximately 1,300 parts per million. The 207-T retention basin appears as an obvious dark brown rectangular object located south of cribs 216-T-15 and 216-T-14, and east of the T tank farm fence. The 207-T retention basin is concrete lined and constructed out of reinforced concrete. It has a high response of 3,100 parts per million to 5,000 parts per million. Anomalies located between the T tank farm fence and the 207-T retention basin and north of T tank farm all show the same dark brown color and response of 3,100 parts per million to 5,000 parts per million. It is likely that these objects are constructed using the same material, concrete reinforced with steel rebar. Compared to Figures A-21 through A-23, the data in Figure A-24 shows a high contrast and more detailed response.

Linear features, bracketed by light blue and highlighted by yellow and orange, are located in the southeast corner of Figure A-24, with responses between 1,800 parts per million and 2,100 parts per million. This response likely represents sewer lines and pipelines going to and from 207-T retention basin and T tank farm. Another linear anomaly follows Camden Road north, turns west along 23rd Street, then turns again north into T tank farm. This arrangement fits nicely with an electrical trench detailed in historical site documents. There are three violet features in the western portion of the figure; two running diagonally in the top northwest corner and one along the far west side oriented north-south. Their response is 300 to 1,200 parts per million and may represent subsurface electrical lines.

B2.4.6 In-Phase 20 kilohertz

The data in Figure A-25 were processed and reduced according to the description in Appendix C.

Figure A-25 shows more background colors and fewer anomalies. The background color shifts to predominately yellow at 1,740 parts per million, punctuated by green and light blue noise at approximately 1,600 parts per million. This effect mutes the high contrast seen in the 15 kilohertz data. However, the shift still shows great detail and continues to display all the previously mentioned features. Within and between cribs 216-T-14 and 216-T-15, a light blue feature appears at approximately 1,500 parts per million. The 207-T retention basin appears as an obvious dark brown rectangular object located south of cribs 216-T-15 and 216-T-14, and east of the T tank farm fence. The 207-T retention basin is concrete lined and constructed out of reinforced concrete. It has a high response of 3,000 parts per million. Anomalies located between the T tank farm fence and the 207-T retention basin, and north of T tank farm, all show the same dark brown color and response of 3,000 parts per million. It is likely that these objects are constructed using the same material, concrete reinforced with steel rebar.

Linear features, bracketed by yellow and highlighted by orange, blues, and violets, appear in the southeast corner of Figure A-25. These features display an in-phase response between 480 parts per million and 2,100 parts per million. This response likely corresponds to sewer lines and pipelines going to and from 207-T retention basin and T tank farm. Another linear anomaly follows Camden Road north, turns west along 23rd Street, then turns again north into T tank farm. This arrangement coincides with an electrical trench detailed in historical site documents. There are two violet features in the western portion of the figure; one running diagonally in the top northwest corner, and one linear response runs along the far west side oriented north-south. Their response is 480 to 2,100 parts per million and may represent subsurface electrical lines.

B2.4.7 Ex-Farm Electrical Conductivity

Figures A-26 through A-30 in Appendix A show the contours of the frequency-dependent electrical conductivity data for the frequencies of 5, 7.5, 10, 15, and 20 kilohertz, respectively. Unlike the magnetic and electromagnetic in-phase data, anomalous responses in the electrical conductivity could result from increased soil moisture or salt deposits, in addition to the presence of ferrous and non-ferrous metals.

Table B-8 presents the summary statistics for the acquired data. The contour map was compiled from data points that were kriged on a 2-meter square grid. The kriging semi-variogram was linear.

Table B-8. Summary Statistics for Ex-Farm, In-Phase Electromagnetic Induction Data.

Statistic	5 kilohertz	7.5 kilohertz	10 kilohertz	15 kilohertz	20 kilohertz	Total
Figure	**A-26**	**A-27**	**A-28**	**A-29**	**A-30**	**A-31**
Violet bracket (min to max)	0 to 8	0 to 8	0 to 8	0 to 8	0 to 8	0 to 8
Data count	43,033	43,033	43,033	43,033	43,033	43,033
Minimum (ppm)	0	0	0	0	0	0
Median (ppm)	6.3	2	1.8	2.1	3	19.6
Maximum (ppm)	563	336	276	165	110	1,068.8
Standard deviation (ppm)	57	35	27	16	12	136

Notes:
ppm = parts per million.

The figures use a color scheme that represents variations in the data. Hues ranging from brown, red, to yellow represent high electrical conductivity. Green, light blue, and dark blue hues represent low electrical conductivity. Blue hues may show additional areas of interest. The median violet colors form the background. White areas represent areas of no data coverage.

The figures also show sporadic electrical conductivity responses over the entirety of the site; these responses are likely noise due to subtle differences within the soil and the limitations of the survey instrument (e.g., the anomaly that curves through the four cribs in the northeastern portion of the figure). Additionally, the monitoring wells produce little response because the sensor was not placed directly over top of their locations.

B2.4.8 Electrical Conductivity at 5 kilohertz

The electrical conductivity data at 5 kilohertz shown in Figure A-26 were processed and reduced according to the description in Appendix C.

The features in Figure A-26 likely represent the buried pipes and other structures outside the T tank farm. The 207-T retention basin appears as an obvious dark brown rectangular object located south of cribs 216-T-14 through 216-T-17, and east of the T tank farm fence. The 207-T retention basin was concrete lined and constructed out of reinforced concrete. It has a high response of 300 millisiemens per meter. Anomalies located between the T tank farm fence and the 207-T retention basin, and north of T tank farm, all show the same dark brown color and response of 300 millisiemens per meter. It is likely that these objects are constructed using the same material, concrete reinforced with steel rebar. Linear features delineated by light blue highlights in the southeast corner of the plot have an electrical conductive response of 20 millisiemens per meter. This response likely corresponds to sewer lines and pipelines going to and from the retention basin and T tank farm.

Another linear anomaly appears to follow Camden Road north, turn west along 23rd Street, then turn north into T tank farm. This linear feature coincides with an electrical trench detailed in historical site documents. There are light blue features in the western portion of the figure, running diagonally in the top northwest corner, and a linear response along the far west side oriented north-south. The large value at 25 millisiemens per meter possibly represents subsurface electrical lines.

B2.4.9 Electrical Conductivity at 7.5 kilohertz

The electrical conductivity data at 7.5 kilohertz shown in Figure A-27 were processed and reduced according to the description in Appendix C.

The features in Figure A-27 electrical conductivity data are likely associated with buried pipes and other structures outside the T tank farm. The 207-T retention basin appears as an obvious dark brown rectangular object located south of cribs 216-T-14 through 216-T-17, and east of the T tank farm fence. The 207-T retention basin was concrete lined and constructed out of reinforced concrete. It has a high response of 200 millisiemens per meter. Anomalies located between the T tank farm fence and the 207-T retention basin, and north of T tank farm, all show the same dark brown color and response of 200 millisiemens per meter. It is likely that these objects are constructed using the same material, concrete reinforced with steel rebar.
Linear features delineated by light blue highlights in the southeast corner of the plot display an electrical conductive response of 20 millisiemens per meter. This response likely corresponds to sewer lines and pipelines going to and from the retention basin and T tank farm.

Another linear anomaly appears to follow Camden Road north, turn west along 23rd Street, then turn north into T tank farm. This linear feature coincides with an electrical trench detailed in historical site documents. There are light blue features in the western portion of the figure, running diagonally in the top northwest corner, and a linear response along the far west side oriented north-south. The large value at 25 millisiemens per meter possibly represents subsurface electrical lines.

B2.4.10 Electrical Conductivity at 10 kilohertz

The electrical conductivity data at 10 kilohertz shown in Figure A-28 have been processed and reduced according to the description in Appendix C.

The features in Figure A-28 are likely associated with buried pipes and other structures outside the T tank farm. The 207-T retention basin appears as an obvious dark brown rectangular object located south of cribs T-14 through T-17, and east of the T tank farm fence. The 207-T retention basin was concrete lined and constructed out of reinforced concrete. It has a high response of 200 millisiemens per meter. Anomalies located between the T tank farm fence and the 207-T-retention basin, and north of T tank farm all show the same dark brown color and response of 200 millisiemens per meter. It is likely that these objects are constructed using the same material, concrete reinforced with steel rebar. Linear features delineated by light blue

highlights in the southeast corner of the plot have an electrical conductive response at 20 millisiemens per meter. This response likely corresponds to sewer lines and pipelines going to and from the retention basin and T tank farm.

Another linear anomaly appears to follow Camden Road north, then turn west along 23rd Street, then turn north into T tank farm. This linear feature coincides with an electrical trench detailed in historical site documents. There are light blue features in the western portion of the figure, running diagonally in the top northwest corner and a linear response along the far west side oriented north-south. The large value at 25 millisiemens per meter possibly represents subsurface electrical lines.

B2.4.11 Electrical Conductivity at 15 kilohertz

The electrical conductivity data at 15 kilohertz shown in Figure A-29 were processed and reduced according to the description in Appendix C.

The many features within Figure A-29 electrical conductivity data are likely associated with the tanks, buried pipes, and other structures within the T tank farm. The 207-T retention basin is the obvious dark brown rectangular object located south of cribs T-14 through T-17 and east of the T tank farm fence. The 207-T retention basin was concrete lined and constructed out of reinforced concrete. It has a high response of 200 millisiemens per meter. Anomalies located between the T tank farm fence and the 207-T retention basin and north of T tank farm all show the same dark brown color and response of 200 millisiemens per meter. It is likely that these objects are constructed using the same material, concrete reinforced with steel rebar.
Linear features delineated by light blue highlights in the southeast corner of the plot display electrical conductive response at 20 millisiemens per meter. This response likely corresponds to sewer lines and pipelines going to and from the retention basin and T tank farm.

Another linear anomaly appears to follow Camden Road north, then turn west along 23rd Street, then turn north into T tank farm. This linear feature coincides with an electrical trench detailed in historical site documents. There are light blue features in the western portion of the figure, running diagonally in the top northwest corner and a linear response along the far west side oriented north-south. The large value at 25 millisiemens per meter possibly represents subsurface electrical lines.

B2.4.12 Electrical Conductivity at 20 kilohertz

The electrical conductivity data at 20 kilohertz shown in Figure A-30 have been processed and reduced according to the description in Appendix C.

The features in Figure A-30 are likely associated with the buried pipes and other structures outside the T tank farm. The 207-T retention basin appears as the obvious dark brown rectangular object located south of cribs T-14 through T-17, and east of the T tank farm fence. The 207-T retention basin was concrete lined and constructed out of reinforced concrete. It has a

high response of 200 millisiemens per meter. Anomalies located between the T tank farm fence and the 207-T retention basin, and north of T tank farm all show the same dark brown color and response of 200 millisiemens per meter. It is likely that these objects are constructed using the same material, concrete reinforced with steel rebar. Linear features delineated by light blue highlights in the southeast corner of the plot display electrical conductive response at 20 millisiemens per meter. This response likely corresponds to sewer lines and pipelines going to and from the retention basin and T tank farm.

Another linear anomaly appears to follow Camden Road north, turn west along 23rd Street, then turn north into T tank farm. This linear feature coincides with an electrical trench detailed in historical site documents. There are light blue features in the western portion of the figure, running diagonally in the top northwest corner, and a linear response along the far west side oriented north-south. The large value at 25 millisiemens per meter possibly represents subsurface electrical lines.

B2.4.13 Total Electrical Conductivity

The total electrical conductivity, which is an average response from all frequencies, is shown in Figure A-31. The data were processed and reduced according to the description in Appendix C.

Figure A-31 shows several pronounced features (red and blue) that stand out against the median color (light purple). The median violet color brackets the values from 0 to 8 millisiemens per meter and a solid line contour is located at 0 millisiemens per meter. The lower values, represented by the color violet and ranging from 0 to 4 millisiemens per meter, may represent the true background electrical conductivity.

The features in the figure are likely associated with the buried pipe and other structures outside the T tank farm. Features that appear to be linear are likely a buried network of pipelines used to move waste.

B2.5 IN-FARM GROUND-PENETRATING RADAR RESULTS

Appendix A contains 14 figures (Figures A-32 through A-45) that represent ground-penetrating radar (GPR) results completed within the T tank farm. Figure A-32 is the base map for the survey and displays the GPR coverage. Approximately 38,500 square meters (9.5 acres) were covered. Both north-south and east-west oriented lines were acquired.

In GPR data, buried pipelines typically cause hyperbolic diffraction patterns that appear within the individual radargrams (Figure B-8). A radargram is a stack of traces plotted next to one another, where the energy level is contoured to show the diffraction patterns. The two-way travel-time of the waveform is converted into an estimated burial depth using a selected or calibrated dielectric constant (Section 5.3.3). For the T tank farm, the velocity was approximately 0.093 meters per nanosecond.

Figure B-8. Sample Ground-Penetrating Radar Plot with Buried Pipelines.

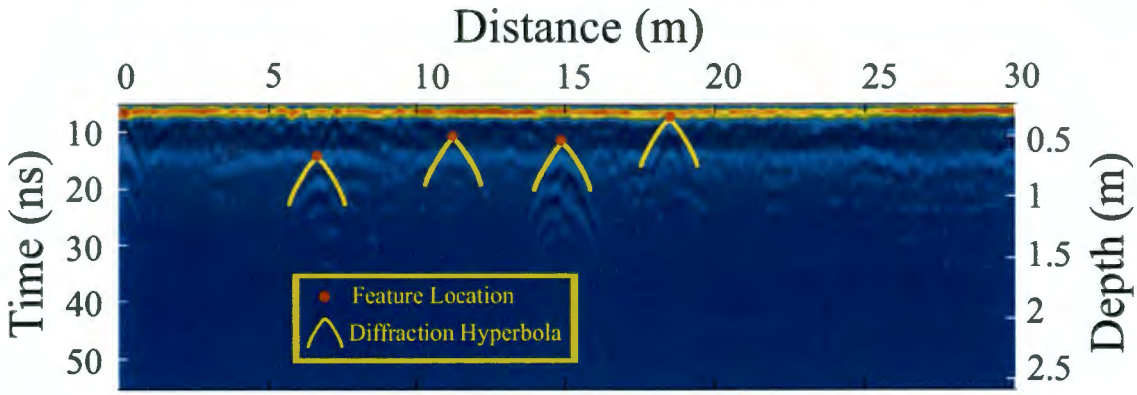

Figure A-33 was used to identify and spatially reference hyperbolic diffraction locations using the results of individual radargrams. These locations were plotted onto the T tank farm base map, which shows the points relative to known infrastructure. As seen in this figure, several pipelines were interpreted based on these manually selected points, and the interpreted pipeline routes usually agree with available infrastructure drawings.

Difficulties arise in several locations with concentrated hyperbolic points (such as the northeast area of the farm), or where herringbone effects occurred. Herringbone effects occur when anomalies are offset to the side of the actual target location. The offsets are caused by inaccuracies in the GPS location data, and are also affected by alternating data acquisition orientations (i.e., data acquisition is alternating from north to south, then south to north). A classic herringbone pattern is seen in the location of the curvilinear utility pipe along the western perimeter of the farm. The manual points do not fit directly over the pipeline.

Although manual points of hyperbolas permitted interpretation of several pipelines, it proved time-consuming. To speed processing, the data were converted into constant time-slices that were contoured and interpreted. This approach permitted burial depth estimations and minimized herringbone effects. The processing methodology for the GPR slices is discussed in Section 5.3.3.

Figure A-34 is a GPR data slice presented at 7.98 nanoseconds (0.37 meters below ground surface). The interpretation of infrastructure from this data is presented in Figure A-35. Thirteen individual pipelines are represented as orange-hued lines. The interpretation is based upon their linear orientation, and extremely high or low energy relative to background response. A portion of a utility corridor located along the west and north sides of the 12-tank complex can be seen in the data. This orientation agrees with an electrical conduit corridor shown in existing tank farm infrastructure maps. A north-south conduit is located between the middle and eastern column of tanks. Several east-west oriented branches also appear. A utility also appears that connects the three north-south utility diversion boxes (along the eastern side of the main tanks). A utility conduit is oriented north-south and begins at the main change-house and runs towards tank T-111. These features agree with the magnetic and electromagnetic utility interpretations, as well as existing infrastructure drawings for the site.

Several diffused (i.e., low energy) responses are associated with other farm infrastructure, and are likely caused by larger buried objects or tanks T-201 through T-204. These diffused

responses occur consistently throughout the time-slice series of GPR results.

Figures A-36 and A-37 represent the contoured GPR data and subsequent interpretation at a constant time-slice of 9.58 nanoseconds. This particular time slice demonstrates the difficulty of interpreting linear responses caused by pipelines due to the overall noise in the response patterns. These figures show a pipeline that runs north-south just east of tanks T-201 through T-204. Just north of tank T-201, this utility turns eastward towards the main tanks. Another north-south pipeline runs along the northern and eastern perimeter of the farm and may connect to a series of diversion boxes.

Figures A-38 and A-39 represent the contoured GPR data and subsequent interpretation at a constant time-slice of 14.37 nanoseconds. Compared with the previous time-slice interpretations, only a few additional utilities are interpreted. An east-west oriented utility crosses over tank T-108 and ends at tanks T-109 and T-107. Another east-west oriented utility appears along the northern edges of tanks T-112, T-111, and T-110. All other interpreted utilities were previously identified.

Figures A-40 and A-41 represent the contoured GPR data and subsequent interpretation at a constant time-slice of 16.77 nanoseconds. At the lower southwest corner of the surveyed area, an east-west oriented utility begins at the 200-W-52 underground structure and continues east. Another east-west oriented utility enters the farm area at the extreme southeast corner of the surveyed area, and continues west towards 200-W-52. This utility may turn 90 degrees north and continue past the T-32 underground structure. The north-south oriented utility seen in Figure A-35 begins at the main change-out facility, and continues northward across tank T-111, where it may connect with an east-west utility. A utility corridor begins at the 241-TR-152 diversion vault and appears to serve as a major utility corridor located between the two northern most tank rows of T-101, T-102, T-103, and T-104, T-105, and T-106. This response correlates to a large pipe trench shown on available tank farm infrastructure drawings.

Figures A-42 and A-43 represent the contoured GPR data and subsequent interpretation at a constant time-slice of 21.55 nanoseconds. A curvilinear response begins at the northern edge of the 200-W-52 underground structure located just east of the T-7 tile field, runs northward and then turns northeast toward tank T-103. This feature represents a possible utility. However, the feature is not indicated on available tank farm infrastructure drawings. Within the southeast farm area, a utility runs slightly northwest and heads towards the 241-TR-152 diversion vault. Just east of the TR series diversion boxes is another north-south oriented utility corridor. The utility appears to angle northwest after passing the northernmost diversion vault, and runs toward tank T-101. The major utility corridor is more defined at this time-slice.

Figures A-44 and A-45 represent the contoured GPR data and subsequent interpretation at a constant time-slice of 27.95 nanoseconds. The linear signatures are interpreted as buried utilities.

To summarize, multiple buried utility corridors were interpreted based on the GPR survey. Many of the interpreted utility routes agree with available tank farm infrastructure maps, but may deviate slightly. The deviation may be caused by survey orientation error, GPS location error, or omissions/errors in design media for the tank farm.

B3.0 REFERENCES

Huang, H. and I.J. Won, 2000, "Conductivity and Susceptibility Mapping Using Broadband Electromagnetic Sensors," *Journal of Environmental and Engineering Geophysics*, 5(4):31-41.

RPP-23752, 2005, *Field Investigation Report for Waste Management Areas T and TX-TY*, Rev. 0-A, CH2M HILL Hanford Group, Inc., Richland, Washington.

APPENDIX C

SUPPLEMENTAL THEORY

TABLE OF CONTENTS

C1.0 SUPPLEMENTAL THEORY C-1
C1.1 RESISTIVITY C-1
C1.1.1 Depth of Investigation C-4
C1.1.2 Electrical Resistivity Tomography C-5
C1.1.3 Well-to-Well and Well-to-Surface Inversion C-8

C2.0 REFERENCES C-14

LIST OF FIGURES

Figure C-1. Dipole-Dipole Array Configuration C-1
Figure C-2. Two-Dimensional Pseudosection Build-Up of Resistivity Data. C-3
Figure C-3. Comparison of Apparent Resistivity Data Presentation Styles C-5
Figure C-4. Example (Worst Case Scenario) of Resistivity Inversion C-6
Figure C-5. Inversion of Line 1 from BC Cribs and Trenches Fiscal Year 2004. ..... C-7
Figure C-6. Comparison of Different Inversion Models of Line 1 Resistivity Data C-8
Figure C-7. Potential (volts) Distribution from a Linear Source (Well). C-10
Figure C-8. Three Plume Models That Would Yield Similar Inversion Results for Well-to-Well or Well-to-Surface Geometry. C-11
Figure C-9. Benchmark Testing of the New Three-Dimensional Inversion Code with Data Collected In a Homogeneous Earth. C-11
Figure C-10. Benchmark Testing of the New Three-Dimensional Inversion Code Using a Scaled T Tank Farm and Tanks T-103 and T-106 ..... C-12
Figure C-11. Results for Inversion of Leak Testing in the Mock T Tank Farm Experiment. C-13

LIST OF TERMS

Terms

SuperSting R8 IP. SuperSting R8 resistivity and induced polarization meter produced by Advanced Geosciences, Inc.

Abbreviations, Acronyms, and Initialisms

HRR	high-resolution resistivity
WTW	well-to-well
WTS	well-to-surface

C1.0 SUPPLEMENTAL THEORY

C1.1 RESISTIVITY

The earth's resistivity is a function of soil type, porosity, moisture, and dissolved salts. The resistivity method detects and maps changes or distortions in an imposed electrical field due to heterogeneities in the subsurface.

Resistivity is a volumetric property measured in ohm-meters that describes the resistance of current flow within a medium. Its inverse, conductivity, in siemens/meter, describes the ease by which current will flow through a medium.

In the field, the electric current is generated by battery or motor-generator depending on the particular application and the amount of power required. Current is introduced into the ground through electrodes (metal rods). Earth-to-electrode coupling is typically enhanced by pouring water around the electrodes. The electrodes are placed along linear transects and provide points for both current transmission and voltage potential measurements. Field data are acquired using a four-electrode array where electric current is injected into the earth through one pair of electrodes (transmitting dipole) and the resultant voltage potential is measured by the other pair (receiving dipole). The most common configurations are dipole-dipole, Wenner and Schlumberger arrays. Figure C-1 depicts the dipole-dipole array configuration.

Figure C-1. Dipole-Dipole Array Configuration.

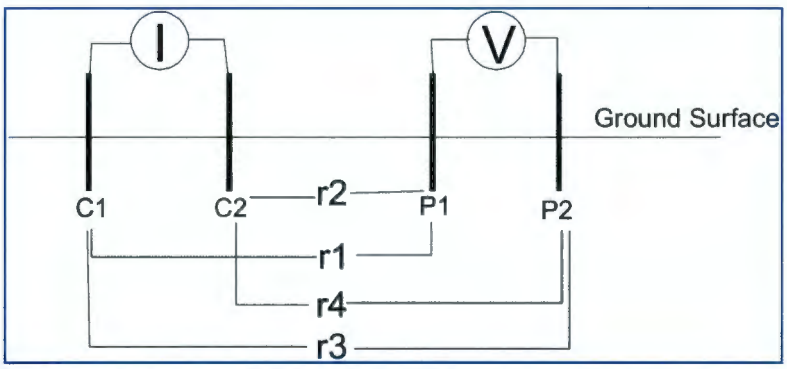

Resistivity is not measured directly. When current (I) is applied and voltage (V) measured. Resistance (R) (ohms) can be calculated using Ohm's Law (Equation C-1):

$$R = \frac{V}{I} \qquad \text{(C-1)}$$

Resistivity and resistance are related through a geometric factor. The simplest example is a solid cylinder with a cross sectional area, A and length, L (Equation C-2):

$$\rho = R\frac{A}{L} \tag{C-2}$$

Resistivity can be calculated by using the voltage, current, and geometry over which the measurement is made. In the earth, a hemispherical geometry exists. The hemispherical geometry is called a half-space, due to the fact that all current applied at the surface travels into the ground; above the ground, air has an infinite resistivity.

For the four-electrode array, the geometric factor, K, is (Equation C-3):

$$K = 2\pi \frac{1}{\left(\frac{1}{r_1} - \frac{1}{r_2}\right) - \left(\frac{1}{r_3} - \frac{1}{r_4}\right)} \tag{C-3}$$

where:

r_1 through r_4 = distance between electrodes.

An inverse calculation (or inverse model) is needed to convert the measured voltage potential to resistivity. Inversion estimates earth parameters, given the measured potential, input current, and boundary conditions. The inverse calculation assumes that each measurement of potential was a result of a homogeneous earth (Equation C-4):

$$\rho_a = 2\pi \frac{V}{I} K \tag{C-4}$$

Equation C-4 assumes isotropy (i.e., no directional dependence of resistivity), no displacement currents (using a direct current or low frequency current application), and the resistivity is constant throughout such that Laplace's equation can be assumed. Because the degree of heterogeneity is not known *a priori*, a true resistivity is not calculated. To obtain a true resistivity requires tomography. Tomography generates a model of true resistivity using the measurements of apparent resistivity, electrode arrangement, and other boundary conditions.

The high-resolution resistivity (HRR) surveys in this report used a pole-pole array. In a pole-pole array, one electrode pair is fixed effectively at infinity, while the other pair acts as a rover. Practically, the infinite electrodes are spaced approximately 2 to 10 times the distance of the furthest separation of the rover electrodes, which can be up to 200 meters (656 feet) apart. The pole-pole array provides higher data density, increased signal to noise ratio, and requires less transmitted energy. Roy and Apparao (1971), "Depth of investigation in direct current methods," discuss the superiority of the pole-pole method when conducting shallow (near-surface) surveys.

The calculation of apparent resistivity is simplified in the pole-pole array (Equation C-5):

$$\rho_a = 2\pi \frac{V}{I}(n * a) \tag{C-5}$$

where:

a = the basic electrode spacing
n = the integer multiplier as the current and potential electrodes incrementally separate.

The schematic below (Figure C-2) demonstrates the idea of a linear transect of electrodes on the surface. For a complete survey, each electrode has one turn at transmission, while potential measurements occur at all other electrodes in the array.

Figure C-2. Two-Dimensional Pseudosection Build-Up of Resistivity Data.

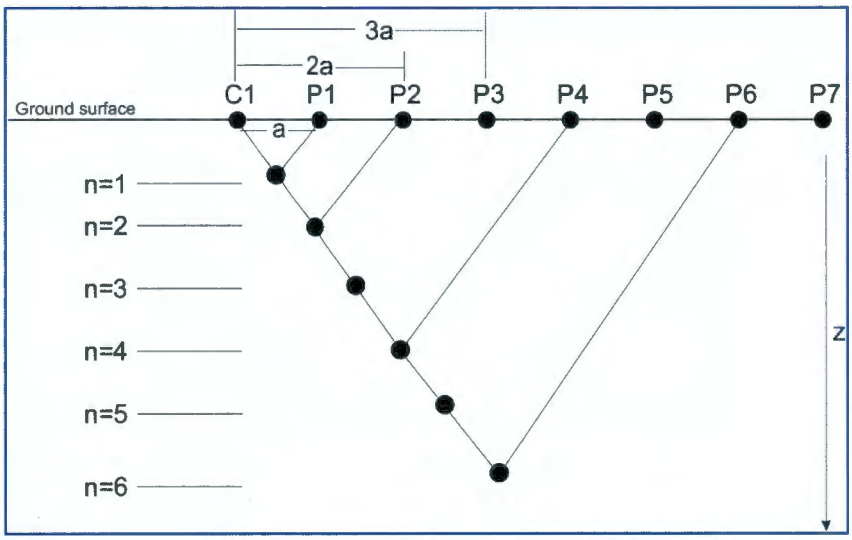

The linear transect arrangement produces a two-dimensional data set of resistivity as a function of x and z, where z is the dimension into the earth and x is along the surface. Although resistivity is a function of the volume over which the measurement is made, its location is typically plotted as a point. The location of the point is a function of n and is referred to as the depth of investigation. Hallof (1957), "On the interpretation of resistivity and induced polarization measurements," demonstrated that the intersection of two 45 degree lines (with respect to the surface) produces a suitable pseudosection for interpretation. The pole-pole array plots depth according to Equation C-6:

$$z = 0.5na \tag{C-6}$$

For HRR, the location of n is a function of the maximum sensitivity of the signal, which decreases as a logarithmic function as n increases. Once z is determined, the two-dimensional data set can then be presented as a contour plot, where isopachs of equivalent values are connected by a common line or color. Figure C-2 depicts such a plot.

C1.1.1 Depth of Investigation

The depth of investigation relates a measurement made at the surface to a depth for target identification (Barker 1989, "Depth of investigation of collinear symmetrical four-electrode arrays"). The depth of investigation is a linear function of electrode spacing with no emphasis on actual resistivity values.

Fink (1989), *Induced Polarization: Electrochemistry, Fractal Geometry, and Geohydrologic Application*, shows that the maximum sensitivity of the depth of investigation characteristics curve was a power function of dipole separation (Equation C-7):

$$Q_{DIC} = 1.5455n^{-0.7542} \tag{C-7}$$

where:

Q_{DIC} = the peak value of the DIC curve for each value of n.

Furthermore, the depth at which the maximum sensitivity occurs, Z_{DIC}, was found to be (Equation C-8):

$$Z_{DIC} = -0.2853n^{0.8732} \tag{C-8}$$

Equation C-8 can be generalized in the form of (Equation C-9):

$$Z_{DIC} = c * n^{b} \tag{C-9}$$

where:

c and b = fitting parameters for measured data, if ground truth data exist for comparison.

Since Fink (1989), parameters to control depth plotting through empirical data analysis have been refined. This report uses a method of depth investigation called "Geometric Inversion," a proprietary algorithm that includes topographic static correction to adjust for terrain effects.

An example of the plotting methodology is presented below (Figure C-3). The data are from Line 1 from the BC cribs and trenches site along trench 216-B-26, and were acquired in August 2004. For comparison, data plotted according to the Hallof (1957) and Roy and Apparao (1971) methodology are also presented to show the advantage of the geometric inversion technique for apparent resistivity plotting. Borehole data of pore fluid electrical conductivity (millisiemens/centimeter) allow the reader to assess the accuracy of each method. The borehole data were collected from well C4191, which is located in the center of trench 216-B-26 (90 meters [295 feet] from the beginning of the resistivity survey line). The borehole conductivity data show high values from approximately 25 to 44 meters (82 to 144 feet) below ground surface, which is coincident with the low-resistivity values seen in the geometric inversion.

Figure C-3. Comparison of Apparent Resistivity Data Presentation Styles.

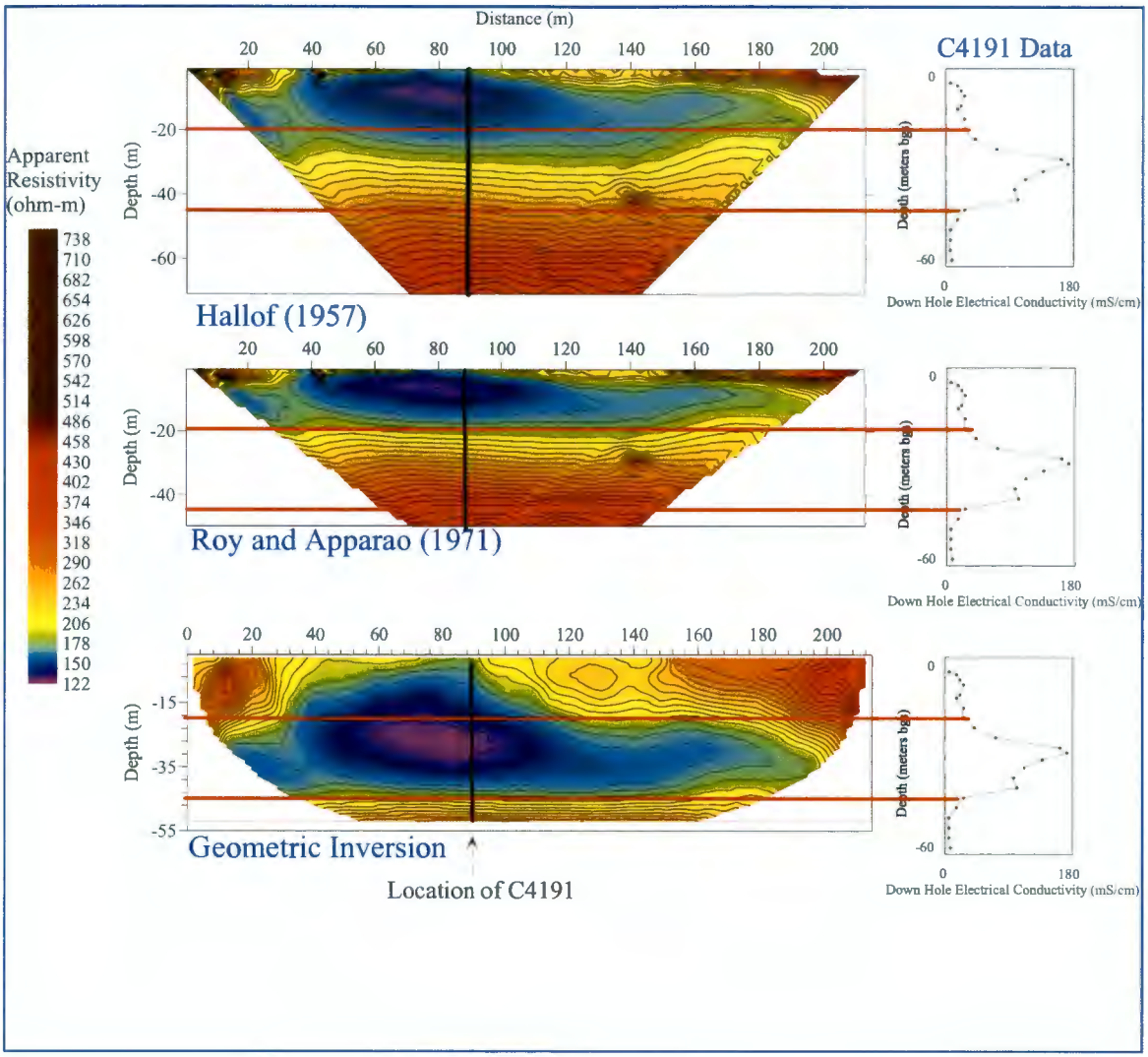

C1.1.2 Electrical Resistivity Tomography

Electrical Resistivity Tomography calculates the true resistivity of the subsurface measured apparent resistivity and Equation C-10:

$$\frac{\partial}{\partial x}\left(\frac{1}{\rho}\frac{\partial V}{\partial x}\right)+\frac{\partial}{\partial x}\left(\frac{1}{\rho}\frac{\partial V}{\partial x}\right)+I=0. \qquad \text{(C-10)}$$

Inversion minimizes the difference between the modeled and measured resistivity.
Several methods of inversion are presented in Oldenburg and Li (1999), "Estimating depth of investigation in DC resistivity and IP surveys"; Loke and Barker (1995), "Least-squares deconvolution of apparent resistivity pseudosections"; and LaBrecque et al. (1996), "The effects of noise on Occam's inversion of resistivity tomography data."

The major disadvantage to inversion is the number of model parameters (i.e., discrete modeling points where the true resistivity is calculated) exceeds the number of measurements. Therefore, the final estimate of true resistivity may be overly sensitive to uncertainty in the data. Finally, the non-linearity requires an iterative solution of the forward model, using an optimization technique to find a global minimum in an objective function.

An example of this limitation is presented below as Figure C-4. The plot was adapted from Figure 2 of Oldenburg and Li (1999). The top image, showing the apparent resistivity, was used in an inverse model to calculate the bottom three images. The differences among the three inverted plots are attributed to variations in the definition of the objective functions. Figure C-4 illustrates a worst-case scenario.

Figure C-4. Example (Worst Case Scenario) of Resistivity Inversion.

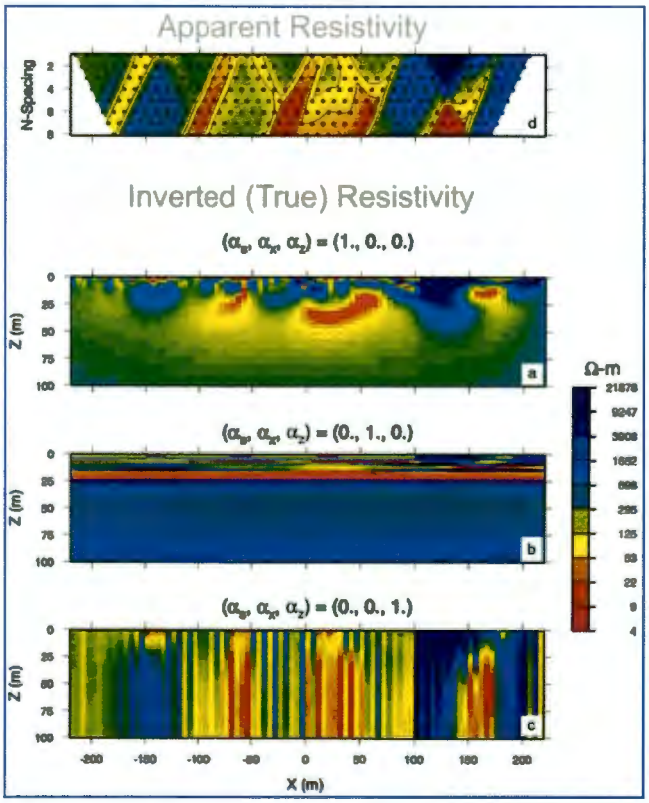

Note: Figure adapted from Oldenburg, D.W. and Y. Li, 1999, "Estimating depth of investigation in DC resistivity and IP surveys," *Geophysics*, 64(2):403-416.

To complete a comparison of inversion results, Line 1 from the BC cribs and trenches fiscal year 2004 survey was inverted with EarthImager2D[1] software. The model requires the measured field data, a starting model, and specification of the various parameters that control the inversion processes. The inversion was tested several times using different built in algorithms (i.e., Robust Inversion, Smooth Model Inversion, and Damped Least Squares Inversion), different starting

[1] EarthImager2D and EarthImager3D are trademarks of Advanced Geosciences, Inc., Austin, Texas.

models (i.e., constant background of 200 ohm-meters, constant background of 1,000 ohm-meters, and using the apparent resistivity data as the starting model), and different parameters (e.g., stabilizing factor of 1 and 10, damping factor of 1 and 10, number of finite element re-meshing, level of noise). Figure C-5 shows an example of the inversion with the smooth model inversion, with a starting model of 200 ohm-meters, and the remaining default parameters in the EarthImager2D program. The top image is the measured data, the lower image is the estimated true resistivity, and the middle image is the apparent resistivity. The objective is to make the top two images match, and statistics such as the root mean square and L2 Norm quantify the difference.

Figure C-5. Inversion of Line 1 from BC Cribs and Trenches Fiscal Year 2004.

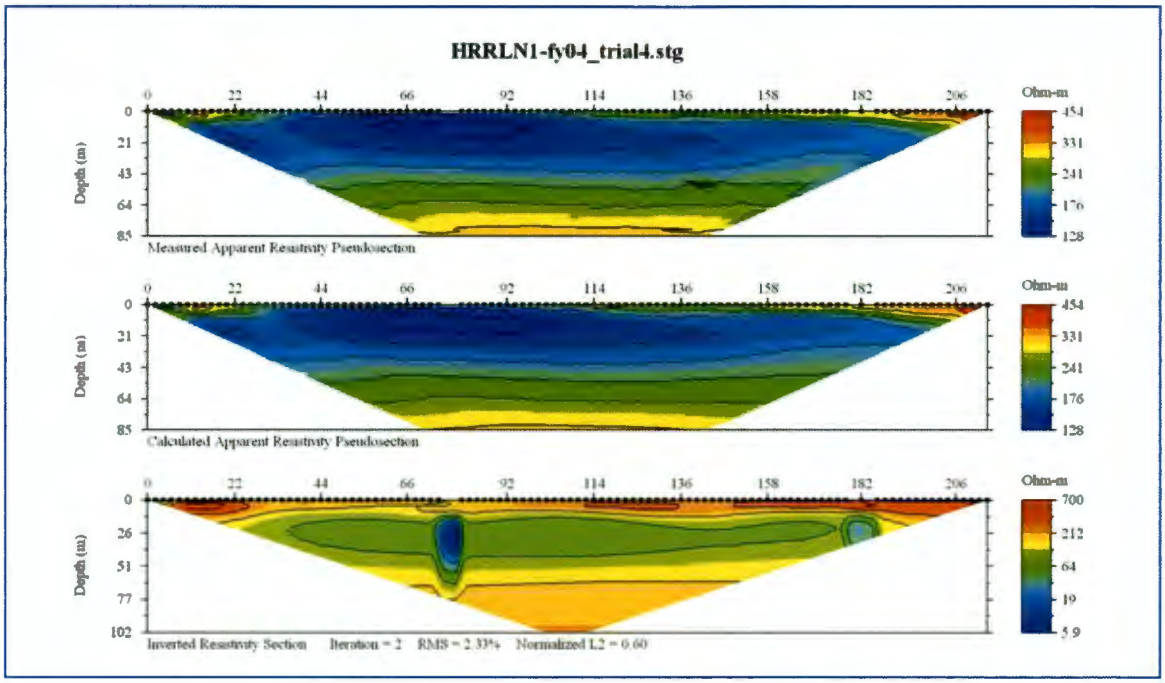

The most striking feature of the inverted section is the very low bulls-eye anomaly about 80 meters along the section. The data around this location is highly suspect, but otherwise the data appear reasonable. The root mean square and L2 Norm statistic confirms that the model was able to converge to a solution that resembles the measured data. Figure C-6 demonstrates another example of inversion, comparing the geometric inversion used in HRR, the above (trial 4) inversion, and an inversion that tests the robust inversion algorithm, a starting model equating to the apparent resistivity, and different values for the inversion-adjusting parameters. The electrical conductivity data from well C4191 is also shown for completeness.

Figure C-6. Comparison of Different Inversion Models of Line 1 Resistivity Data.

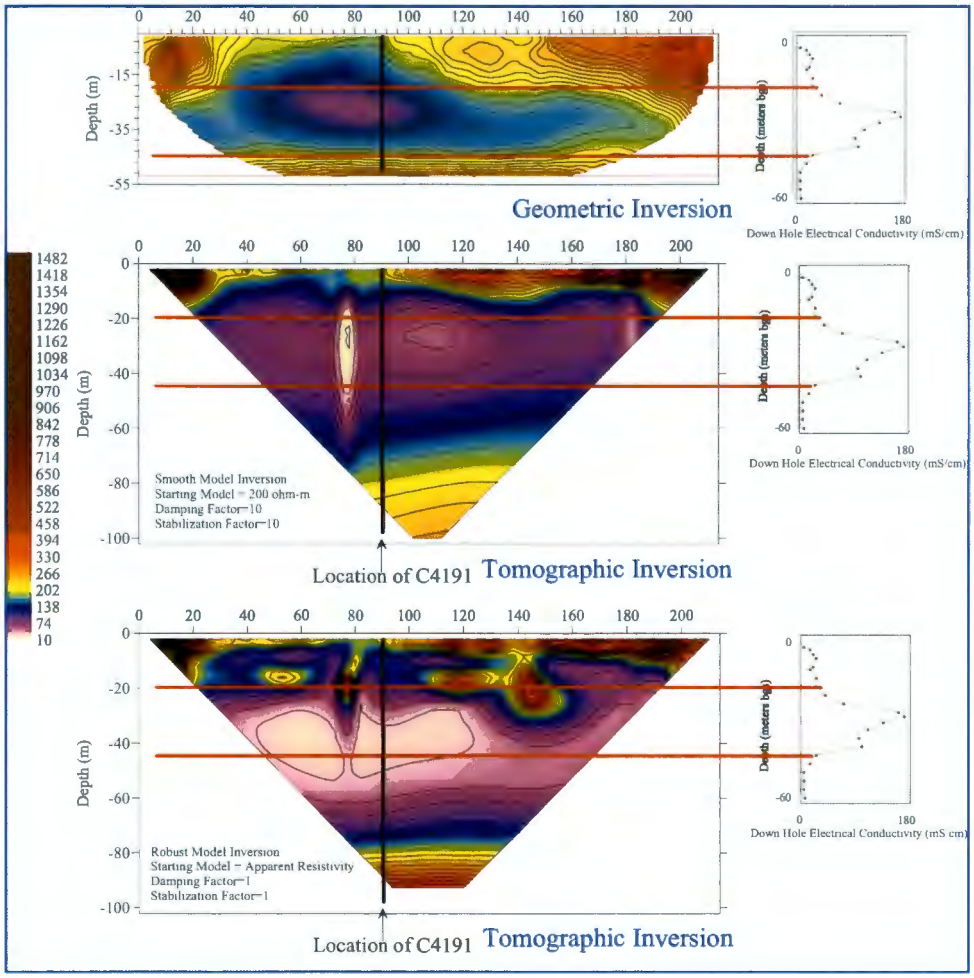

When the different interpretation schemes are compared to borehole data, the geometric inversion with HRR shows the best correlation. The tomographic inversion results, on the other hand, show a highly smeared plume that cannot replicate the conductive anomaly below 30 meters (98 feet). Oldenburg and Li (1999) discuss this failure with tomographic inversion. That report devises a Depth of Investigation Index that calculates reliability (or believability) versus depth.

C1.1.3 Well-to-Well and Well-to-Surface Inversion

For inversion of well-to-well (WTW) and well-to-surface (WTS) data, observations of voltage potential are used to calculate the distribution of electrical resistivity around an area bound by the well locations. The major difference is the geometry of the electrodes for the wells. The typical electrode used in electrical resistivity is a stake that penetrates no more than 29 centimeters (11.5 inches) into the ground. The stake is modeled as a point in space. A well is a very long stake that must be modeled as a line source in the model.

The following example (Equation C-11) uses a homogeneous and isotropic earth with a well located at r=0. Laplace's Equation in cylindrical coordinates solves for the voltage potential around a well:

$$\frac{1}{\rho}\frac{\partial}{\partial r}\left(r^2\frac{\partial V}{\partial r}\right)=0 \qquad \text{(C-11)}$$

Equation C-13 does not explicitly model the current source. Instead, it changes the boundary conditions to apply a source, I (amps), at r=0, z=0. Other boundary conditions are:

V=0 at z=-infinity (very deep)

$\frac{\partial V}{\partial z}=0$ at z=0 (surface)

V=0 at r=infinity

The potential distribution around a well of length, b, is shown in Equation C-12. It was derived from integrating the solution resulting from a point source, which assumed a uniform current distribution, over the length of the well.

$$V(r,z)=\frac{I\rho}{4\pi b}\ln\left[\frac{z+b+\left[r^2+(z+b)^2\right]^{0.5}}{z-b+\left[r^2+(z-b)^2\right]^{0.5}}\right] \qquad \text{(C-12)}$$

Figure C-7 shows the results (as colored contours) of modeling the forward solution in Equation C-14 for potential distribution around a 10-meter (33-foot) long well with an infinitesimal resistivity. Close to the well, the iso-potential line is elongated. As the distance from the well increases, the shape of the contour becomes similar to the point electrode (i.e., spherical).

Figure C-7. Potential (volts) Distribution from a Linear Source (Well).

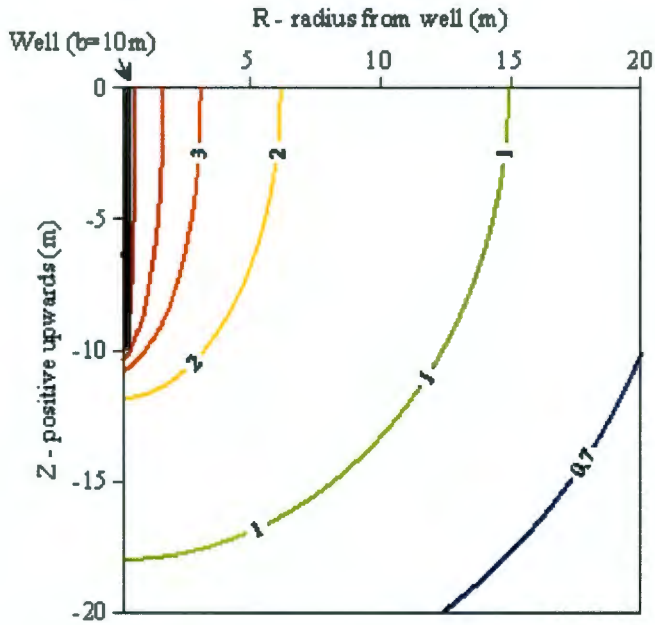

For heterogeneous earth and the WTW and WTS data collected at T tank farm, a new inverse code was developed based on the finite difference method. Advanced Geosciences, Inc. upgraded their commercial EarthImager3D[2] software to accommodate the new geometries. It simulated the wells as linear conductors, where a group (i.e., a vertical line) of cells within the model are assigned an electrical resistivity several orders of magnitude lower than the surrounding earth. During the course of the inversion calculations, the properties of the well cannot change, unlike the other cells in the model.

WTW and WTS results are only valid in a two-dimensional X-Y plane. The depth information is lost and only an aerial model of plume migration can be inferred. Figure C-8 below shows three plumes at different depths or orientations. All three would model similarly.

[2] EarthImager2D and EarthImager3D are trademarks of Advanced Geosciences, Inc., Austin, Texas.

Figure C-8. Three Plume Models That Would Yield Similar Inversion Results for Well-to-Well or Well-to-Surface Geometry.

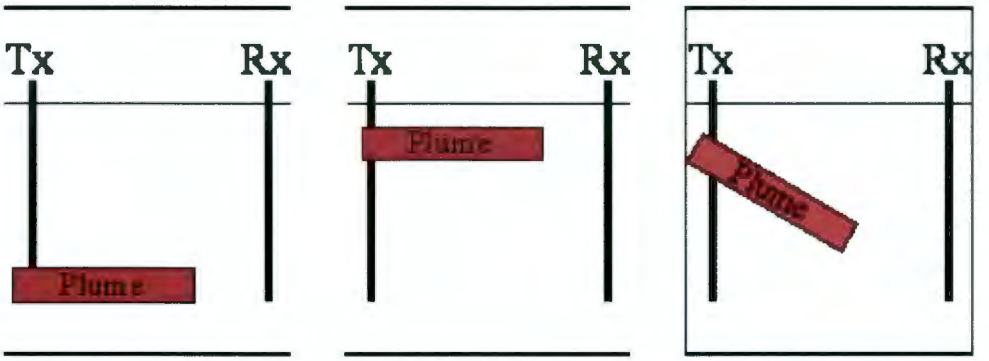

Before using the new inversion model on T tank farm data, the model was tested. The tests included laboratory-scaled experiments designed to check the results against the expected outputs. The first test collected data from a set of wells in a homogeneous background earth. The model was expected to invert the potential data to verify that the earth is homogeneous. For the homogeneous earth test, the wells were placed in a swimming pool mixed continually by the filtration system. Figure C-9 shows the experimental setup and results for the test. Fourteen wells with a length of 16.5 centimeters (6.5 inches) were placed in a ring. The minimum distance between rings was 8.5 centimeters (3.3 inches) and the maximum distance was 38.1 centimeters (15 inches). The wells were connected to the SuperSting R8[3] resistivity and induced polarization meter (SuperSting R8 IP), and data collected using a pole-pole array. The infinites were placed approximately 3 meters (9.8 feet) away in opposite directions.

Figure C-9. Benchmark Testing of the New Three-Dimensional Inversion Code with Data Collected In a Homogeneous Earth.

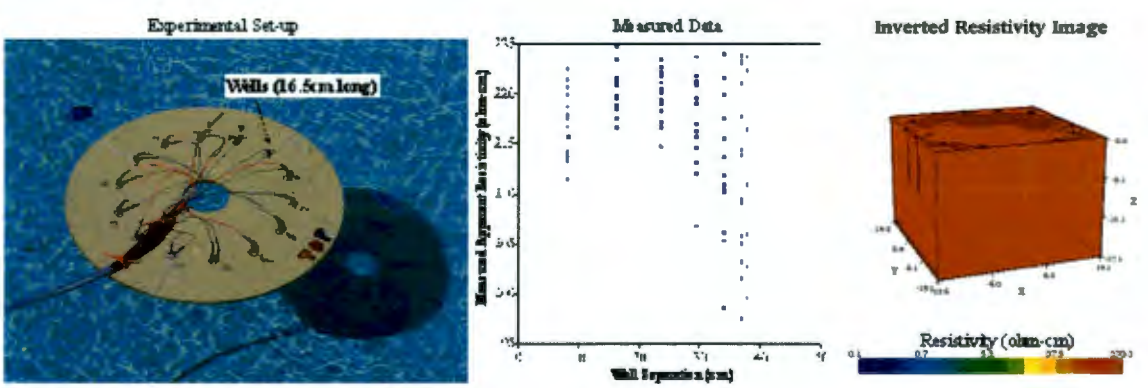

The middle plot of Figure C-9 shows the measured results in apparent resistivity. For a homogeneous earth, the apparent resistivity is equal to the actual (inverted) resistivity.

[3] SuperSting R8 and SuperSting R8 IP are trademarks of Advanced Geosciences, Inc., Austin, Texas.

An apparent resistivity function, similar to Equation C-5, can be derived for the WTW geometry by rearranging Equation C-12 and solving for ρ at z=0 (Equation C-13):

$$\rho_a = 4\pi \frac{V}{I} \frac{b}{\ln\left[\frac{-\left(b+\left[r^2+b^2\right]^{0.5}\right)}{b-\left[r^2+b^2\right]^{0.5}}\right]} \tag{C-13}$$

The distribution of apparent resistivity shows that some noise does exist in the data, likely due to the movement of the water. The inverted resistivity on the right hand side of the plot shows that the calculated true resistivity is homogeneous (within a given noise envelope).

The test simulated a leak in a scaled (1:138.5) version of T tank farm. The scale used a 16.5-centimeter (6.5-inch) diameter metal paint can to simulate a tank. Figure C-10 shows the experimental setup for the testing. The tests simulated leaks from tanks T-106 and T-103. The geometry of the collection system included HRR on the surface electrodes, WTW, and WTS. Many of the drywells and groundwater wells in the vicinity of tanks T-103 and T-106 were used to map the leaks.

Figure C-10. Benchmark Testing of the New Three-Dimensional Inversion Code Using a Scaled T Tank Farm and Tanks T-103 and T-106.

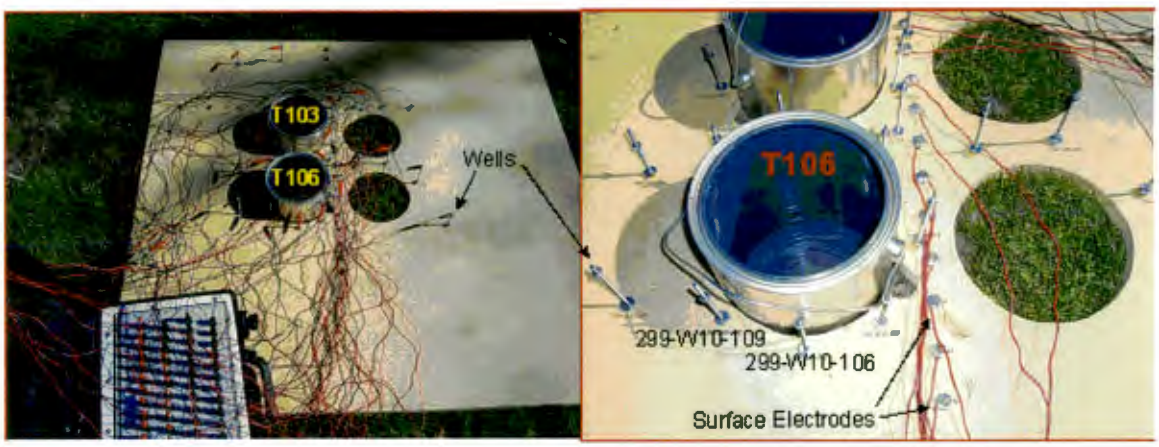

Leaks were simulated by pouring a sodium chloride supersaturated salt solution into the bottom of the empty paint cans. The cans had 1.6-centimeter (5/8-inch) holes drilled in the bottom for infiltration. The bottom of the cans were approximately 12.7 centimeters (5 inches) below the surface. A total of three leak simulations were tested. The first test represented a leak from tank T-106, where 0.34 kilograms (12 ounces) of solution was poured into the can. At the scale of the mock tank farm, the 0.34 kilograms (12 ounces) represents 379,000 liters (100,000 gallons). The second test included added an additional 0.68 kilograms (24 ounces) of solution in the simulated tank T-106. The last test simulated a leak of 0.34 kilograms (12 ounces) of solution from tank T-103.

Prior to leaking, a data set of initial voltage potential was collected and inverted using the three-dimensional inversion code. The background data set was compared with post-leak data. Figure C-11 shows the results of the pre-leak inversion. The red dots are the locations of the wells used in the WTW inversion. The figure shows that the lower left corner is less resistive and the upper right corner is more resistive. The tanks do not appear in the results of the inversion. This could be due to the fact that they were not very well grounded to the earth. Contact resistance was checked prior to data collection, and the resistance between the tanks was approximately 50 ohms.

Figure C-11. Results for Inversion of Leak Testing in the Mock T Tank Farm Experiment.

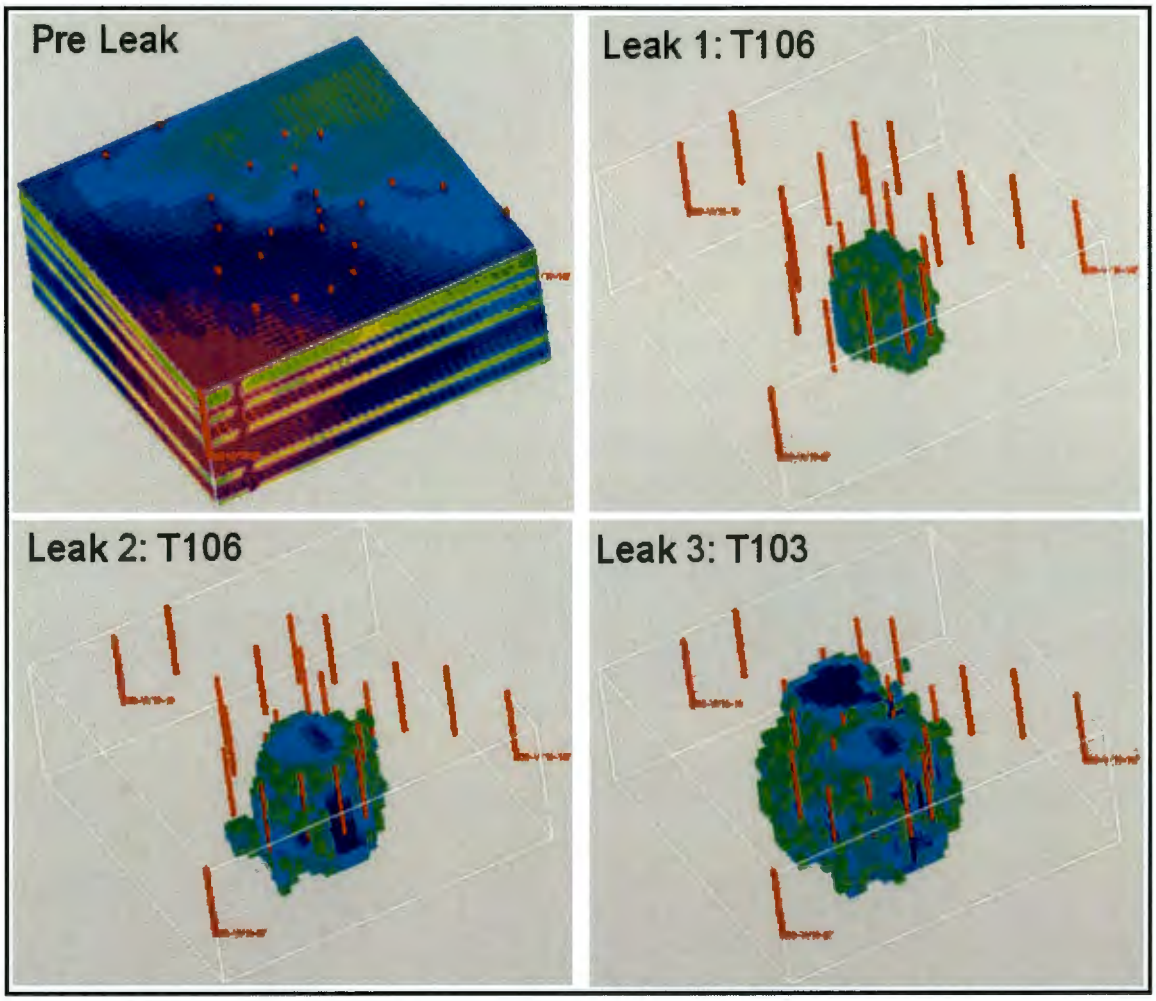

For the first leak test, the solution was poured into the bottom of the tank and allowed to infiltrate for approximately 12 hours. The upper right hand corner of Figure C-11 shows the results of the inversion. The results are displayed as percent difference in resistivity compared to the initial pre-leak case. Green represents a lower change and blue represents a higher change. The results show the migration pattern that was expected from infiltration. The salt water moved outward from beneath tank T-106.

The results for the second test are shown in the lower left corner of Figure C-11. For this leak, more solution was added to tank T-106 and the data were collected approximately 6 hours after infiltration. The results show that the plume has migrated laterally, but is fairly concentrated around tank T-106.

The results of the last test are shown in the bottom right of Figure C-11. For this test, the salt solution was poured into tank T-103 and left standing for about 4 hours. The salt plume is seen beneath tanks T-103 and T-106. Hydrologically speaking, the results appear consistent with expectations (i.e., the plume is confined to areas beneath tanks where infiltration was initiated).

C2.0 REFERENCES

Barker, R.D., 1989, "Depth of investigation of collinear symmetrical four-electrode arrays," *Geophysics*, 54(8):1031-1037.

Fink, J.B., 1989, *Induced Polarization: Electrochemistry, Fractal Geometry, and Geohydrologic Application*, Ph.D. Dissertation, University of Arizona, Tucson, Arizona.

Hallof, P.G., 1957, "On the interpretation of resistivity and induced polarization measurements," Ph.D. Dissertation, Massachusetts Institute of Technology, Boston, Massachusetts.

LaBrecque, D.J., M. Miletto, W. Daily, A. Ramirez, and E. Owen, 1996, "The effects of noise on Occam's inversion of resistivity tomography data," *Geophysics*, 61(2):538-548.

Loke, M.H. and R.D. Barker, 1995, "Least-squares deconvolution of apparent resistivity pseudosections," *Geophysics*, 60(6):1682-1690.

Oldenburg, D.W. and Y. Li, 1999, "Estimating depth of investigation in DC resistivity and IP surveys," *Geophysics*, 64(2):403-416.

Roy, A. and A. Apparao, 1971, "Depth of investigation in direct current methods," *Geophysics*, 36(5):943-959.

APPENDIX D

LIMITATIONS

TABLE OF CONTENTS

D1.0 LIMITATIONS OF SURFACE GEOPHYSICAL EXPLORATION IN THE TANK FARM ENVIRONMENT D-1
D1.1 LIMITATIONS IN INTERPRETING HIGH-RESOLUTION RESISTIVITY AND RESISTIVITY INVERSION RESULTS D-1
D1.1.1 High-Resolution Resistivity Interpretation with Infrastructure D-1
D1.1.2 Limitations with Resistivity Inversion D-7

D2.0 REFERENCES D-8

LIST OF FIGURES

Figure D-1. High-Resolution Resistivity Processing of a Single Plume (10 ohm-meters) in a Homogeneous Background Sand (1,000 ohm-meters). D-2

Figure D-2. High-Resolution Resistivity Processing of a Plume (10 ohm-meters) in a Homogeneous Background Sand (1,000 ohm-meters) with a Pipe (0.01 ohm-meter) at the Surface. D-3

Figure D-3. Modeling of Conductive Tank (Plots A, D, and G) and Resistive Tank (Plots B, C, E, F, and H) in a Background Uniform Soil D-4

Figure D-4. Modeled Sections and High-Resolution Resistivity Processing with a Water Table. D-6

Figure D-5. Modeling and High-Resolution Resistivity Processing of a Plume beneath Three Tanks. D-7

Figure D-6. Electrical Resistivity Tomography Inversion of a Plume (10 ohm-meters) in a Homogeneous Background Sand (1,000 ohm-meters) with a Pipe (0.01 ohm-meters) at the Surface. D-8

D1.0 LIMITATIONS OF SURFACE GEOPHYSICAL EXPLORATION IN THE TANK FARM ENVIRONMENT

The T tank farm has features that prevent optimal surface geophysical survey.
Buried infrastructure has the greatest negative effect on acquisition of data, data interpretation, and data visualization. Near-subsurface and above-surface structures (e.g., pipelines, well heads, overhead power lines, tanks, metal buildings) can prevent access to areas, or contribute electrical and magnetic responses that mask changes caused by subsurface hydrogeologic changes.

D1.1 LIMITATIONS IN INTERPRETING HIGH-RESOLUTION RESISTIVITY AND RESISTIVITY INVERSION RESULTS

Infrastructure was mapped using a multi-method geophysical reconnaissance survey consisting of magnetic gradiometry, electromagnetic induction, and ground penetrating radar.
The reconnaissance survey mapped the location and relative signal strength of underground pipelines and tanks. To put the high-resolution resistivity (HRR) and resistivity inversion results in context, the discussion below outlines many of the limitations of viewing resistivity data with respect to these infrastructure related interferences.

D1.1.1 High-Resolution Resistivity Interpretation with Infrastructure

Sample models illustrate the limitations of HRR processing in relation to a high degree of infrastructure. These models show different levels of complexity, by sequentially adding subsurface components, such as a tank or pipe. The simplest model illustrates a plume within a homogeneous unsaturated background soil. The plume has an electrical resistivity of 10 ohm-meters, and the background soil has a resistivity of 1,000 ohm-meters. The following continuity equation (Equation D-1) describes electrical potential:

$$\frac{\partial}{\partial x}\left(\frac{1}{\rho}\frac{\partial V}{\partial x}\right)+\frac{\partial}{\partial z}\left(\frac{1}{\rho}\frac{\partial V}{\partial z}\right)-\frac{k^2}{\rho}V=-I\cdot\delta(x)\cdot\delta(z) \qquad \text{(D-1)}$$

where:

V = scalar voltage potential in the Fourier transform domain

I = electrical current source

k = wave number

ρ = electrical resistivity as a function of (x,z), solved with a Finite Element scheme with Dirichet boundary conditions at infinity.

The first model assumes a plume 200 meters long and 14 meters high with its top surface 19 meters below ground surface.

EarthImager2D[1] models the plume by calculating apparent resistivity for every electrode combination using a pole-pole array. The apparent resistivity from the EarthImager2D model is then processed as typical HRR data. Figure D-1 shows the results, with the blue box representing the original location of the plume during modeling. The black box shows the HRR interpreted plume. The interpreted plume, which represents 384 ohm-meters, is derived from the weighted logarithm average of the background resistivity and plume resistivity using Equation D-2:

$$\log(\rho) = \left[\left(\frac{L-h}{L}\right)\log(\rho_{back}) + \left(\frac{h}{L}\right)\log(\rho_{plume})\right] \qquad \text{(D-2)}$$

where:

L = height of the domain imaged by HRR (67 meters)
h = height of the original modeled plume (14 meters).

Figure D-1. High-Resolution Resistivity Processing of a Single Plume (10 ohm-meters) in a Homogeneous Background Sand (1,000 ohm-meters).

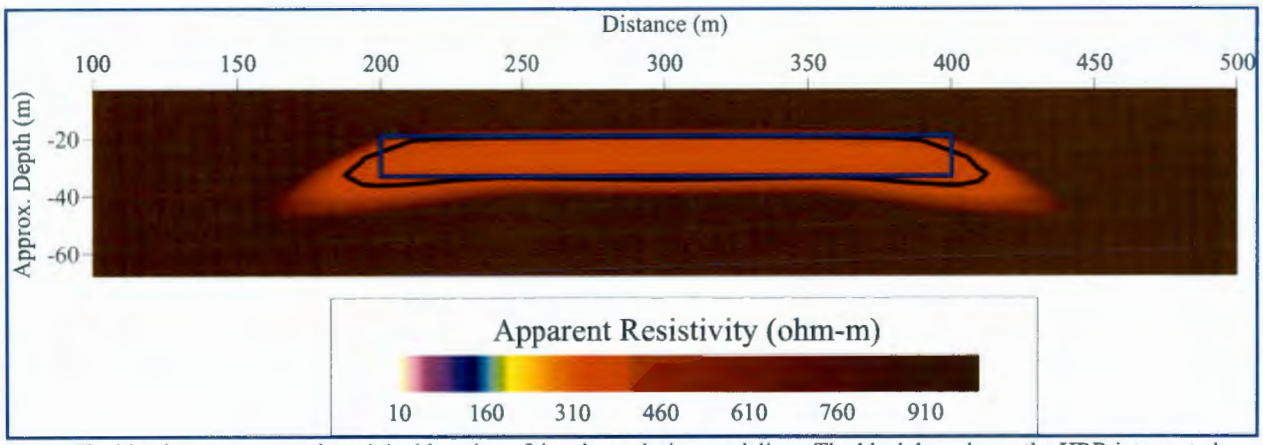

Note: The blue box represents the original location of the plume during modeling. The black box shows the HRR interpreted plume.

In Figure D-1, the interpreted plume and modeled plume have nearly the same location and size. However, HRR represents the plume with an apparent resistivity value 1.5 orders-of-magnitude larger than originally modeled.

A more complicated model assumes a plume and pipe. The pipe has a location of 297 meters along the line, a resistivity of 0.01 ohm-meter, and a cross section of 1.5 meters (smallest cell size available within the finite element model). Figure D-2 shows the HRR results for this model. Figure D-2 shows that the interpreted HRR plume has a slightly larger size and deeper

[1] EarthImager2D and EarthImager3D are trademarks of Advanced Geosciences, Inc., Austin, Texas.

location than the previous plume model due to the additive effect of potential field theory. Potential field theory assumes that the total potential distribution has (nearly) the same value as the sum of each subsurface feature (e.g., background soil, plume, and pipe) modeled separately, as shown in Equation D-3:

$$\Psi_{total} = \Psi_{background} + \Psi_{plume} + \Psi_{pipe} \tag{D-3}$$

where:

Ψ = potential field distribution

Figure D-2. High-Resolution Resistivity Processing of a Plume (10 ohm-meters) in a Homogeneous Background Sand (1,000 ohm-meters) with a Pipe (0.01 ohm-meter) at the Surface.

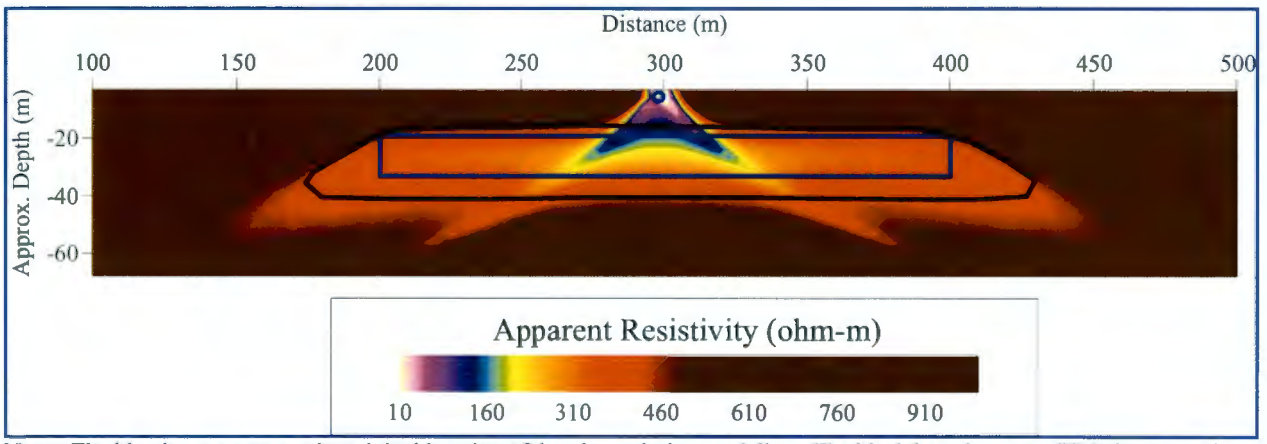

Note: The blue box represents the original location of the plume during modeling. The black box shows the HRR interpreted plume.

For processing simplistic survey lines, a filtering algorithm removes the virtual pant leg effect caused by the pipe. These pant leg features can be seen in Figure D-2 just below the position of the pipe. Wells have a similar response. The drawback of filtering is that it does not move the plume back to the original position and size.

A model with greater complexity adds a tank to the domain. The tanks at T tank farm have a single wall consisting of a 0.63-centimeter (¼-inch) inner steel liner and an approximately 0.3-meter (1-foot) outer concrete shell. Asphalt covers the concrete. According to Dr. William Daily (personal communication) the tanks have a high conductivity. Dr. Daily stated that the asphalt, typically a resistive material, degrades over time. The degradation allows water, waste, and other conductive fluids to contact the concrete. The concrete may have breaches that allow fluids inside the tank to flow out to contact the soil.

Dr. Jim Fink (personal communication) believes that intact (non-leaking) tanks have high resistivity. The outer shells provide electrical insulation for the steel liner inhibiting electrical flow through the tank. Therefore, non-leaking tanks are not grounded to the soil. The following model shows the effects of both conductive and resistive tanks, with and without a plume. The forward model simulations were conducted with the EarthImager2D and HRR processing of

apparent resistivity. A 1 ohm-meter resistivity simulates the conductive tank and a 10,000 ohm-meter resistivity simulates the resistive tank. A 20 ohm-meter resistivity simulates the plume; tank waste in Hanford Site soil has a resistivity of approximately 20 ohm-meters.

Figure D-3 shows the results of modeling a resistive and conductive tank. Plots A, B, and C model the effects of a tank only. Plot A, in the upper left corner, shows the HRR data of a conductive tank. The pant legs, typical of a conductive body in a resistive soil (modeled as 1,000 ohm-meters) extend below the tank. The tank has a size of 28 meters (92 feet) long and 9 meters (30 feet) high. The top of the tank extends to about 2.5 meters (8.2 feet)below ground surface. The green square shows the location of the tank.

Figure D-3. Modeling of Conductive Tank (Plots A, D, and G) and Resistive Tank (Plots B, C, E, F, and H) in a Background Uniform Soil.

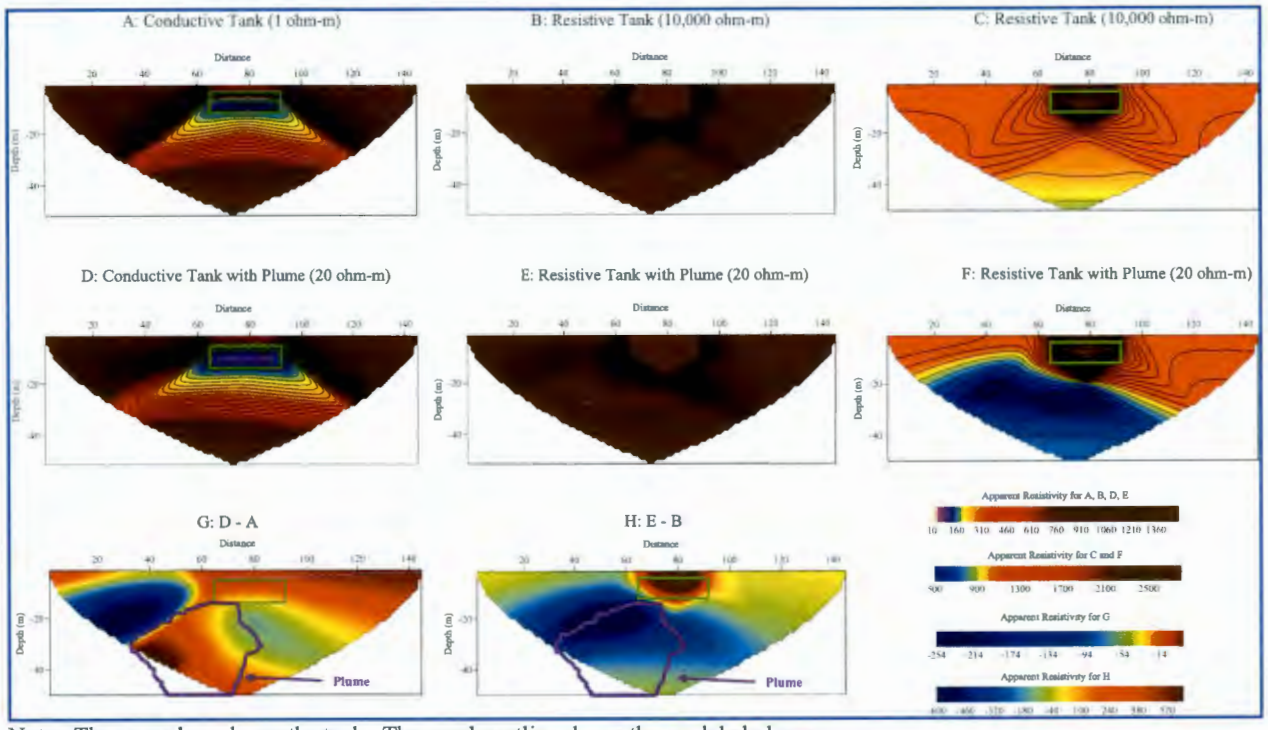

Note: The green box shows the tank. The purple outline shows the modeled plume.

Plot B shows the HRR section of a resistive tank. Plot B uses the same color scheme as the one used for all T tank farm processing. Plot C applies a new color scheme to enhance readability. The resistive tank also shows a pant leg effect.

Plots D, E, and F in Figure D-3 show the results of adding a plume with a resistivity of 20 ohm-meters. Plot D shows the plume beneath the conductive tank, Plot E shows a plume beneath the resistive tanks, and Plot F provides the same information as Plot E but with a new color scheme to enhance readability. In Plot D, the conductive tank nearly obscures the plume beneath it because it has conductivity an order-of-magnitude greater than the plume. It does, however, affect the HRR data in the upper left corner of the section. The plume beneath a resistive tank, on the other hand, contrasts sharply with the tank in Plot F. Therefore, a

conductive plume beneath a resistive tank can easily be identified in an HRR data processing model. A conductive plume beneath a conductive tank cannot be easily identified.

Plots G and H in Figure D-3 illustrate HRR data pre- and post-plume. Removing the pre-leak data from the post-leak data removes much of the tank effects. Plot G (i.e., data from Plot A subtracted from the data in Plot D) shows large changes in apparent resistivity in the upper left corner. The light blue and green colors beneath the tank show the pant legs from the plume. Within the center of the modeled plume (outlined in purple) the plume goes slightly more resistive. Plot H (i.e., data from Plot B subtracted from the data of Plot E) shows a plume with high contrast. Plot F does not require the application of a different color scheme because the plume beneath the resistive tank has high visibility without it.

The most complex model adds a water table with a resistivity of 100 ohm-meters. The water table sits approximately 72 meters (236 feet) below ground surface at the T tank farm. Figure D-4 shows the results of modeling using EarthImager2D. As before, the pant leg effect extends from the corner of the tank. However, Figure D-4 shows a more pronounced pant leg effect than Figure D-3 because of the water table. Although the water table sits 72 meters (236 feet) below ground surface, and has a discrete change in electrical properties relative to the background, the apparent resistivity function acts as a smoothing operator. Wait (1982), *Geo-electromagnetism*, developed the apparent resistivity function for a two layer case as shown in Equations D-4 through D-6:

$$\rho_a = 2\pi r \frac{V}{I} \cdot \frac{1}{G(r,K)} \tag{D-4}$$

where:

r_1 = resistivity of top layer (i.e., dry soil)
r_2 = resistivity of bottom layer (i.e., saturated soil)
r = distance between current and potential electrodes
h = depth to layer 2

$$K = \frac{\rho_2 - \rho_1}{\rho_2 + \rho_1} \tag{D-5}$$

$$G(r,K) = 1 + 2Kr + \sum_{n=0}^{\infty} \frac{K^n}{\sqrt{r^2 + [(n+1)2h]^2}} \tag{D-6}$$

Figure D-4. Modeled Sections and High-Resolution Resistivity Processing with a Water Table.

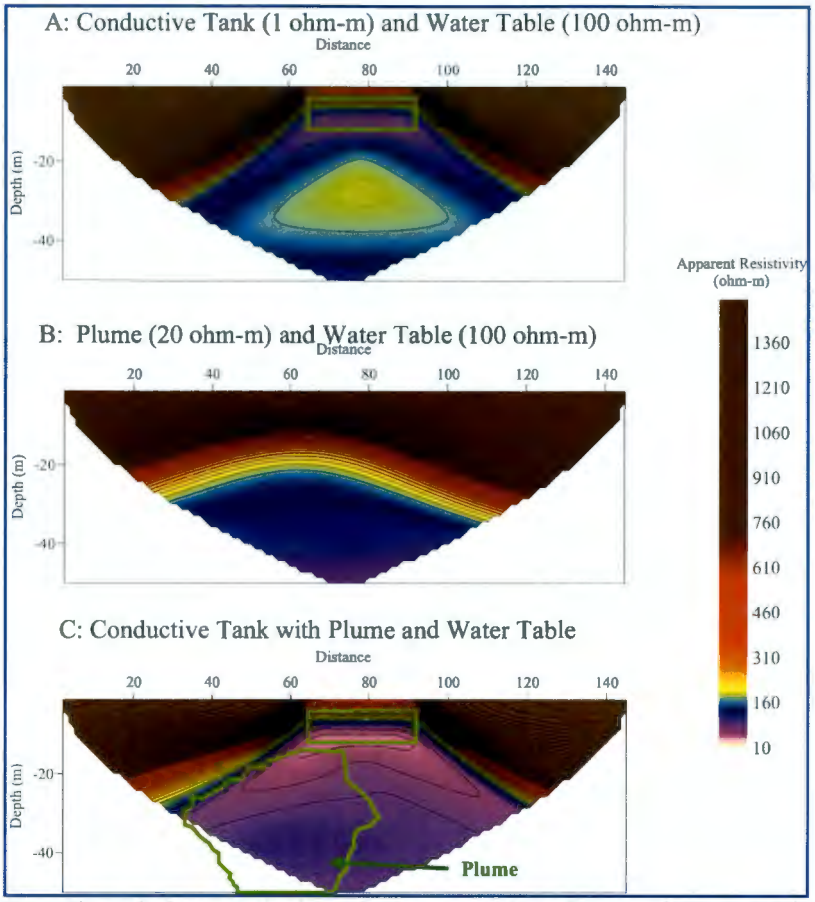

Note: Plot A depicts a conductive tank with water table at 70 meters below ground surface. Plot B depicts a plume with a water table. Plot C depicts a tank, plume, and water table. The green rectangle represents the tank. The green outline represents the plume.

The apparent resistivity function can affect the overall apparent resistivity of data that seem remotely far from the source layer. Figure D-4, Plot A demonstrates this by increasing the overall effects of the pant legs and creating a conductive layer at about 50 meters (164 feet) below ground surface. Plot A also shows a distinctive high apparent resistivity area directly beneath the tanks relative to the pant legs.

Figure D-4, Plot B shows the plume with a water table and no tank. The modeled plume resembles the overall shape of the original plume but it does not have a bottom due to the water table, and the pant legs from the plume makes it appear much larger.

Figure D-4, Plot C shows HRR processing after modeling a tank, water table, and plume. The difference between Plots A and C, modeled without and with a plume, respectively, demonstrates the effects of a plume beneath a conductive tank. The area beneath the tank in Plot C exhibits greater conductivity, and becomes more conductive as the depth increases. The differences between Plots A and C can be used to discriminate plumes beneath tanks within the HRR data collected in the T tank farm.

Note: Figure D-4, Plot C resembles T tank farm Lines 4E - 8E and 1N – 5N.

The final model depicts a tank-like environment, with three conductive tanks and a large plume directly beneath them. A water table also exists at approximately 72 meters (236 feet) below ground surface. Figure D-5 shows the results from HRR processing, with the tanks and plume outlined in green. The results show a plume that extends beyond the edges of the tanks. The extension of the plume in the HRR data is shown by conductive earth that protrudes beyond the pant leg. The location of the pant leg on the left side of the tank is highlighted in a yellow band. The pant leg location coincides with the last transmitter electrode location above the tank. Transmitter electrodes to the left of the yellow line are not over the tank, and the decrease in resistivity (increased conductivity) in this area is due to the plume. Plumes, therefore, can be identified in HRR sections if they protrude beyond the tanks and the resistivity decreases with distance from the last transmitter over the tank. Again, the conceptual model depicted in Figure D-5 can be used to help interpret HRR data collected within the T tank farm environment.

Figure D-5. Modeling and High-Resolution Resistivity Processing of a Plume beneath Three Tanks.

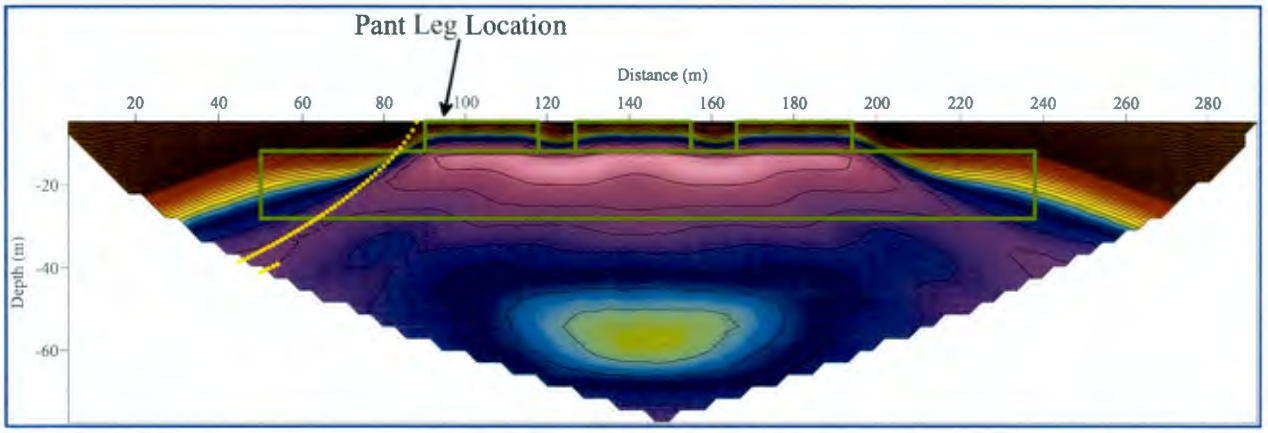

Note: The yellow pant leg location coincides with the last transmitter influenced by a tank. Figure D-5 looks similar to HRR Line 8E (Figure A-55).

D1.1.2 Limitations with Resistivity Inversion

Resistivity inversion removes the pant legs resulting from pipe and tank effects. The end goal of inversion is to return a plume to original size, location, and electrical properties. However, inversion does not adequately restrain the depth of the plume when data are collected from the surface only. Additionally, material property contrasts over short distances provide an additional level of difficulty for the inversion. Constraints are necessary to increase the number of model equations to ensure the uniqueness in the solution. Figure D-6 shows the results of inverting the apparent resistivity of the plume and pipe example described in Figure D-2. Inversion was completed using EarthImager2D with a smooth inversion scheme (LaBrecque et al. 1996, "The effects of noise on Occam's inversion of resistivity tomography data").

Figure D-6. Electrical Resistivity Tomography Inversion of a Plume (10 ohm-meters) in a Homogeneous Background Sand (1,000 ohm-meters) with a Pipe (0.01 ohm-meters) at the Surface.

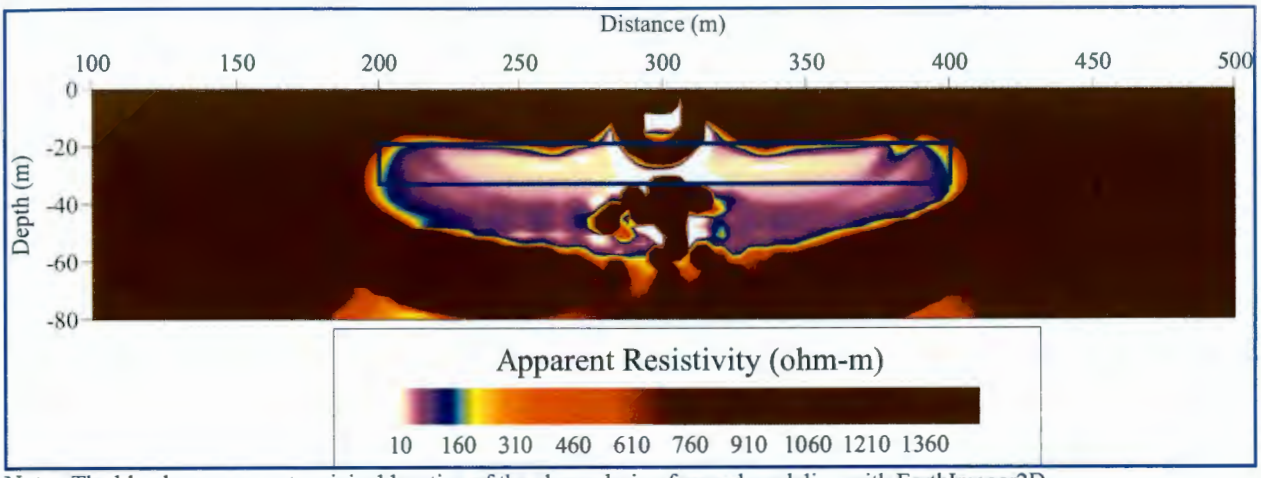

Note: The blue box represents original location of the plume during forward modeling with EarthImager2D.

The inversion results reproduced the plume more or less accurately. However, the bottom of the plume is not well resolved, and the plume is highly pock-marked with the effects of pipe removal. Additional constraints, such as core data, geophysical logging, or flow and transport modeling results help to define the bottom edge of these features. Resistivity electrodes placed deep in the vadose zone also help define the vertical extent of a plume.

D2.0 REFERENCES

Daily, W., personal communication in regards to electrical measurements recorded around S-112 tank, hydroGEOPHYSICS, Inc., Tucson, Arizona.

Fink, J.B., personal communication in regards to electrical measurements recorded around S-112 tank, hydroGEOPHYSICS, Inc., Tucson, Arizona.

LaBrecque, D.J., M. Miletto, W. Daily, A. Ramirez, and E. Owen, 1996, "The effects of noise on Occam's inversion of resistivity tomography data," *Geophysics*, 61(2):538-548.

Wait, J.R., 1982, *Geo-electromagnetism*, Academic Press, New York, New York.

APPENDIX E

NON-EXCAVATING OR -PENETRATING ELECTRODE TESTING

TABLE OF CONTENTS

E1.0 BACKGROUND E-1

E2.0 TEST METHODOLOGY E-2
- E2.1 TEST LOCATION E-2
- E2.2 TEST EQUIPMENT E-2
- E2.3 ELECTRODE CONFIGURATION E-3

E3.0 DATA ACQUISITION E-4
- E3.1 GROUP 1 – DRY MEASUREMENTS E-5
- E3.2 GROUP 2 – WET MEASUREMENTS E-6
- E3.3 GROUP 3 – SOIL BENEATH NEP ELECTRODE E-6
- E3.4 GROUP 4 – SOIL COVERING NEP ELECTRODE E-6
- E3.5 GROUP 5 – SOIL COVERING NEP ELECTRODE WITH SALT WATER E-6

E4.0 DATA PROCESSING E-6
- E4.1 DOWNLOADING, PARSING, QUALITY CONTROL, AND POINT REJECTION – ONSITE E-7
- E4.2 PROCESSING AND PLOTTING – OFFICE E-7
  - E4.2.1 Graphical Processing and Analysis E-7
  - E4.2.2 Numerical Processing and Analysis E-9

E5.0 RESULTS E-12
- E5.1 GRAPHICAL RESULTS E-12
- E5.2 NUMERICAL RESULTS E-12

E6.0 CONCLUSIONS E-13

LIST OF FIGURES

Figures E-1a and E-1b. HRR Electrode Deployment Strategies. E-1

Figure E-2. NEP Test Location. E-2

Figure E-3. Electrode Array Configuration. E-3

Figures E-4a and E-4b. (left) Comparison of NEP, Depth Limited, and Traditional Electrodes; (right) Expanded View of NEP Electrode. E-3

Figure E-5. Setup and Testing of NEP Electrode. E-4

Figure E-6. Comparison of Apparent Resistivity Pseudosections for the Three Electrode Types. E-8

Figure E-7. Difference Grids Showing Apparent Resistivity Pseudosections for the Three Electrode Types. E-9

Figure E-8. Comparison of Standard Deviation Pseudosections for the Three Electrode Types. E-10

Figure E-9. Chart Showing Percent Difference Between the Three Electrode Types. E-11

Figure E-10. Chart Showing a Comparison of the Standard Deviation for the Three Electrode Types. E-11

LIST OF TABLES

Table E-1. Test Group 1 Under Dry Conditions. E-4

Table E-2. Test Group 2 Under Wet Conditions. E-5

Table E-3. Test Group 3 through 5 NEP with Different Amounts of Soil Cover. E-5

Table E-4. Statistical Comparison for the Three Electrode Types. E-11

Table E-5. Repeatability and Accuracy Evaluation. E-12

LIST OF TERMS

Terms

SuperSting R8 IP. SuperSting R8 resistivity and induced polarization meter produced by Advanced Geosciences, Inc.

Abbreviations, Acronyms, and Initialisms

HRR	high-resolution resistivity
IP	induced polarization
NEP	non-excavating or -penetrating

E1.0 BACKGROUND

Installation of standard surface electrodes is a challenge for high-resolution resistivity (HRR) deployment within a tank farm. Standard HRR surface electrodes are traditionally installed by excavating a small hole, driving a stainless steel rod, and moistening of the ground with salt solution. Electrodes are used to provide direct electrical contact of the HRR equipment with the ground surface. The traditional electrode is driven into the ground using a hammer at the center of a small hole (0.15-meter diameter, 0.15 meter deep [6 inches diameter, 6 inches deep]) and penetration by the electrode usually extends up to 0.38 m (15 inches) below ground surface (Figure E-1a). The hole is then filled with a low concentration salt solution. Electrode installation within the tank farm environment is labor intensive and costly because the ground beneath each electrode location must first be cleared by site personnel by surveying for subsurface equipment. Significant savings could be attained if a new resistivity electrode were developed that would prevent any excavation or penetration into the earth.

A new electrode was designed, fabricated, and tested to determine if it was acceptable for use in collecting resistivity data. The new electrode design was termed the non-excavating or -penetrating (NEP) electrode. The NEP electrode would require sufficient contact with the ground and the ability to remain stable and upright during HRR data collection. The concept of the NEP electrode would use a stainless steel base of sufficient diameter for stability and a stem for connection to the HRR equipment (Figure E-1b). The NEP electrode would be buried beneath engineered soil, which would help in providing additional electrical contact with the ground.

Figures E-1a and E-1b. HRR Electrode Deployment Strategies.

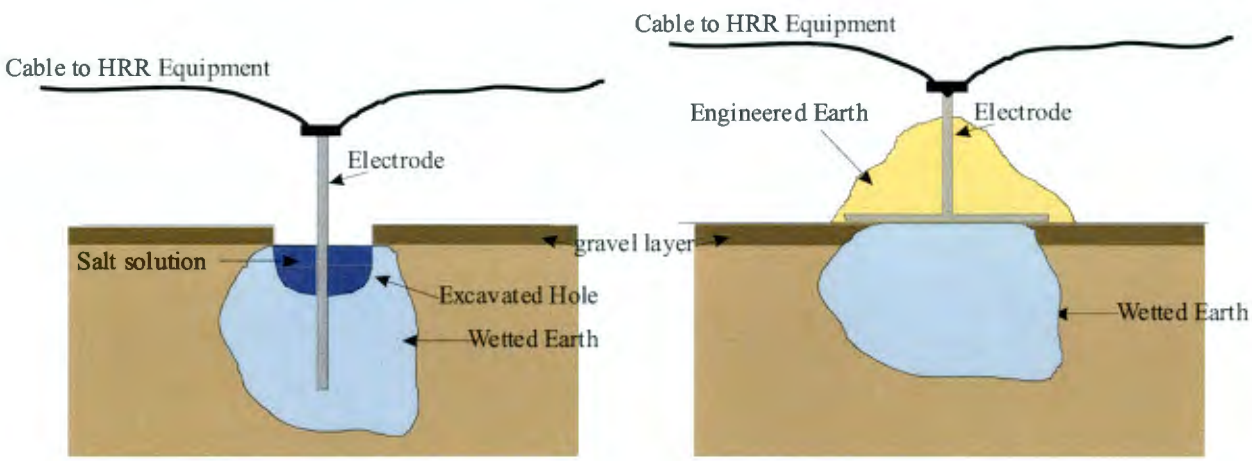

A) Traditional HRR electrode deployment

B) New HRR electrode with no excavation

E2.0 TEST METHODOLOGY

E2.1 TEST LOCATION

The NEP electrode test was conducted along a gravel road within the BC cribs site, south of the 200 East Area. To maximize the likelihood of tank farm conditions, the test was conducted over a gravel road directly over trench 216-B-26 (Figure E-2)

Figure E-2. NEP Test Location.

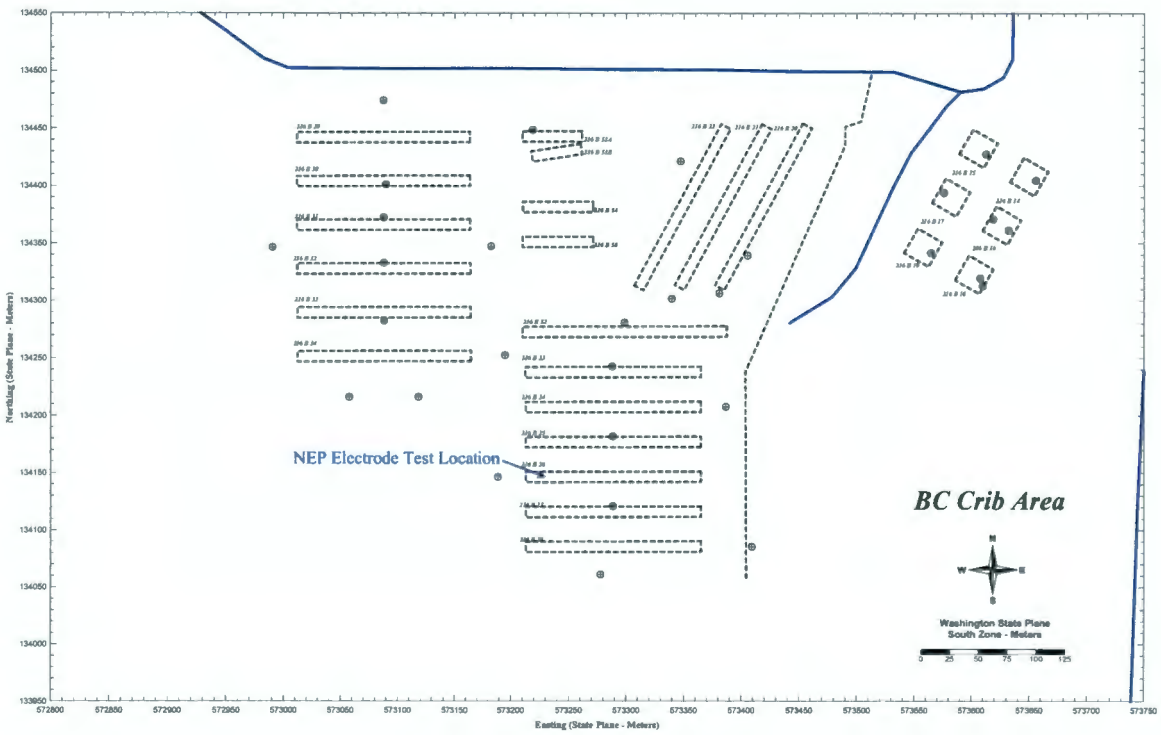

E2.2 TEST EQUIPMENT

The same SuperSting R8[1] resistivity and induced polarization (IP) meter (SuperSting R8 IP) data acquisition system used at BC cribs and T tank farm was used to acquire the NEP testing data. The system included the resistivity meter, a 28-channel switch box, a 28-takeout passive resistivity cable, a 12-volt battery as the power source, 12 NEP electrodes, 12 depth limited electrodes, and 12 traditional electrodes.

[1] SuperSting R8 and SuperSting R8 IP are trademarks of Advanced Geosciences, Inc., Austin, Texas.

E2.3 ELECTRODE CONFIGURATION

Figure E-3 demonstrates the electrode configuration for the test. Three rows of electrodes were placed on the surface: a traditional electrode, a depth limited electrode designed to penetrate no more than 0.3 meters (11.5 inches) into the ground, and the NEP electrode. The 12 electrodes of each type were set 3 meters apart in the same manner as T tank farm data acquisition. Figures E-4a, E-4b, and E-5 are photos of the test setup.

Figure E-3. Electrode Array Configuration.

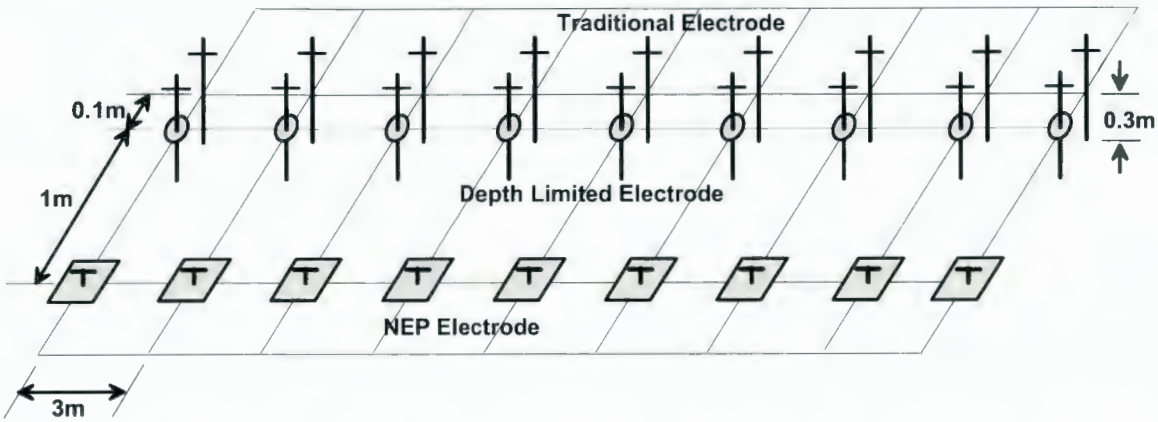

Figures E-4a and E-4b. (left) Comparison of NEP, Depth Limited, and Traditional Electrodes; (right) Expanded View of NEP Electrode.

Figure E-5. Setup and Testing of NEP Electrode.

E3.0 DATA ACQUISITION

Data acquisition for the 18 tests were conducted on May 19, 2006, where the traditional stake electrode was the control for evaluating differences between it, the depth limited electrode (stake with plate), and the NEP electrode. A summary of the test parameters for the individual tests is provided in Tables E-1 through E-3.

Table E-1. Test Group 1 Under Dry Conditions.

Test Parameters	GROUP 1: DRY					
Electrode Type	Stake	Stake	Stake w/ Plate	Stake w/ Plate	NEP	NEP
Command File	DD-NE	DD-NE	DD-NE1	DD-NE1	DD-NE1	DD-NE1
Output File	A1-1	A1-2	B1-1	B1-2	C1-1	Not Completed
No. Data Sets	3	3	3	3	3	3
Max I (mAmps)	1250	1250	1250	1250	1250	1250
Max V (volts)	400	400	400	400	400	400
Error Cutoff (%)	2	2	2	2	2	2
Cycles	3	3	3	3	3	3
Repeats	2	2	2	2	2	2
Res or IP/Res	RES	IP/RES	RES	IP/RES	RES	IP/RES
No. Electrodes	12	12	12	12	12	12
Electrode Spacing (m)	3	3	3	3	3	3
Array	Dipole-Dipole	Dipole-Dipole	Dipole-Dipole	Dipole-Dipole	Dipole-Dipole	Dipole-Dipole
Salt Water	None	None	None	None	None	None
Top Soil	None	None	None	None	None	None

Table E-2. Test Group 2 Under Wet Conditions.

Test Parameters	GROUP 2: WET					
Electrode Type	Stake	Stake	Stake w/ Plate	Stake w/ Plate	NEP	NEP
Command File	DD-NE1	DD-NE1	DD-NE1	DD-NE1	DD-NE1	DD-NE1
Output File	D1-1	D1-2	E1-1	E1-2	F1-1	F1-2
No. Data Sets	3	3	3	3	3	3
Max I (mAmps)	1250	1250	1250	1250	1250	1250
Max V (volts)	400	400	400	400	400	400
Error Cutoff (%)	2	2	2	2	2	2
Cycles	3	3	3	3	3	3
Repeats	2	2	2	2	2	2
Res or IP/Res	RES	IP/RES	RES	IP/RES	RES	IP/RES
No. Electrodes	12	12	12	12	12	12
Electrode Spacing (m)	3	3	3	3	3	3
Array	Dipole-Dipole	Dipole-Dipole	Dipole-Dipole	Dipole-Dipole	Dipole-Dipole	Dipole-Dipole
Salt Water	0.5L	0.5L	0.5L	0.5L	0.5L	0.5L
Top Soil	None	None	None	None	None	None

Table E-3. Test Groups 3 through 5 NEP with Different Amounts of Soil Cover.

Test Parameters	GROUP 3: SOIL 1		GROUP 4: SOIL 2		GROUP 5: SOIL 3	
Electrode Type	NEP	NEP	NEP	NEP	NEP	NEP
Command File	DD-NE1	DD-NE1	DD-NE1	DD-NE1	DD-NE1	DD-NE1
Output File	G1-1	G1-2	H1-1	H1-2	I1-1	I1-2
No. Data Sets	3	3	3	3	3	3
Max I (mAmps)	1250	1250	1250	1250	1250	1250
Max V (volts)	400	400	400	400	400	400
Error Cutoff (%)	2	2	2	2	2	2
Cycles	3	3	3	3	3	3
Repeats	2	2	2	2	2	2
Res or IP/Res	RES	IP/RES	RES	IP/RES	RES	IP/RES
No. Electrodes	12	12	12	12	12	12
Electrode Spacing (m)	3	3	3	3	3	3
Array	Dipole-Dipole	Dipole-Dipole	Dipole-Dipole	Dipole-Dipole	Dipole-Dipole	Dipole-Dipole
Salt Water	None	None	0.5L	0.5L	None	None
Top Soil	1" under	1" under	1" under	1" under	2" on top	2" on top

E3.1 GROUP 1 – DRY MEASUREMENTS

The first group of tests was conducted under dry conditions where the traditional stake electrode was driven to no greater than 0.3 meters (11.5 inches) below ground surface; the depth limited stake electrode (stake with plate) was driven in until the limiting plate touched the ground surface (0.3 meters of penetration [11.5 inches]); and the NEP electrode was simply placed on the ground surface. No solution was added. Three sets of full resolution dipole-dipole apparent resistivity, contact resistance, and IP data were acquired for each electrode type. No IP data were recorded for the NEP electrode because the ground coupling was insufficient for measurement.

E3.2 GROUP 2 – WET MEASUREMENTS

For the Wet Measurements Group, 0.5 liters (0.13 gallons) of salt water was applied to the gravel surface directly surrounding or beneath all the electrodes. Three sets of full resolution dipole-dipole apparent resistivity, contact resistance, and IP data were then acquired. The measurements within this group for the traditional stake electrode would be used as the control set. Measurements within this group for the depth limited stake electrode were subsequently compared to the control group.

E3.3 GROUP 3 – SOIL BENEATH NEP ELECTRODE

For Group 3 tests, 1 inch of top soil was placed within a wooden form (0.4 meters [1.3 feet] square) directly over the area where the previous 0.5 liters (0.13 gallons) of salt water was applied in Group 2 testing. The soil was patted down with the flat edge of the NEP electrode four or five times which increased inter-grain contact. Soil was added until the total height reached 2.5 centimeters (1 inch) in height. The NEP was then placed on top of the soil mound. Three sets of full resolution dipole-dipole apparent resistivity, contact resistance, and IP data were then acquired.

E3.4 GROUP 4 – SOIL COVERING NEP ELECTRODE

Group 4 was an extension of Group 3 testing. While the NEP electrode was sitting on top of the 2.5-centimeter (1-inch) soil mound, 5 centimeters (2 inches) of additional soil was placed on top within the form. The soil was packed with the flat edge of the geophysicist's hand or a tool with a flat edge. Three sets of full resolution dipole-dipole apparent resistivity, contact resistance, and IP data were then acquired.

E3.5 GROUP 5 – SOIL COVERING NEP ELECTRODE WITH SALT WATER

For the final test group, the soil form was removed and an additional 0.5 liters (0.13 gallons) of salt water was added to the top of the soil mound. Three sets of full resolution dipole-dipole apparent resistivity, contact resistance, and IP data were then acquired. The final NEP measurements within this group were subsequently compared against the control set (wet stake electrode).

E4.0 DATA PROCESSING

The NEP testing resulted in 18 data sets corresponding to various electrode test configurations. Data sets were acquired for each of the three electrode configurations: 1) standard stake electrode, 2) depth limited stake electrode, and 3) the NEP electrode. All data were recorded and

stored in a binary format within the SuperSting R8 IP for the duration of the field testing. A single command file, which contained a list of the desired transmitter and receiver electrodes to be interrogated, was used for all electrode tests.

E4.1 DOWNLOADING, PARSING, QUALITY CONTROL, AND POINT REJECTION – ONSITE

The individual binary data files from the SuperSting R8 IP were downloaded through Advanced Geosciences, Inc. SS Administrator software and exported, in ASCII format, to a laptop computer. Each data file was inspected, while still onsite, to ensure adequate data quality. Onsite data inspection consisted of a cursory evaluation of signal-to-noise, percent error for the three data stacks, and a comparison of the scatter between the data sets. The ASCII data files were parsed into usable columns (e.g., Record No., Date, Current, Normalized Potential, Error, Apparent Resistivity, Geometry, Transmitter Gain) using Microsoft Excel[2]. Each data file contained three readings which were then averaged to obtain a more reliable measurement.

A standard deviation value was computed for the three repeat measurements within each electrode set. Erroneous data points with a standard deviation that exceeded 1 ohm-meter were removed from all three data sets so that a one-for-one comparison could be performed. This resulted in the removal of 10 data points out of the total 59 data points.

E4.2 PROCESSING AND PLOTTING – OFFICE

E4.2.1 Graphical Processing and Analysis

A geo-electric pseudosection was used to produce a cross section each electrode set. The resulting data were plotted (Figure E-6) using Surfer 8[3], a software package used to develop a two-dimensional grid and contour. The resulting sections were first visually inspected for erroneous data points that persisted through the data reduction (quality assurance/quality control) steps. The grids (mesh) were subtracted from each other to produce difference grids (Figure E-7), where the resulting contour plot would highlight any differences in data obtained from each electrode.

---

[2] Microsoft and Excel are either registered trademarks or trademarks of Microsoft Corporation in the United States and/or other countries.

[3] Surfer and Surfer8 are registered trademarks of Golden Software, Golden, Colorado.

Figure E-6. Comparison of Apparent Resistivity Pseudosections for the Three Electrode Types.

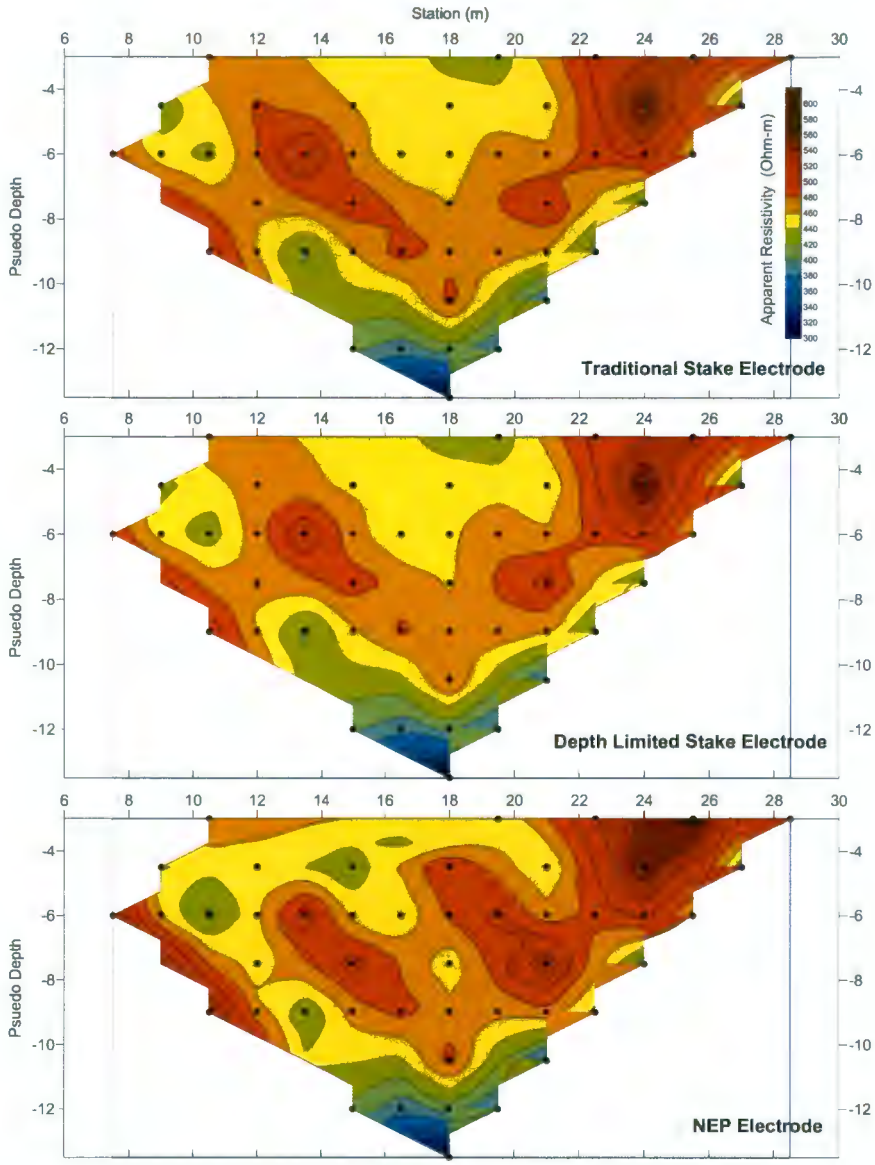

Figure E-7. Difference Grids Showing Apparent Resistivity Pseudosections for the Three Electrode Types.

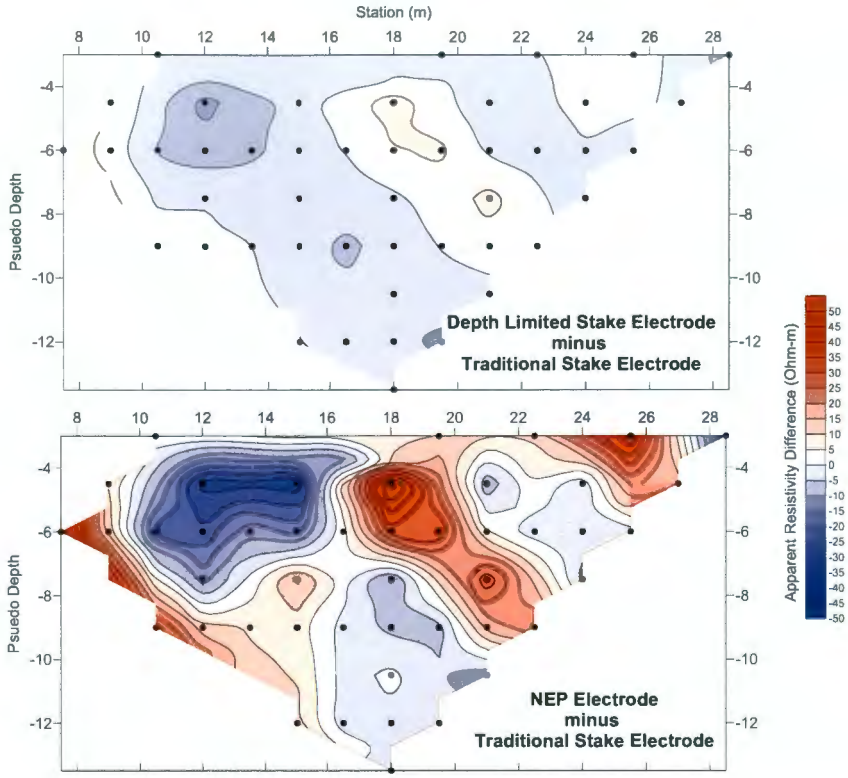

E4.2.2 Numerical Processing and Analysis

A statistical comparison of the apparent resistivity for three electrode types was evaluated in Microsoft Excel. A comparison the accuracy (percent difference) and repeatability (standard deviation) was the primary focus, but additional statistics were derived for a comparison of signal strength (current output vs. voltage received), and data acquisition error consistency. Figure E-8 shows a comparison of the percent difference between: 1) the traditional stake electrode and the depth limited stake electrode, and 2) the traditional stake electrode and the NEP electrode. Figure E-9 shows the percent difference between the three electrode types. Figure E-10 shows a comparison of the standard deviation values for the three electrode types. A summary of the statistical analysis can be viewed in Table E-4.

Figure E-8. Comparison of Standard Deviation Pseudosections for the Three Electrode Types.

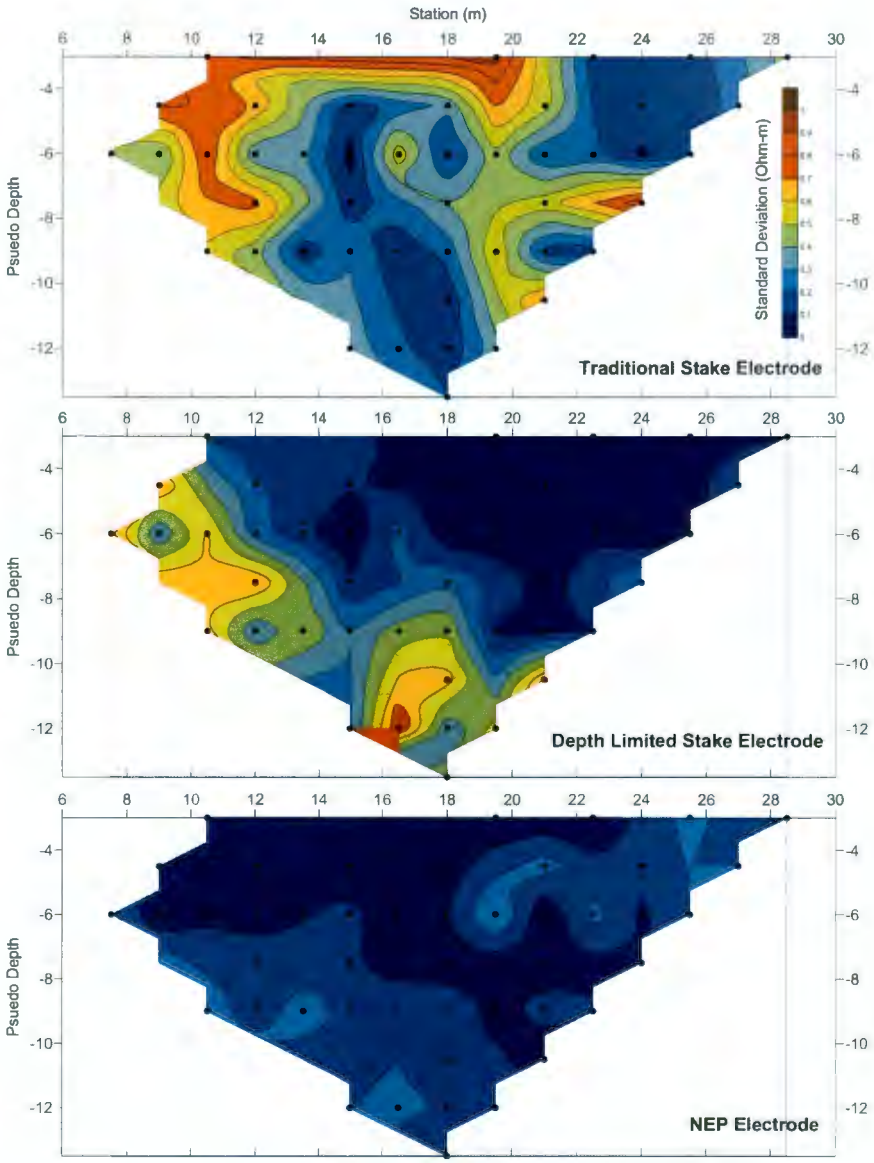

Figure E-9. Chart Showing Percent Difference Between the Three Electrode Types.

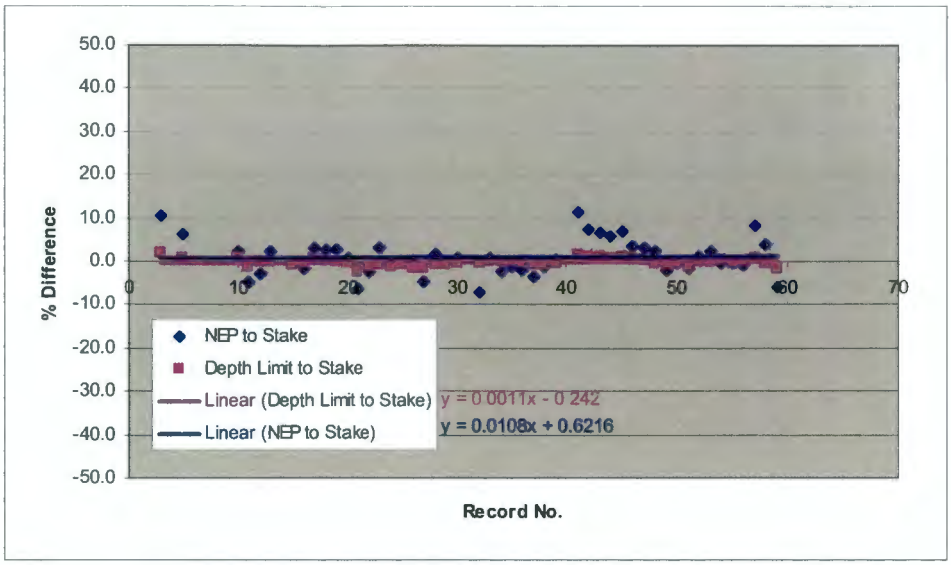

Figure E-10. Chart Showing a Comparison of the Standard Deviation for the Three Electrode Types.

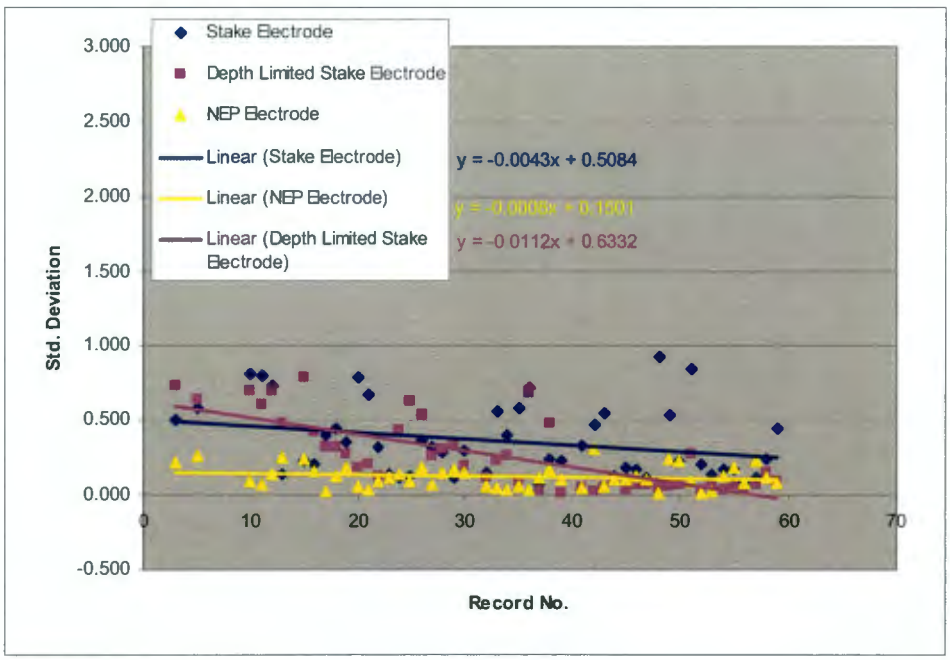

Table E-4. Statistical Comparison for the Three Electrode Types.

	D1 - Wet Stake					E1 - Wet Depth Limit Stake					I1 - NEP WET + 2" soil top electrode				
	R1	R2	R3	Ravg	Rstdev	R1	R2	R3	Ravg	Rstdev	R1	R2	R3	Ravg	Rstdev
Count	49.0	49.0	49.0	**49.0**	**49**	49	49	49	**49**	**49**	49	49	49	**49**	**49**
Average	457.1	457.1	457.1	**457.1**	**0.36**	456.2	456.2	456.2	**456.2**	**0.26**	461.9	461.8	461.7	**461.8**	**0.12**
Maximum	557.4	557.3	557.1	**557.3**	**0.93**	559.0	558.9	558.9	**558.9**	**0.78**	570.667	570.5	570.2	**570.5**	**0.31**

E5.0 RESULTS

E5.1 GRAPHICAL RESULTS

Analysis of the apparent resistivity pseudosection data plot for the three electrode types shows that the magnitude and character of depth limited stake electrode data more closely approximates the traditional stake electrode. The magnitude and character of the NEP electrode is not as close as the depth limited electrode, but from a geophysical imaging perspective, the difference is small enough that it will not affect profiling accuracy. The greater difference on the NEP electrode is attributed to the difference in location from the traditional electrode and most likely represents the changing geology over the 1-meter distance (Figure E-3). The resulting difference plots (Figure E-7) shows the difference between traditional and stake electrode is ± 10 ohm-meters and the difference between traditional and NEP electrode is approximately ± 50 ohm-meters. Another problem with direct comparison of electrode types is that one has to assume that the data acquired for the control set, in this case the traditional stake electrode, is correct and that any differences are caused by problems with the other electrode types. However, the increased surface area of the depth limited stake and NEP electrode make apparent resistivity measurements more reliable than the control set.

Comparison of the repeatability (Figure E-8) for the three electrode sets shows that the NEP electrode has a much smaller standard deviation for the three repeat measurements than the depth limited stake electrode, which in turn has a lower standard deviation than the traditional stake electrode. This indicates that the NEP electrode is more stable and more likely to produce repeatable data than the stake electrodes.

E5.2 NUMERICAL RESULTS

The statistical analysis shows a similar result to the graphical analysis. The average percent difference between the three electrode types was less than 1% and the average difference in standard deviation was less than 0.26 ohm-meters. Table E-5 shows a summary of the accuracy and repeatability statistics. This indicates that both alternative electrode types are well within an acceptable range for use within a tank farm.

Table E-5. Repeatability and Accuracy Evaluation.

	Percent Difference		Std Deviation Compariosn	
	NEP to Stake Electrode	Depth Limit to Stake Electrode	NEP to Stake Electrode	Depth Limit to Stake Electrode
Count	49	49	49	49
Average	0.98	-0.21	0.26	0.22
Maximum	11.61	1.80	0.92	0.88

E6.0 CONCLUSIONS

The NEP electrode was tested against traditional stake electrode and a depth limited stake electrode, and was found to produce suitable data if deployed with approximately 1 liter (0.26 gallons) of salt solution over 0.014 cubic meters (0.5 cubic feet) of surface cover (soil). Deploying the NEP electrode instead of a penetrating electrode could provide a significant time and cost savings by eliminating the need for prior subsurface clearing (ground penetrating radar scanning or 60 hertz electrical scanning). Logistical concerns were raised about the quantity of soil that would have to be introduced into the farm, transported to each electrode location, and potentially collected for disposal following data acquisition. A typical deployment may contain as many as 300 in-farm electrodes which would require approximately 4.3 cubic meters (150 cubic feet) of soil. Soil could be delivered to an area just outside the tank farm entry point where salt water could be added before the soil is loaded onto small landscaping carts. Deployment of traditional electrodes already requires transport of salt water via wheeled carts. Testing results show that the NEP electrode and the depth limited electrode are suitable alternate electrode configurations for resistivity data collection in and around the tank farms.

APPENDIX F

LESSONS LEARNED AND STREAMLINING FUTURE SURFACE GEOPHYSICAL EXPLORATION SURVEYS

TABLE OF CONTENTS

F1.0 INTRODUCTION F-1

F2.0 SITE ACCESS RESTRICTIONS AND TRAINING F-1

F3.0 INFRASTRUCTURE AND TRENCH MAPPING F-2
- F3.1 CRIBS AND TRENCHES F-2
- F3.2 GROUND-PENETRATING RADAR VS. G.O. CART F-2
- F3.3 GROUND-PENETRATING RADAR SURVEY RESOLUTION F-2

F4.0 RESISTIVITY DATA COLLECTION F-3
- F4.1 EXTRA CABLE SETS AND ELECTRODES F-3
- F4.2 REFERENCE ELECTRODE MAINTENANCE F-3
- F4.3 TEMPORARY VERSUS PERMANENT SURFACE ELECTRODES F-3
- F4.4 SURVEY RESOLUTION (SURFACE ELECTRODE SPACING) F-4

F5.0 EQUIPMENT F-5
- F5.1 INTEGRATED GLOBAL POSITIONING SYSTEM F-5
- F5.2 IMPROVING THE GLOBAL POSITIONING SYSTEM F-6
- F5.3 G.O. CART PLATFORM AND INTEGRATED GEOPHYSICAL SENSORS F-7
- F5.4 RESISTIVITY EQUIPMENT F-7

LIST OF FIGURES

Figure F-1. Cable Layout Across T Tank Farm F-5

Figure F-2. Shows a Selection of Ground-Penetrating Radar Features (colored crosses), Interpreted Pipelines (colored lines), and the Ground-Penetrating Radar Survey Line Coverage (black dots) F-6

LIST OF TERMS

Terms

SuperSting R8 IP. SuperSting R8 resistivity and induced polarization meter produced by Advanced Geosciences, Inc.

Abbreviations, Acronyms, and Initialisms

G.O. Cart	Geophysical Operations Cart
GPR	ground-penetrating radar
GPS	global positioning system
UL	Underwriters Laboratories, Inc.

F1.0 INTRODUCTION

This appendix provides lessons learned through the field work performed at the T tank farm and subsequent analysis of the data collected. These lessons learned can be used to streamline and improve follow-on deployments.

F2.0 SITE ACCESS RESTRICTIONS AND TRAINING

Lack of well defined training requirements for data collection activities that included both in-farm and ex-farm areas resulted in schedule delays. The area within the T tank farm fence (in-farm area) was controlled by CH2M HILL Hanford Group, Inc. while the areas outside the tank farm (ex-farm) were controlled by Fluor Hanford, Inc. Site access and safety training requirements for both CH2M HILL Hanford Group, Inc. and Fluor Hanford, Inc. had to be satisfied. Training requirements were not well defined and some required training courses are not recognized between contractors (e.g., lock and tag training for CH2M HILL Hanford Group, Inc. does not satisfy the Fluor Hanford, Inc. lock and tag training requirements). Additional training requirements were identified during field work planning which delayed start of data collection efforts.

Additional tank farm operations support on an as needed basis will reduce data acquisition time. Work within the ex-farm areas required a field work supervisor and a health physics technician when entering contaminated areas. Work in the farm required a field work supervisor, a health physics technician, and a minimum of two operators equipped with masks and respirators. The deployment of resistivity electrodes and cables was labor intensive, and under summer temperatures, the supplied air bottles lasted approximately 30-40 minutes. On average, operators were able to work through 6 bottles a day which provided for approximately 4 hours of in-farm work. No additional cable or electrode maintenance could occur once the operators left the farm. If electrode and/or cable connections were not satisfactory, then data acquisition was delayed until the next time operators could enter the farm and fix the faulty connection(s). Many of the survey lines required 7 to 8 hours to acquire, but the limited farm access time sometimes required the data acquisition be split over two days. Additional time is needed when a line is collected over multiple days because portions have to be repeated in order to accommodate changing conditions (e.g., instrument drift, electrode contract resistance changes). Often this limitation almost doubled data acquisition time. The ability to provide longer access hours when needed would reduce future data acquisition efforts.

F3.0 INFRASTRUCTURE AND TRENCH MAPPING

F3.1 CRIBS AND TRENCHES

Electromagnetic and magnetic surveys performed outside the tank farm with the Geophysical Operations Cart (G.O. Cart) were not effective for identifying subsurface metallic waste, solid waste, and plume characterization beneath the crib and trench areas (as was performed over the trench and cribs at the BC cribs site). Subsequent evaluation of the G.O. Cart results in comparison to the resistivity imaging showed a lack of sensitivity to the plumes beneath the northeast trenches and the 241-T-7 tile field. The resistivity results show that the plumes are deeper than the detection capabilities of the electromagnetic instrument (no greater than 6 meters [20 feet]), and magnetics results were limited because little metal was disposed of within the areas. The method was capable of detecting subsurface infrastructure that was not shown on available maps. Limiting G.O. Cart surveys to trench and crib areas of concern may greatly reduce project costs without impacting project goals. Future deployment of the G.O. Cart should be dependent on the expected depth of the imaging target. The G.O. Cart should be effective for targets that are no deeper than 6 meters (20 feet).

F3.2 GROUND-PENETRATING RADAR VS. G.O. CART

The abundance and proximity of the pipelines within the farm overwhelmed the electromagnetic and magnetic sensors on the G.O. Cart and individual responses could not be easily resolved. Instead, a grouped feature was mapped that represented a collection of responses.
The ground-penetrating radar (GPR) survey by contrast, provided sufficient resolution to separate individual responses and allowed hydroGEOPHYSICS, Inc. to verify the location of the subsurface infrastructure. Future projects may benefit from more GPR coverage and less G.O. Cart coverage within the tank farm area.

F3.3 GROUND-PENETRATING RADAR SURVEY RESOLUTION

The survey resolution along the line was approximately 5 centimeters (2 inches), but the resolution between the lines averaged 3.05 meters (10 feet) in the easting direction and 6.1 meters (20 feet) in the northing direction. Subsequent processing of the GPR data showed that increasing the total survey resolution by decreasing the line spacing would improve the accuracy of the interpreted infrastructure location.

F4.0 RESISTIVITY DATA COLLECTION

F4.1 EXTRA CABLE SETS AND ELECTRODES

Two complete sets of cables and electrodes would enhance data collection efforts by allowing for relocation and setup of one cable set while collecting resistivity data on the other set.
Only 100 electrodes were manufactured for the T tank farm demonstration which prevented the field crew from working ahead of the data collection by completing the setup on the next resistivity line. Future projects would benefit from an additional set(s) that could be installed along a successive line while acquiring data on the initial set.

F4.2 REFERENCE ELECTRODE MAINTENANCE

An electric fencer significantly reduces maintenance on the reference electrode wires. The wire that was used to connect the remote reference electrode arrays to the project site was run along the ground surface. Significant down time was caused by animals chewing through the wire. The wire is protected by a thin insulation that is designed to electrically insulate the wire and not provide a strength shield. Breaks caused by animals seemed to only occur at night or at times when the wire was not in use.

Subsequent work at S tank farm (December 2005) suggested that the small electrical signal from the resistivity instrument caused small animals to stay clear of the wire. A 12-volt DC powered electric fencer was used to apply a signal during periods when data were not being collected.
A dramatic decrease in wire breaks occurred after implementing the electric fencer.
The cumulative schedule impact associated with troubleshooting and repair of the reference electrode wires was approximately one week.

F4.3 TEMPORARY VERSUS PERMANENT SURFACE ELECTRODES

Permanent surface electrodes should be considered at sites where repeated data collection efforts may be performed. Resistivity data collection at the T tank farm was performed in two separate periods. Time period one, June to August 2005, was used to acquire the electromagnetic, magnetic, GPR, and surface resistivity data, while period two, January to February 2006, was used to acquire the well-to-well and well-to-surface data. The second deployment required that surface electrodes be replaced along survey lines recorded on during the first deployment.
The endpoints of the surface resistivity surface lines were located by global positioning system (GPS) during the first deployment, but could only be relocated within approximately 10 centimeters (3.9 inches) during the second deployment. A portion of a surface resistivity line was repeated prior to well-to-surface measurements, to evaluate any electrode-to-ground changes that occurred as a result of replacing electrodes at different times. The overall character of the data was consistent between the two deployments, however, the specific magnitudes and noise characteristics were different.

Dynamic measurements at S tank farm, where data was acquired at two different times when electrodes were installed twice, showed similar electrode-to-ground changes. Like T tank farm, the overall character of the data was consistent between data acquisition periods, but significant noise was observed when evaluating dynamic changes (subtracting data from Deployment 2 from data at Deployment 1). Resistivity is a relative measurement, so replacing electrodes for each deployment changes the electrode-to-ground contact properties (electrochemical) which alter the measured resistivity value. These changes are typically so small that non-dynamic measurements are not influenced. However, dynamic measurements are greatly affected by these changes and future deployments should consider using a permanently installed surface electrode to greatly reduce this noise source. Additionally, using permanent electrodes would eliminate time required to pull the electrodes and have a radiological survey performed prior to removing the electrodes from the tank farm.

F4.4 SURVEY RESOLUTION (SURFACE ELECTRODE SPACING)

Surface electrode spacing for future tank farm surveys can be increased from 3 meters (9.8 feet) to 6 meters (18.7 feet) with minimal loss of resolution. The 3-meter (9.8-foot) resolution of the surface resistivity survey was controlled by the electrode spacing along the line which was derived from a variety of factors including:

1. Physics – survey resolution is a function of the target body size and the desired smoothness of the fit to the character of the target body. The target body size and character was not well understood prior to the T tank farm deployment, so a maximum survey resolution was selected.

2. Equipment – the higher the resolution, the smaller the electrode spacing, and the greater the number of electrode channels needed to cover a specific distance. The critical distance for the T tank farm project was the largest distance across the farm (Figure F-1). In order to keep the resistivity data acquisition equipment outside of the farm, the cables had to be long enough to span the critical distance with no greater electrode take-outs than the number of available electrode channels.

3. Logistics – in theory, the higher the survey resolution, the greater the imaging accuracy, however, there is a point of diminishing return. Installation of electrodes at a spacing less than two to three meters would be challenging to deploy and the resolution increase would be minimal given the expected target body size.

Figure F-1. Cable Layout Across T Tank Farm.

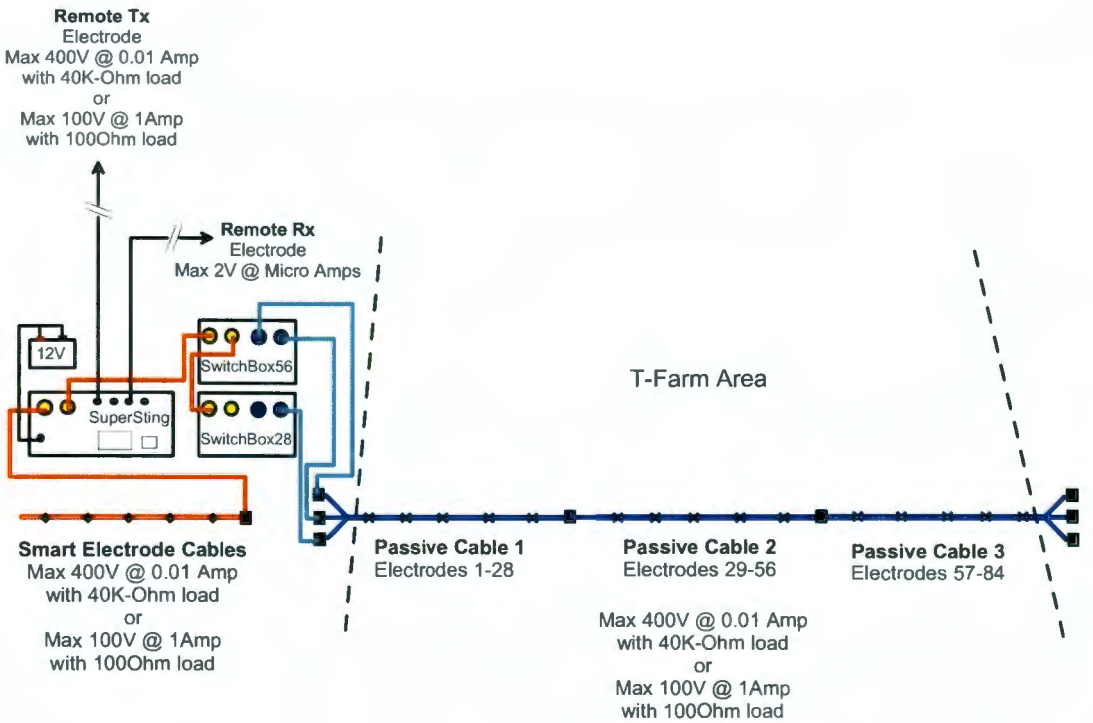

Subsequent analysis of the T tank farm surface data shows a negligible difference in the character of the plume body when using a 6-meter (19.7-foot) electrode spacing rather than a 3-meter spacing. In the future, the 6-meter (19.7-foot) spacing may be implemented to save time and resources with an acceptable resolution of data.

F5.0 EQUIPMENT

F5.1 INTEGRATED GLOBAL POSITIONING SYSTEM

The use of a sub-meter accuracy GPS integrated with the GPR and G.O. Cart instrumentation proved valuable in performing surveys around surface obstacles. The GPS unit provided a spatial (easting, northing) location that was appended to each geophysical data point.
This allowed operators the freedom to survey around surface obstacles, such as above ground structures and large vegetation, while still maintaining an accurate position. Traditional, non-GPS equipped surveys require survey lines that are spaced at regular intervals and run straight from end to end. Accommodating surface obstacles without GPS requires either separate survey grids that exclude areas around the obstacle or many hours of post processing.
The abundant surface obstacles within the project site made a non-GPS survey too time consuming and costly. The use of an integrated GPS for G.O. Cart and GPR surveys at T tank farm greatly reduced data acquisition time while increasing survey accuracy.

F5.2 IMPROVING THE GLOBAL POSITIONING SYSTEM

The GPS unit selected for the project acquired a data point every 1 second which was slower than the sampling rates of the GPR system. The mismatch between the two data acquisition rates meant that much of the position information was interpolated to match the GPR data point. This reduced the accuracy of the point location. In addition, the GPS unit achieved an average accuracy of 1 to 1.5 meters (3.3 to 5 feet) and not the sub-meter that was listed by the manufacturer. The limited accuracy was highlighted when imaging a straight pipeline with multiple lines. During GPR processing, an operator selects the center point of hyperbolic responses that are indicative of subsurface features. Since the GPR data is synchronized with GPS location, the location of the feature within the project site is known. The operator then plots the various features on a plan map and connects like features to represent a pipeline. The limited accuracy of the GPS caused small inconstancies between the actual location of the pipe and the resolved image of the pipe. Figure F-2 shows a selection of GPR features (colored crosses), interpreted pipelines (colored lines), and the GPR survey line coverage (black dots). Notice the GPR features are offset along the survey line coverage and the interpreted pipeline fits between the GPR features. Comparison of the GPR results to known features (historical maps and site inspection), shows an average accuracy of 1 to 2 meters (3.3 to 6.6 feet). With more accurate GPS location, there should be less scatter to the GPR features in plan view, which will increase the accuracy of the pipeline location.

Figure F-2. Shows a Selection of Ground-Penetrating Radar Features (colored crosses), Interpreted Pipelines (colored lines), and the Ground-Penetrating Radar Survey Line Coverage (black dots).

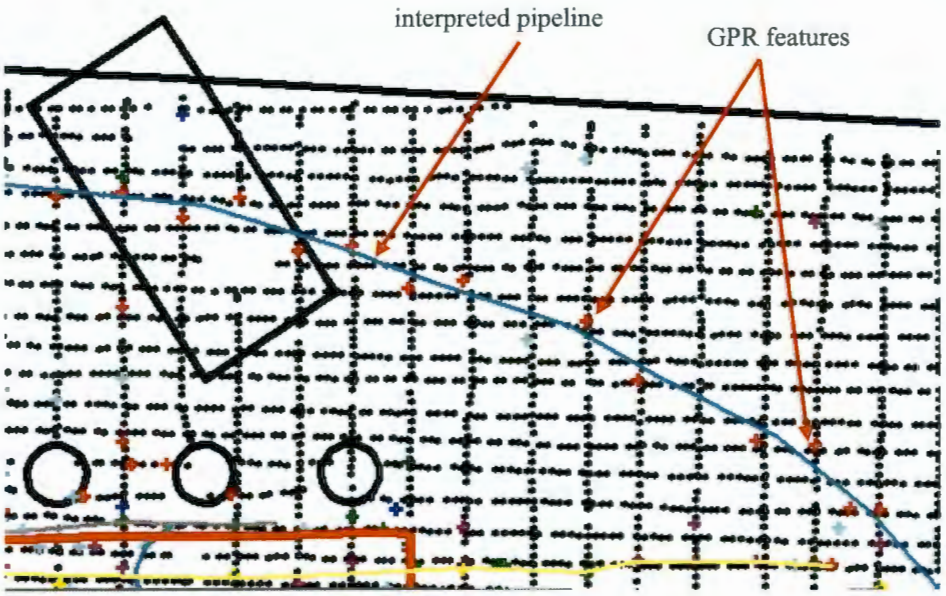

F5.3 G.O. CART PLATFORM AND INTEGRATED GEOPHYSICAL SENSORS

The following design improvements should be considered if the G.O. Cart is used on future deployments:

- Add a non-metallic suspension system to better accommodate rough terrain.
- Add a larger capacity data logger to increase survey time.
- Add an auxiliary high capacity battery to increase survey time.

F5.4 RESISTIVITY EQUIPMENT

Deployment of electrical equipment should include sufficient time for identification and resolution of National Electric Code/Underwriters Laboratories, Inc. (UL) issues. During the work package planning process, concerns were raised about the National Electric Code/UL requirements for using the equipment in the tank farms. This resulted in delaying the work package and subsequent deployment of the SuperSting R8[1] resistivity and induced polarization meter (SuperSting R8 IP) due to National Electric Code/UL review of the system and resolution of potential safety concerns. Previous use of the resistivity equipment at other locations on the Hanford Site considered the instrument a temporary use, test, or experimental system, and a UL certification was not required. Work within and around the tank farms is subject to inspection by a National Electric Code qualified inspector and required a UL certification or exemption for the resistivity equipment.

The SuperSting R8 IP was operated in 200 and 400 watt mode using one 12-volt DC car battery. The transmitter outputs an intermittent, pulsed, DC frequency waveform that is less than 1 hertz with a 67 percent duty cycle square wave; meaning the output transmit power is *not* continuous. When measurements are acquired, the SuperSting R8 IP routes the input power to the transmitter which contains a signal generator. The system applies a low power pulse to the transmitting electrodes to determine the contact resistance. The system then determines the maximum output power based on the contact resistance of the ground and the limiting voltage and current specified by the operator. There are then two boundary conditions for voltage and current that depend on the supplied load.

Condition 1: High ground resistance

A ground resistance of 40,000 ohms would cause the SuperSting R8 IP transmitter to produce a 400-volt signal at 0.01 amperes.

Condition 2: Low resistance

A ground resistance of 100 ohms would cause the SuperSting R8 IP transmitter to produce a 100-volt signal at 1 ampere.

---

[1] SuperSting R8 and SuperSting R8 IP are trademarks of Advanced Geosciences, Inc., Austin, Texas.

Therefore, the system can produce a maximum voltage of 400 volts and a maximum current of 1 ampere, but not at the same time. This will naturally follow Ohms Law: $V = I*R$.

Following review of the SuperSting R8 IP system, it was determined that it was acceptable for use in the tank farms providing lock and tag procedures were used to prevent energizing the equipment while personnel were in the farm moving the cables or electrodes.

DISTRIBUTION SHEET

To	From	Page 1 of 2
Distribution	David Myers, Vadose Zone Project	Date June 28, 2006
Project Title/Work Order		EDT No.
RPP-RPT-28955, Rev. 0, Surface Geophysical Exploration of the T Tank Farm at the Hanford Site		ECN No.

Name	MSIN	Text With All Attach.	Text Only	Attach./ Appendix Only	EDT/ECN Only
Jaraysi, Moses	H6-03	X			
Anderson, Frank	H6-03	X			
Connelly, Michael	H6-03	X			
Jones, Thomas	H6-03	X			
McMahon, William	H6-03	X			
Sydnor, Harold	H6-03	X			
Myers, David (5)	H6-03	D			
Watson, David J.	H6-03	X			
Mann, Fred J.	H6-03	X			
Lober, Robert	H6-60	D			
Wood, Marc	H8-44	X			
Khaleel, Raz	E6-17	X			
Benecke, Mark	E6-35	X			
Rohay, Virginia	E6-35	X			
Todd-Robertson, Mary	E6-35	X			
Horton, Duane	K6-75	D			
Narbutovskih, Susan	K6-76	D			
Weekes, David	H6-62	X			
Krogsrud, L.S.	S7-24	X			
Sweeney, Mark	K6-75	D			
Wiegman, Steven	H6-60	X			
Parker, Danny	H6-03	D			
Voogd, Jeff	H6-03	X			
Field, James	H6-62	X			
Koch Michael R.	S7-83	X			
Popielarczyk, Bob	R2-58	X			
Thomas, Greg	E6-35	X			
Byrnes, Mark	E6-35	X			
Swanson, L.C.	E6-35	X			
Erb, David	E6-35	X			
Cummins, Gloria	E6-35	X			
Yasek, Robert	H6-60	X			

DISTRIBUTION SHEET

To	From	Page 2 of 2
Distribution	David Myers, Vadose Zone Project	Date June 28, 2006
Project Title/Work Order		EDT No.
RPP-RPT-28955, Rev. 0, Surface Geophysical Exploration of the T Tank Farm at the Hanford Site		ECN No.

Name	MSIN	Text With All Attach.	Text Only	Attach./ Appendix Only	EDT/ECN Only
Morse, John	H6-60	X			
Thompson, K. Michael	H6-60	X			
Lyon, Jeff	H0-57	D			
Caggiano, Joseph	H0-57	D			
Uziemblo, Nancy	H0-57	D			

A-6000-135 (10/97)